

THE DEVELOPMENT OF METHODOLOGIES AND
A NOVEL TEST FACILITY FOR THE CHARACTERISATION
OF THERMOELECTRIC GENERATORS

The Development of Methodologies and a Novel Test Facility for the
Characterisation of Thermoelectric Generators

By

DONAL FINNERTY, B.A., B.A.I.

A Thesis

Submitted to the School of Graduate Studies
in Partial Fulfillment of the Requirements

for the Degree

Master of Applied Science

McMaster University

© Copyright Donal Finnerty, May 2013

MASTERS OF APPLIED SCIENCE (2013)
(Mechanical Engineering)

McMaster University
Hamilton, Ontario

TITLE: The Development of Methodologies and a Novel Test Facility for the Characterisation of Thermoelectric Generators

AUTHOR: Donal Finnerty, B.A., B.A.I. (McMaster University)

SUPERVISOR: Dr. J.S. Cotton

NUMBER OF PAGES: xviii, 127

Abstract

With the rising prices of energy and the harmful environmental effects many of conventional energy generation techniques the world is pushing for new, cleaner, more efficient and more environmental renewable energy sources. Thermoelectric generators are one of the potential solutions to these problems of unclean and expensive energy. Thermoelectric generators are solid state devices that convert thermal energy into useful electrical energy.

Over the last ten years the progress in materials science have led to advancements in thermoelectrics. However as of yet no standardised method of testing thermoelectric generators has been established and as such data provided for thermoelectric generators is regarded as questionable. This thesis deals with two commercial thermoelectric generator models, TEG1 12610-5.1 AND TEG1B 12610-5.1, and quantifies the deviation of the manufacturer's specifications to what is experimentally achieved by the generators as 147% and 22% respectively. The variance of the outputs between thermoelectric generators was measured by comparing the maximum power output for the models in question over a sample size of four, it was found to be as much as 20% and 8% respectively.

A full characterisation of the thermoelectric generators is performed on the two generator models to obtain the data as to their power output and thermal conductivity for the purpose of design of a waste energy harvesting device. The full characterisation was also used to validate the testing apparatus as a device capable for the use as a standardised method of characterising the performance of thermoelectric generation modules.

A mechanistic model is created using the experimental characterisation data. This mechanistic model has the ability to accurately predict the voltage and current output of the thermoelectric generator models under any given temperatures and electrical loading condition with a minimum R-squared value of 0.94. The thermal conductivity is also

found to be predictable using an established equation modified with an empirical constant.

Acknowledgements

I really have to acknowledge my supervisor, Dr. James Cotton, in this work because it was not only his guidance and help throughout all my time in Canada but his belief in me which frequently was greater than my belief in myself. Without his support this thesis would never have gotten written and I would have been deported months ago.

I would like to thank Dr Hossam Sadek who's selflessness and level headedness helped me find my feet not only in researching but also in a foreign country.

To Dr. Chan Ching who kept me appraised of my own progress and helped motivate me.

Corbin, Jeff, Mike, Raf and Yakoob who made the TEG Team the most fun and most enthusiastic research group and the best friends I could ask for.

To all the members of TMRL who patiently listened to my presentations on how little I had achieved that week, for their help and helping me consume copious amounts of sushi

To all the members of the Deep Homers over the past two years who made the stifling heat of the Canadian summers more bearable.

To all my Canadian friends who kept me sane and kept me company over many a pitcher at the Phoenix.

To Sarah for always sharing the tea and keeping me company all these long years.

Most importantly to my family who have stuck with me through thick and thin and who's love and support gave me the courage to move five thousand kilometres to see what was on the other side of the ocean.

To the project's financial sponsors N.S.E.R.C., O.C.E., Pizza Pizza and Thermal Electronics Corp..

If I failed to mention you, yet you are still taking the time to read the acknowledgements page of my thesis then I would like to thank you as well.

Table of Contents

Abstract	i
Acknowledgements	vi
Table of Contents	vii
List of Figures	x
List of Tables	xiv
Nomenclature	xv
1 Introduction	1
1.1 Scope of Work	4
2 Literature Review	6
2.1 Historical Background	6
2.2 Thermoelectric Phenomena	6
2.2.1 The Seebeck Effect	6
2.2.2 The Peltier Effect	8
2.2.3 The Thomson Effect	9
2.3 Thermoelectric Generators	10
2.4 Materials	12
2.5 Thermoelectric Equations	15
2.5.1 Power Generated	15
2.5.2 Matched Resistance and Max Power	16
2.5.3 Efficiency	17
2.6 Applications	17
2.7 A Review of TEG Power Generation Modelling Methodologies	18

2.8 A Review of Experimental TEG Characterisation Methodologies.....	23
3 Experimental Facility.....	28
3.1 The Experimental Facility.....	28
3.2 The Energy Balance	32
3.3 Qualification	38
3.4 Data Acquisition System.....	40
3.5 Data Reduction.....	42
3.6 Experimental Procedure	44
3.7 Uncertainty Analysis.....	46
4 Results and Discussion	51
4.1 Manufacturer’s Data	51
4.2 Test Parameters	55
4.3 TEG Variability	56
4.4 Typical Results.....	63
4.5 Experimental and Manufacturer’s Data Comparisons	69
4.6 TEG1 and TEG1B Comparisons	75
4.7 Thermal conductivity	83
4.8 Mechanistic Model.....	84
5 Conclusion and Future Work	93
5.1 Future work:	95
References	97
APPENDIX A.....	101
APPENDIX B	115
APPENDIX C	124

List of Figures

Figure 1.1 A simplified schematic diagram of an overall typical heat transfer system used in heat recovery and the corresponding resistance network.	3
Figure 2.1 Simple thermoelectric circuit containing two dissimilar materials demonstrating the Seebeck effect..	7
Figure 2.2 Simple thermoelectric circuit containing two dissimilar materials demonstrating the Peltier effect	8
Figure 2.3 Basic schematic of a Thermoelectric Generator	10
Figure 2.4 3D rendering of a typical design for a thermoelectric generator	11
Figure 2.5 Sketch of occupied electron states in a p-type semiconductor	13
Figure 2.6 Sketch of occupied electron states in a n-type semiconductor	13
Figure 2.7 Figure of merit of various materials used for thermoelectric applications as a function of temperature.	14
Figure 2.8 %Difference between Chen’s commercial software models and measurements performed to qualify them.	20
Figure 2.9 Experimental Facility used to characterize the performance of thermoelectric generators used by Carmo.....	24
Figure 2.10 Image of Ahsika’s T.E.P.A.S. experimental facility.	25
Figure 3.1 Schematic representation of the TEMTester	29
Figure 3.2 Simplified Sketch of the TEMTester	31
Figure 3.3 Energy Balance for the experiments performed on the TEG1 12610-5.1	35
Figure 3.4 Energy Balance for the experiments performed on the TEG1B 12610-5.1	36
Figure 3.5 Energy into TEG vs Energy out for all TEG1 12610-5.1 experiments	37
Figure 3.6 Energy into TEG vs Energy out for all TEG1B 12610-5.1 experiments.....	38
Figure 3.7 Thermal Conductivity results of MACOR machinable glass ceramic	39
Figure 3.8 Thermal contact resistances between the copper blocks with varying applied pressure	40
Figure 3.9 Examples of the power curve resultant from the detailed test, “A”, and the spot testing	45

Figure 4.1 Performance data for a TEG1 12610-5.1 digitized from the manufacturer's specifications.....	52
Figure 4.2 Current and voltage adopted from manufacturer's data for a cold side temperature, T_c , of 30°C and varying hot side temperatures.....	53
Figure 4.3 Curves of Power output of a TEG1 12610-5.1 at different load resistances for a constant cold side temperature, T_c , of 30°C and various hot side temperatures.....	54
Figure 4.4 Experimental results for the short circuit current and open circuit voltage of four separate TEG1 12610-5.1 at a temperature difference of 200°C-50°C	57
Figure 4.5 Results for the maximum power output of four separate TEG1 12610-5.1 at a temperature difference of 200°C-50°C.....	58
Figure 4.6 Values for the Seebeck coefficient and internal resistance of four separate TEG1 12610-5.1 at a temperature difference of 200°C-50°C.....	58
Figure 4.7 Experimental results for the open circuit voltage and short circuit current of four separate TEG1B 12610-5.1 at a temperature difference of 250°C-50°C.....	59
Figure 4.8 Results for the maximum power output of four separate TEG1B 12610-5.1 at a temperature difference of 250°C-50°C.....	60
Figure 4.9 Values for the Seebeck coefficient and internal resistance of four separate TEG1B 12610-5.1 at a temperature difference of 250°C-50°C.....	60
Figure 4.10 Experimentally measured voltage of a TEG5.1 12610-5.1 as a function of load resistance at a constant cold side temperature of 50°C and different hot side temperatures.....	65
Figure 4.11 Experimentally measured current of a TEG5.1 12610-5.1 as a function of load resistance at a constant cold side temperature of 50°C and different hot side temperatures.....	66
Figure 4.12 Experimentally measured power output of a TEG5.1 12610-5.1 as a function of load resistance at a constant cold side temperature of 50°C and different hot side temperatures.....	67
Figure 4.13 Experimentally measured V-I curve of a TEG1-12610-5.1 measured at a constant cold side temperature of 50°C and different hot side temperatures.....	68

Figure 4.14 Experimentally measured curve of the thermal resistance of aTEG1-12610-5.1 measured at a constant cold side temperature of 50°C and different hot side temperatures.....	69
Figure 4.15 Comparison of manufacturer data and experimental results for a TEG1B 12610-5.1 and TEG 12610-5.1 for a constant cold side temperature of 30°C and varied hot side temperatures.. ..	72
Figure 4.16 Comparison of manufacturer data and experimental results for a TEG1B 12610-5.1 and TEG 12610-5.1 for a constant cold side temperature of 50°C and varied hot side temperatures.	73
Figure 4.17 Comparison of manufacturer data and experimental results for a TEG1B 12610-5.1 and TEG 12610-5.1 for a constant cold side temperature of 80°C and varied hot side temperatures.. ..	74
Figure 4.18 Experimentally measured maximum power output of the TEG1 12610-5.1 and the TEG1B 12610-5.1.	75
Figure 4.19 Experimentally measured open circuit voltage of the TEG1 12610-5.1 and the TEG1B 12610-5.1.....	76
Figure 4.20 Experimentally measured short circuit current of the TEG1 12610-5.1 and the TEG1B 12610-5.1.....	77
Figure 4.21 Experimentally measured voltage of the TEG1 12610-5.1 and the TEG1B 12610-5.1.at the maximum power output.	78
Figure 4.22 Experimentally measured current of the TEG1 12610-5.1 and the TEG1B 12610-5.1.at the maximum power output.	79
Figure 4.23 Experimentally measured electrical resistance of the TEG1 12610-5.1 and the TEG1B 12610-5.1.at which max power occurs.....	80
Figure 4.24 Thermal componenet of the overall thermal conductivity of a TEG1 and a TEG1B	84
Figure 4.25 Open circuit voltage of the TEG1 12610-5.1 predicted by the mechanistic model.....	86

Figure 4.26 Open circuit voltage of the TEG1B 12510-5.1 predicted by by the mechanistic model	87
Figure 4.27 Short circuit current of the TEG1 12610-5.1 predicted by the mechanistic model.....	888
Figure 4.28 Short circuit current of the TEG1B 12610-5.1 predicted by by the mechanistic model	89
Figure 4.29 Experimentally measured thermal conductivity of the TEG1 12610-5.1 and thermal conductivity predicted by standard equation	90
Figure 4.30 Experimentally measured thermal conductivity of the TEG1 12610-5.1 and thermal conductivity predicted by modified equation	90

List of Tables

Table 2.1 Review of assumptions and methodologies used in TEG performance models	22
Table 2.2 Review of a selection of TEG characterization facilities.....	27
Table 3.1 Parameters measured in TEMTester apparatus.....	41
Table 3.2 Maximum Uncertainty of measured and calculated values of the TEG1-12610-5.1	47
Table 3.3 Maximum Uncertainty of measured and calculated values of the TEG1B-12610-5.1	48
Table 3.4 Uncertainty of measured and calculated values of the TEG1-12610-5.1 at the matched load condition	49
Table 3.5 Uncertainty of measured and calculated values of the TEG1B-12610-5.1 at the matched load condition	50
Table 4.1 Table of Testing Parameters for both TEG1 12610-5.1 and TEG1B 12610-5.1	56
Table 4.2 2 Measured values and calculated variance of TEG1-12610-5.1 along with a comparison to manufacturer's data	61
Table 4.3 Measured values and calculated variance of TEG1B-12610-5.1 along with a comparison to manufacturer's data	62
Table 4.4 Percentage difference between the prediction with the manufacturer's data and the experimental data for a TEG1 12610-5.1	71
Table 4.5 Percentage difference between the prediction with the manufacturer's data and the experimental data for a TEG1B 12610-5.1	71
Table 4.6 Difference of the electrical characteristics of the TEG1B-12610-5.1 over the TEG1-12610-5.1	82
Table 4.7 Difference of the electrical characteristics of the TEG1B-12610-5.1 over the TEG1-12610-5.1	82

Nomenclature

α	Seebeck Coefficient of a Material [V/K]
α_{TEG}	Effective Seebeck coefficient of a thermoelectric generator [V/K]
ΔT	Temperature difference between the hot and cold sides of a thermoelectric generator [°C]
η_{TEG}	Conversion efficiency of a thermoelectric generator
λ	Thermal Conductivity of a Material [W/mK]
μ	Thomson Coefficient of a Material [V/K]
ρ	Electrical Resistivity of a Material [Ω m]
π	Peltier Coefficient of a Material [W/A]
A	Area [m ²]
C_P	Specific heat capacity of water [J/kg K]
I	Current [A]
I_m	Current output of the thermoelectric generator at matched resistance condition [A]
I_{TEG}	Current produced by a thermoelectric generator [A]
I_{SC}	Short circuit current of a thermoelectric generator [A]
K	Effective thermal conductivity of a thermoelectric generator [W/K]
k_{C110}	Thermal conductivity of Copper C110 [W/mK]
$K_{ELECTRICAL}$	Thermal conductivity component of a thermoelectric generator dependent on current flow [W/K]

K_{TEG}	Thermal conductivity of a thermoelectric generator [W/K]
$K_{THERMAL}$	Thermal conductivity of a thermoelectric generator generating no current [W/K]
\dot{m}	Mass flow rate of chilling water [kg/s]
N	Number of thermoelectric couples in a thermoelectric generator
P_m	Power output of the thermoelectric generator at matched resistance condition [W]
P_{MAX}	The maximum electrical power achievable by a thermoelectric generator [W]
P_{TEG}	The electrical power output of a thermoelectric generator [W]
Q	Heat Flow [W]
Q_C, Q_{COLD}	Heat flowing from a thermoelectric generator to a heat sink [W]
$Q_{ELECTRICAL}$	Electrical power produced by the TEG [W]
$Q_{HEATERS}$	Heat produced by the heaters [W]
Q_H, Q_{HOT}	Heat flowing to a thermoelectric generator from a heat source [W]
Q_{WATER}	Heat extracted from the TEMTester via the chilling loop [W]
R	Resistance [Ω]
R_{LOAD}	The resistance of the electrical load applied to the thermoelectric generator [Ω]
R_m	Electrical load resistance equivalent to the internal resistance thermoelectric generator [Ω]
R_{TEG}	The internal electrical resistance of a thermoelectric generator [Ω]

$R_{TEG,TH}$	The effective thermal resistance of a thermoelectric generator [K/W]
T	Temperature [°C]
T_{AVG}	Average temperature of a thermoelectric generator [°C]
T_C, T_c	Temperature of the cold side of a thermoelectric generator [°C]
T_{COLD}	Temperature of the cold side of a thermoelectric generator [°C]
T_{COLD}	Temperature at a specific point in the cold block [°C]
$T_{COLD,SURF}$	Temperature at the contact surface of the thermoelectric generator and cold block extrapolated from temperature gradient in the cold block [°C]
T_H, Th	Temperature of the hot side of a thermoelectric generator [°C]
T_{HOT}	Temperature of the hot side of a thermoelectric generator [°C]
T_{HOT}	Temperature at a specific point in the hot block [°C]
$T_{HOT,SURF}$	Temperature at the contact surface of the thermoelectric generator and hot block extrapolated from temperature gradient in the hot block [°C]
$\bar{T}_{W,I}$	Average temperature of chilling water entering heat exchanger [°C]
$\bar{T}_{W,O}$	Average temperature of chilling water exiting heat exchanger [°C]
u_{bias}	The bias uncertainty associated with a measurement device
$u_{temporal}$	The uncertainty of a measurement due to fluctuations of the reading with time
$u(x)$	Uncertainty of a measured value.
$u(R)$	Uncertainty of a calculated value.
V	Voltage [V]

V_m	Voltage output of the thermoelectric generator at matched resistance condition [V]
V_{OC}	Open circuit voltage of a thermoelectric generator [V]
V_{TEG}	voltage produced by a thermoelectric generator [V]
x	General spatial coordinate [m]
x_{COLD}	Position of a thermocouple sensor in the cold block [m]
x_{HOT}	Position of a thermocouple sensor in the hot block [m]
ZT	Thermoelectric Figure of Merit, dimensionless number indicative of a materials effectiveness for thermoelectric conversion

1 Introduction

Thermal energy (heat) was the first type of energy that humans first learned to harness to keep themselves warm and cook their meat [1,2]. Three hundred thousand years, and that reliance on heat has not abated but only become more sophisticated. The vast majority of electricity produced is converted from heat, through the combustion of materials or the nuclear decay of isotopes. In 2012 Canada produced 35% of its electricity using various thermal processes [3] which is in general considered relatively low on a global scale because of Canada's access to hydroelectric power. The United States' production of electricity shows a different story; 88% of electricity produced there uses thermal processes which with only an average efficiency of approximately 30-40% means as much as 2.1 PetaWatt hours of waste thermal energy [4].

Society has come to realise that the reliance on those sources of heat are not sustainable and are possibly having a negative effect on the climate. Efforts have been made to relieve the reliance on thermal energy and branch out into renewable sources. Solar, wind, wave and tidal are all receiving a huge push both socially and economically to reduce the amount that we rely on heat. However with the sheer magnitude of worldwide consumption of electricity and the relatively small amount of infrastructure devoted to renewable energy, it is still a long way from powering the world. With the steady increase in the worldwide demand for energy this goal is not becoming any easier.

The major problem with the heat energy that we create is that in doing useful work that thermal energy emerges from the process at a lower grade which is considered useless. This useless heat is considered a waste, a bi-product of the process and is vented to the atmosphere. In 2008, Arun Majumdar Director of the Advanced Research Projects Agency – Energy (ARPA-E) and professor of UC Berkley estimated that of the average 100 Quadrillion BTUs of energy are produced in the United States and as much as 55-60QBTU [5] are lost to the atmosphere or reservoirs of water as waste heat. According to his presentation given in the “Energy 2009: Lean and Green Conference” Sean Bedard of

CanmetEnergy estimated that 2,300 Peta Joules of waste heat is produced in Canada from various industries with pulp and paper, metallurgy, chemical and petrochemical and oil refining being the main sources. Bedard went on to say that numerous studies performed by various institutions indicated that 25% of that waste heat energy is recoverable using contemporary waste heat recovery technology [6].

Thermoelectric generators are one such technology. They are solid state devices that have the ability to convert heat directly into useful electricity. The major benefit of these devices is that the heat does not have to be high grade to be converted; Thus they can be used to recover the waste heat energy that has until now been rejected to the atmosphere as waste. The benefits of this technology over others is that the generators are long life solid state devices that have no moving parts to convert the waste heat. They provide a long term passive solution to producing electricity with waste heat from any process.

The research presented in this thesis is a component in a larger research project, P.O.W.E.R. – Pizza Oven Waste Energy Recovery, done in conjunction with Pizza Pizza Corp. with the goal of recouping the heat from the pizza oven exhaust gases. There are other students researching different areas such as thermal energy storage, energy auditing and heat transfer. One aim of the project is to create two heat transfer systems, one that captures the heat in the exhaust gas and transfers it to one side of the thermoelectric generator and another that extracts the heat from the cold side. Both of these heat transfer systems are being designed to have high heat transfer while providing isothermal surfaces for the generators. Another aim is to take the thermal energy that is extracted with the cold side heat transfer system, that which was not converted directly to electricity, and store it so the store can use it for heating, absorption chilling or hot water needs. All this research is being performed with a view to combine all the research to provide Pizza Pizza with a complete waste heat recovery system using waste heat to make their stores more energy efficient. Another benefit from the overall project is that the solution will provide Pizza Pizza with autonomous power from the grid allowing them to still function in the event of a power outage. The research presented in this thesis is a full characterisation of a thermoelectric generator with a view to providing accurate data and

mechanistic models for design and optimisation of energy recovery employing these devices.

In the design of a power generation system using thermoelectric generators the, generator plays a fundamental role both in the generation of electricity but also as a critical component in the heat flow path. The generator represents a significant thermal resistance in the heat flow path from the heat source to heat sink, Fig. 1.1. The generator's thermal resistance is affected by many factors including its temperature and how much power it is producing. The heat flow through the system determines the temperature difference across the generators and thus the power generated by the system. In turn the heat flow is affected by the thermal resistance. This causes a delicate and complicated problem to designing these systems.

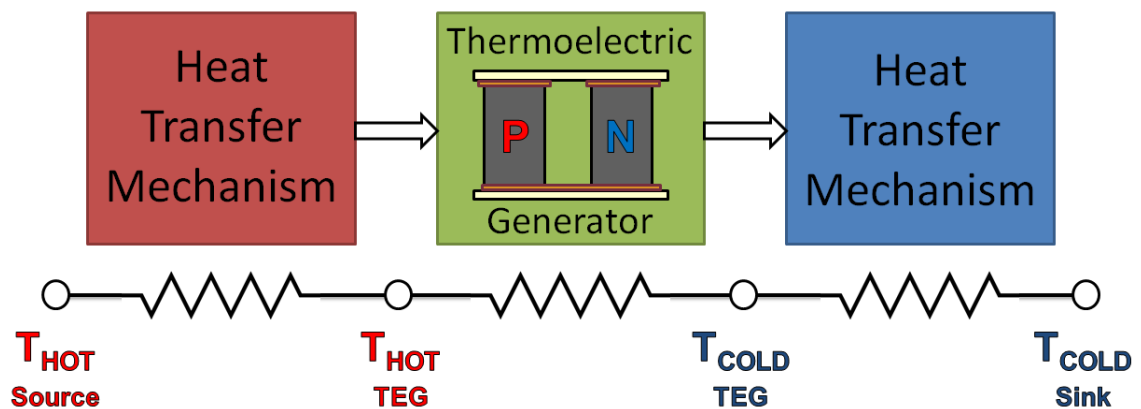


Figure 1.1 A simplified schematic diagram of an overall typical heat transfer system used in heat recovery and the corresponding resistance network.

The development of a power generation system requires accurate and detailed data of the thermoelectric generator used, focusing on the power generated and thermal conductivity as a function of both temperature and electrical current. The specifications supplied by the manufacturer only provide data at a single electrical current for a given temperature difference. Thermal conductivity data provided is limited to the heat flow through a generator for a single temperature difference at a specific current. Information regarding how the manufacturer data is generated is not supplied and there is no mention of a

measurement facility, the repeatability of these results or a reported uncertainty. This leaves designers without a reliable tool to make predictions as to how the generator will interact with their system.

While the physics behind thermoelectric generators has been known since the 1800s, numerical modelling of thermoelectrics still proves to be exceedingly difficult to provide accurate data. This is mainly due to the high sensitivity of the thermoelectric material properties which change drastically with temperature and the electric current. Even the most detailed models developed to capture all the physical processes that occur in thermoelectric generation report up to 20% error to the measured value of power output [7]. With the difficulty in modelling the performance of thermoelectric generators, the relevant data will need to be found experimentally.

Numerous papers exist detailing the experimental results from thermoelectric generators [15,17,20,21,27,29-34]. However no single paper yet exists that contains all the relevant data that is needed to accurately design a power generation system over a range of conditions different from the the rated matched power specifications. These investigations tend not to focus on the thermal conductivity, instead focusing more on the power generation aspect. Those papers that deal with power generation tend to focus heavily only on already optimised systems where the generator puts out the maximum power possible. This data is not sufficient for design for two reasons: it does not take into account that the manufacturing process of thermoelectric generators and of the thermoelectric materials can lead to high variability of their performance [8,9] and it does not allow for design constraints that may cause the generation system to operate at a non-optimal condition.

1.1 Scope of Work

This thesis will focus on characterising two commercial thermoelectric generators at different thermal conditions over a large range of electrical conditions. The purpose of these characterisations is to provide designers of thermoelectric generation systems with

well quantified and validated data as to how thermoelectric generators will work in a waste heat recovery device. A mechanistic model will be derived from the experimental results which will be capable of accurately predicting the performance of a thermoelectric generator under a wide range of temperatures and electrical loads. This model will provide designers to accurately predict what a thermoelectric generator will produce electrically under varied electrical conditions and how it will affect the flow of heat through the system.

The experiments for this research will be performed using a novel facility specifically designed for the characterisation of thermoelectric generators. The facility accurately tracks the heat flowing through the system with an energy balance of 6%. The thermal properties of thermoelectric generators can be evaluated while also allowing for any thermal condition to be set to test the generated power. The system can also be maintained in these conditions while the electrical conditions are varied to observe their effects on the thermal properties. Overall, the data provided will give a full accounting of the thermal and electrical coupling involved in the thermoelectric generators.

2 Literature Review

2.1 Historical Background

Thermoelectrics is the study of the coupling of thermal and electrical phenomena, which occurs when heat flow induces a flow of electrons or an electric current induces a flow of heat. The study of thermoelectrics was established in 1821 when the first discovery was made in the field but has not been much utilised commercially.

Today, with the field of mechanical engineering focusing more and more on efficient and sustainable forms of energy, thermoelectrics has become a viable area of research. The main reason for the resurgence of thermoelectrics was the vast improvement in materials science. The creation of semiconductors, which when used in thermoelectrics can yield higher efficiencies than previously attainable. Another reason for the revival of thermoelectrics is the large amount of heat that is produced as waste in many industrial and commercial processes. This waste heat is considered to be at too low a temperature to be used as a driving force any sort of useful work in traditional thermal plant systems but with thermoelectrics even that flow of low grade heat can be converted directly into electrical energy.

2.2 Thermoelectric Phenomena

Thermoelectrics deals mainly with three phenomena which are the Seebeck effect the Peltier effect and Thomson effect which all involve the coupling of thermal and electronic energy flow:

2.2.1 The Seebeck Effect

The Seebeck effect is most easily observed in a circuit of two dissimilar metals joined together at two separate points, called a thermocouple circuit. Fig. 2.1 shows a schematic of the thermocouple with which Thomas Johann Seebeck first observed the Seebeck

effect in 1821 [10]. Seebeck found that when heat was applied to one joint in the circuit and heat removed from the other joint, an electromotive force is generated in the circuit.

Seebeck further found that the magnitude of the EMF was proportional to the temperature difference between the two joints and was directly related to the materials used. All conductive materials have a Seebeck coefficient, α , which is the material property responsible for generating the EMF. The EMF generated in the thermocouple circuit is proportional to the difference in Seebeck coefficient between the two materials:

$$\alpha_{CIRCUIT} = \alpha_{MATERIAL A} - \alpha_{MATERIAL B} \quad 2.1$$

$$E.M.F = \alpha_{CIRCUIT}(T_H - T_C) \quad 2.2$$

The Seebeck coefficient of a material cannot be measured independently as it only develops from the difference between two materials; as such platinum was designated as having a Seebeck coefficient of zero. The direction of the electromotive force depends on the Seebeck coefficient of the materials used and which joint in the circuit is at a higher temperature.

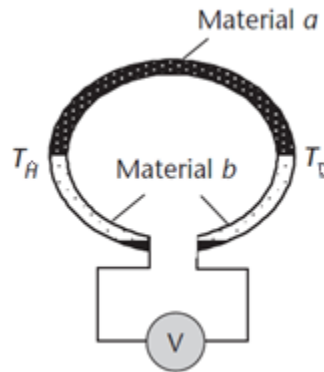


Figure 2.1 Simple thermoelectric circuit containing two dissimilar materials. A voltage is measurable in the circuit when the joints are held at different temperatures. [11]

2.2.2 The Peltier Effect

The Peltier effect can be loosely considered the Seebeck effect in reverse. Jean Charles Peltier discovered in 1834 that if a current were flowing through a circuit of dissimilar metals, a thermocouple, that heat would be given off the circuit at one joint while heat would simultaneously be absorbed at the opposite joint. Similar to Seebeck's experiment it was found that the amount of energy being evolved and absorbed at either joint was related to the materials used. It was also found that the heat was proportional to the current flow through the circuit.

As it was found for the Seebeck effect, it is a material property that is responsible for the Peltier effect. This material property is the Peltier coefficient, π , and it is the difference between that coefficient in the two materials that causes the heat flow.

$$\pi_{CIRCUIT} = \pi_{MATERIAL A} - \pi_{MATERIAL B} \quad 2.3$$

$$Q = \pi_{CIRCUIT} \times I \quad 2.4$$

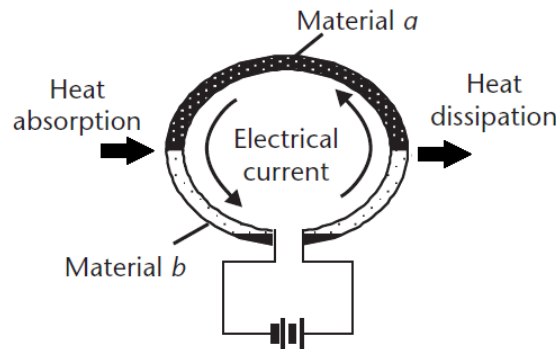


Figure 2.2 Simple thermoelectric circuit containing two dissimilar materials. A current is applied to the circuit causing heat to be absorbed and rejected at opposite joints in the circuit. [11]

The joint at which heat is being evolved is dependent on the direction of the current and the relative Peltier coefficients. For example, in Fig. 2.2, heat is being rejected by the joint on the right and absorbed on the left, which is true given the direction of current

flow if “material b” has a higher Peltier coefficient than that of “material a”. However if “material a” were replaced with a “material c” that had a Peltier coefficient higher than that of “material b”, then given the same current direction heat would be dissipated at the joint on the left and absorbed at the joint on the right. Performing the same action on the circuit for the Seebeck effect will cause the direction of the EMF to change.

2.2.3 The Thomson Effect

The Thomson effect was discovered by Lord Kelvin when he was investigating the discoveries of Peltier and Seebeck. Kelvin found when a conductor is experiencing a temperature difference along its length while carrying an electronic current, heat will either be absorbed by or emitted from the conductor due to the Thomson effect. The heat generated in a conductor experiencing a temperature gradient is then the combination of this heating or cooling and the joule heating:

$$Q = I^2R - \mu I \frac{dT}{dx} \quad 2.5$$

Equation 2.5 above evaluates the heat generation. The first term is the Joule heating and the second the Thomson effect. Whether heat is absorbed or generated by the Thomson effect is dependent on the relative direction of the temperature gradient and electric current. The magnitude of the Thomson effect is proportional to the Thomson coefficient, μ , electrical current, I , and the temperature gradient, dT/dx , along its length.

The Thomson effect results from the change of Seebeck coefficient of the material as a function of temperature. Along the conductor the Seebeck coefficient changes as it is a function of the temperature. As the electrical current travels through the conductor, the electrons must either absorb or reject heat energy due to a changing Seebeck coefficient. The Thomson coefficient is thus proportional to the change in Seebeck coefficient with temperature. Kelvin expressed his ideas in two equations called the Thomson relations:

$$\mu = T \frac{d\alpha}{dT} \quad 2.6$$

$$\pi = \alpha T \quad 2.7$$

2.3 Thermoelectric Generators

The power generated by a single thermocouple circuit is not large enough to be of much use considering the Seebeck coefficient of even the best metal pairings is of the order of millivolts per Kelvin. To create a device that outputs a useful amount of power many thermocouples are connected electrically in series, causing the driving EMFs to add together. They are also connected thermally in parallel between the same heat source and heat sink. These devices are referred to as thermoelectric generators or TEGs.

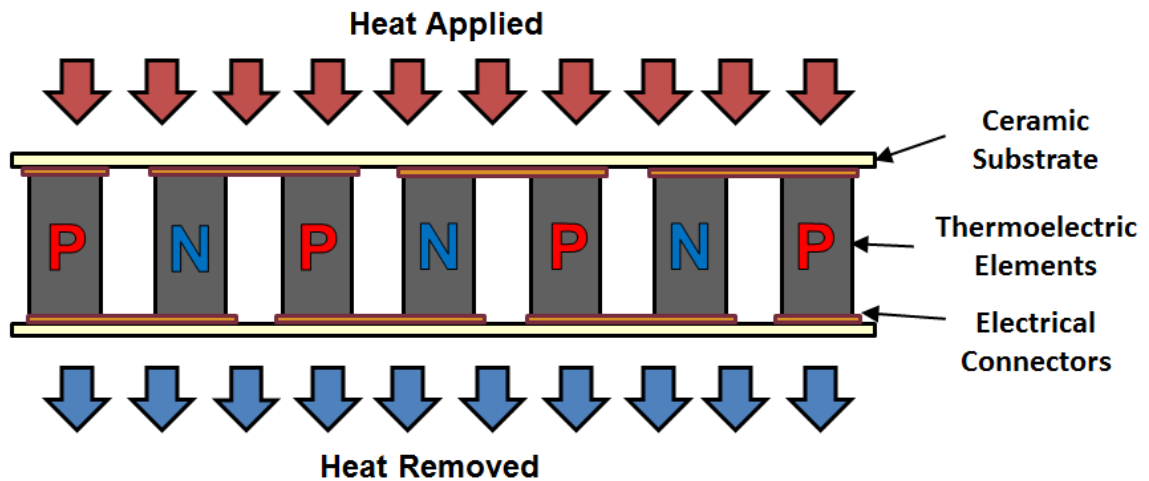


Figure 2.3 Basic schematic of a Thermoelectric Generator

Figure 2.3 above shows the basic schematic of a thermoelectric generator, a thermoelectric circuit specifically designed to give high output power. There are three main components to the typical thermoelectric generator:

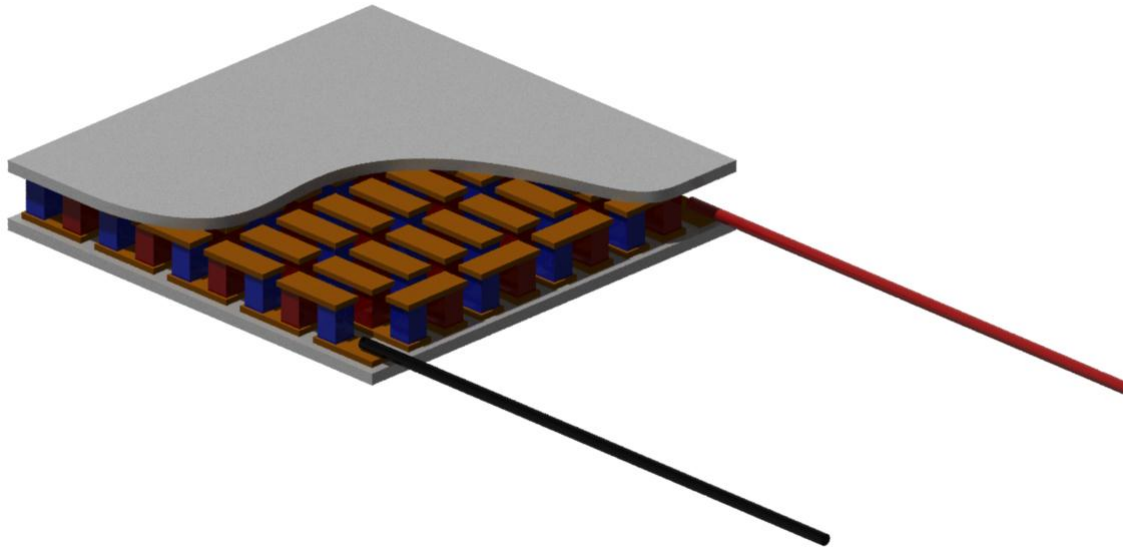


Figure 2.4 3D rendering of a typical design for a thermoelectric generator

1. The ceramic substrate: The device is held together by two ceramic substrates which sandwich the thermoelectric material. The substrate is ceramic to provide structural support and also electrically isolate the circuit from the heating and cooling surfaces.
2. The electrical connectors: The thermoelectric elements are not directly connected to each other but are electrically connected via metallic electrical connectors. Copper is generally used because of its high thermal and electrical conductivity but it has to be nickel coated to prevent diffusion of dopants between the semiconductors and the copper. The higher electrical conductivity of the electrical connectors results in less power generated by the thermoelectric generator being wasted internally as Joule heating.
3. The thermoelectric elements: The thermoelectric elements in a thermoelectric generator vary depending on the application. The main factors in the choice of material used are application temperature range and output conditions.

A typical thermoelectric generator can contain between 50-200 thermoelectric couples depending on the necessary output power conditions and can range greatly in size from a few square millimetres to 100 cm².

2.4 Materials

The effectiveness of a material for power generation via thermoelectrics is based on three material properties:

- The Seebeck coefficient α ; the higher the Seebeck coefficient, the higher the driving force for the electrons and thus the potential for higher power output.
- The thermal conductivity λ ; the lower the thermal conductivity of material, the less thermal energy is needed to generate a temperature difference between the joints in the thermoelectric couple.
- The electrical resistivity ρ ; the lower the electrical resistivity, the less energy of the system will be dissipated by generating internal heat.

These three material properties are used to indicate how well a material will perform in a thermoelectric application and they are frequently combined in the non-dimensional figure of merit, ZT , for comparison.

$$ZT = \frac{\alpha^2 T}{\lambda \rho} \quad 2.8$$

Before the emergence of semiconductors, the most suitable conductors for the use in thermoelectrics were metals which have a low figure of merit and are not capable of producing much power. Semiconductors are metals that have been doped with either excess electrons, resulting in an n-type semiconductor, or excess electron holes, resulting in a p-type semiconductor.

Semiconductors are extremely good thermoelectric materials because the doped impurities allow for easy excitation of the electrons and holes to the conduction band, while still having a thermal conductivity higher than metals.

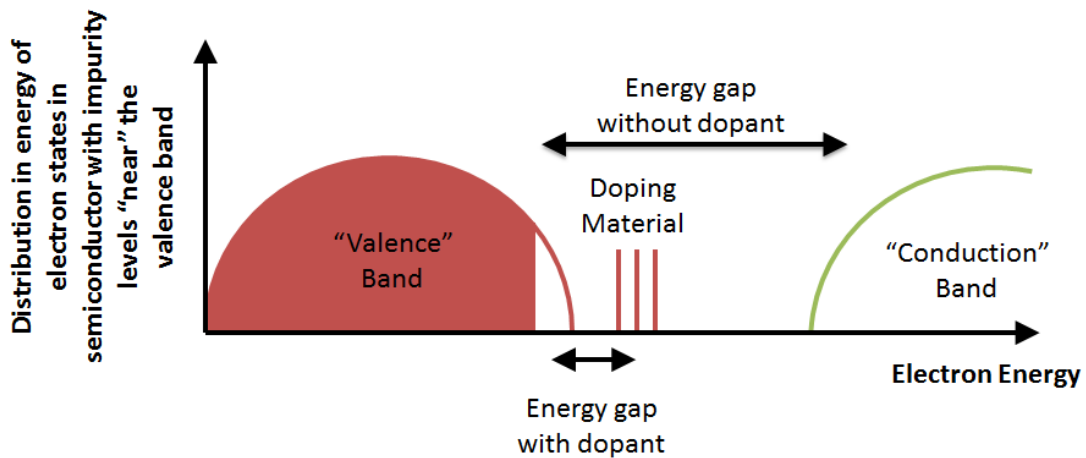


Figure 2.5 Sketch of occupied electron states in a p-type semiconductor [12]

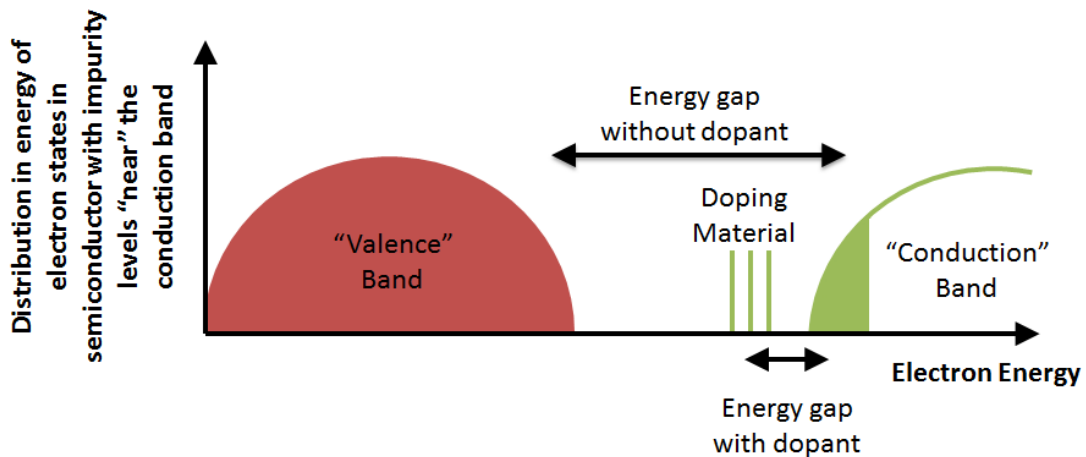


Figure 2.6 Sketch of occupied electron states in an n-type semiconductor[12]

In a thermoelectric circuit, holes will flow from hot to cold in p-type material and electrons will flow from hot to cold in n-type material. In a thermocouple circuit made of p and n type material the net flow of positive electron holes and negative electrons results in a higher current than with metals alone. The sketches Fig. 2.5 and Fig. 2.6 show how in

semiconductors less energy is required to create the conduction electrons as they only have to jump from the dopant to the conduction band and similarly less energy is required to create the conduction holes as they only have to jump from the dopants to the valence band.

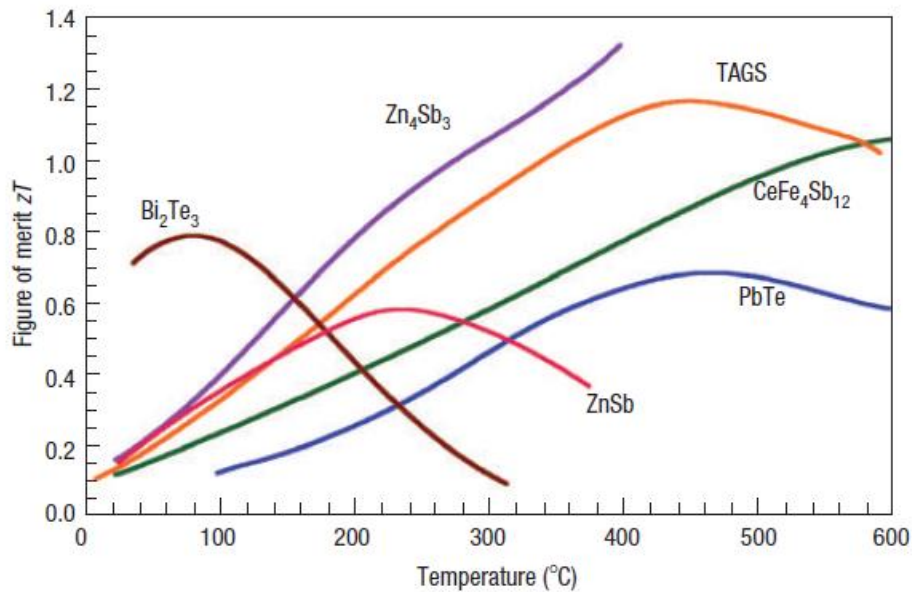


Figure 2.7 Figure of merit of various materials used for thermoelectric applications as a function of temperature [13]

As can be seen in Fig. 2.7, different thermoelectric materials have an optimal point at which they perform. For instance for low temperature range applications, Bismuth Telluride (Bi_2Te_3) performs well but is not as good as Lead Telluride (PbTe) at higher temperatures. Because of this high variation in thermoelectric properties as a function of temperature, a thermoelectric generator has to be designed with a specific temperature difference in mind to ensure the right material is chosen for optimum performance.

Once the material has been chosen, the geometry must be considered as the output characteristics of the TEG can be highly influenced by the geometry of the thermoelectric elements [14, 15].

2.5 Thermoelectric Equations

The following section outlines some of the fundamental models of thermoelectric generators as to power generation, optimum generating conditions and calculating efficiency of generators.

2.5.1 Power Generated

The power output of a thermoelectric generator is related to the heat flow through the generator. If the heat flow through the thermoelectric circuit is simplified down to a single dimension, the heat flow “into a” and “out of a” thermoelectric generator can be expressed by equations 2.9 and 2.10 respectively [16.]

$$Q_H = N\alpha_{CIRCUIT}T_H I + K(T_H - T_C) - \frac{I^2 R}{2} \quad 2.9$$

$$Q_C = N\alpha_{CIRCUIT}T_C I + K(T_H - T_C) + \frac{I^2 R}{2} \quad 2.10$$

In the above equations ‘K’ is an effective thermal conductivity of the thermoelectric generator which includes the ceramic substrates, the electrical connectors and the thermoelectric pellets. Similarly ‘R’ is the electrical resistance of the thermoelectric generator which is the sum of the electrical resistances of the electrical connectors and the thermoelectric material. The Seebeck coefficient of the circuit is for one thermocouple circuit and thus has to be multiplied by the number of thermocouples in the TEG, “N”. The first term is the thermoelectric phenomenon in the system, the second the conductive heat transfer and the third is the joule heating occurring in the circuit.

According to conservation of energy the power output of the generator converted from the heat flow through the TEG must result in a difference in the heat flowing in and out of the TEG i.e.:

$$P_{TEG} = Q_H - Q_C = N\alpha_{CIRCUIT}I(T_H - T_C) - I^2 R \quad 2.11$$

The output power of the generator is clearly independent of the conductivity of the TEG as a whole which was present in both equations in 2.9 and 2.10. However as mentioned above the temperature difference depends heavily on the thermal conductivity of the components individually as that determines the temperature difference across the thermoelectric elements. This circular path can lead to difficulty in modelling TEGs.

2.5.2 Matched Resistance and Max Power

The Seebeck effect generates a voltage difference across the circuit and the current produced is a function of that voltage difference and the resistance of the whole circuit as determined by Ohm's law which can be written as follows:

$$I = \frac{V}{R} = \frac{N\alpha_{CIRCUIT}(T_H - T_C)}{R_{TEG} + R_{LOAD}} \quad 2.12$$

In the above equation the electrical resistances of the circuit have been split up to the internal resistance of the generator, R_{TEG} , and the resistance of the load that is being powered, R_{LOAD} . As stated above the generator follows Ohm's law where the voltage and current produced are linearly related to each other by the internal resistance. Given this fact, the power output can be rewritten from equation 2.11 as:

$$P_{TEG} = \frac{(N\alpha_{CIRCUIT})^2(T_H - T_C)^2}{R_{TEG} + R_{LOAD}} - \left[\frac{N\alpha_{CIRCUIT}(T_H - T_C)}{R_{TEG} + R_{LOAD}} \right]^2 R_{TEG} \quad 2.13$$

For a given temperature difference and a given TEG the power output is only a function of the load resistance applied to the circuit. Differentiating the power equation to find the maximum, we find that the maximum power is achieved when the load applied to the TEG is equal to the resistance of the TEG. This condition is referred to as "matched" resistance when the two component resistances are matched and the maximum power possible by the TEG is achieved.

$$P_{MAX} = \frac{(N\alpha_{CIRCUIT})^2(T_H - T_C)^2}{4 \times R_{TEG}} \quad 2.14$$

2.5.3 Efficiency

The efficiency of a thermoelectric generator is judged by the amount of electrical power that is converted from thermal energy. The conversion efficiency then is calculated from the ratio of output power to heat flow into the system:

$$\eta_{TEG} = \frac{P_{TEG}}{Q_H} \quad 2.15$$

Given the Seebeck coefficients of the materials used in thermoelectric generators today, a typical value for the conversion efficiency of a typical commercial TEG is between 3%-5% efficient.

2.6 Applications

Given that the conversion efficiency of thermoelectric generators is still quite low for effective use they must be used in the correct application. One of the more ideal uses for thermoelectrics is the harvesting of energy from waste heat produced by various industrial and commercial processes. There are a few ways of recouping the energy from this low grade heat but thermoelectrics present one of the most practical solutions.

Devices that are built for the generation of power by converting waste heat using thermoelectrics are complex devices. Depending on the magnitude of the desired output power they can contain up to hundreds of individual thermoelectric generators [17]. Considering the vast opportunities for waste heat recovery from many different processes, there is no one device that will satisfy all possible situations. The scenarios in which thermoelectric generators can be used can vary considerably with temperature range, heat flow, space and geometry, material (for highly regulated environments such as the food industry), electrical load and many other possible constraints that have to be imposed on the device so as not to negatively affect the original process.

The varied constraints create a situation for which there exists no “one size fits all” device. Designing devices for harvesting the energy from heat flows with such variable

parameters, knowledge of how a thermoelectric generator performs under a wide range of thermal and electrical conditions must be known.

2.7 A Review of TEG Power Generation Modelling Methodologies

The most practical method of designing a thermoelectric system would of course be modelling the performance of the device analytically considering that the physics of thermoelectrics is well known. Modelling thermoelectric processes, however, is not as simple as the above equations would indicate. The highly non-linear nature of the many material properties involved in thermoelectrics as a function of temperature and the steep temperature gradients they experience make modelling thermoelectric generation a difficult endeavour.

There are several assumptions that are frequently made to make modelling of the power generated from a thermoelectric generator much simpler.

- Averaging the thermal and thermoelectric properties over the range of temperatures for each material.
- Ignoring the effect of the Thomson effect and/or the Joule heating inside the generator
- Assuming the thermal and electrical conditions experienced by the generator are optimal and constant.

Researchers have been tackling the problem in both ways: simplifying the system or trying to capture all thermoelectric phenomena occurring in the generator. However to date, no one model has provided a workable solution for both the power generation and heat transfer of a thermoelectric generator.

The first assumption that the properties are all constant or relatively constant is one of the most common assumptions. This simplification was investigated in 2012 by Ahsika [18] who presented a paper on measuring the time constant of a thermoelectric generator using his proposed testing apparatus the TEPAS [19]. In this paper Ahsika states how

thermoelectric properties can be up to 30% off if the material properties of the generator are considered constant as a function of the temperature gradient across them and current flow through them.

In Min's paper in 2001[20] he proposed a new method of calculating the figure of merit of a thermoelectric generator. Min reports on the two most common current methods of measuring these internal parameters: the Harman technique and the direct measurement of the properties separately. According to the paper, the first method, using the Harman technique to calculate the figure of merit can have a 20% error. The second method, measuring the parameters (Seebeck, electrical and thermal conductivities) directly leads to a 10% error in the calculation of figure of merit. Min's novel method, though, yields better results as it considers the parameters in the figure of merit as both functions of temperature and current. The new method calculates the figure of merit using the temperature differences at the open circuit condition and short circuit condition given a fixed heat flow. However it does not account for the change in Seebeck coefficient as a function of temperature at different load conditions.

Neglecting the Thomson effect has been proven to be impractical by Lazard in her 2009 paper [21]. The paper focuses mainly on the design of thermoelectric generators for large temperature differences by utilizing multiple materials in one pellet. As part of that analysis, Lazard analyses the heat transfer through a single pellet with and without the Thomson effect. The results of the analysis show that over a total temperature difference of 30°C across the element, the temperature at a point can differ between the two simulations by as much as 4°C. This difference occurs over a temperature difference of 30°C but in most conventional power generation systems the temperature difference would be much larger, 100°C to 800°C, resulting in a larger current and Thomson effect.

Yu [22] outlined his method of design for generation devices with multiple TEGs in a parallel plate heat exchanger. Yu tackled the problem very well balancing the heat transfer of the hot and cold supply to the TEG with power output. However when his model came to trying to predict the electrical part of the thermoelectric generator it was

very simplistic using averaged values for the thermoelectric properties of the material. Another major assumption was that the device was running at the matched load condition for all situations considered without looking into how a change in load resistance might affect the system in either the thermal or electrical aspects.

Of the papers that try to capture all the complexity of thermoelectric generation, the heat transfer and the thermoelectric phenomenon Chen's paper in 2011 [23] deals best with the interaction of the two phenomena. Chen's paper utilizes commercial computational fluid dynamics software and the user defined functions included to model a thermoelectric generator. Chen comments on previous studies making use of commercially available software criticizing how they only capture the heat transfer aspect of the generator ignoring the specific thermoelectric phenomena. However Chen's model fails to predict the output of the generator. His results are adapted and presented in figure 2.8.

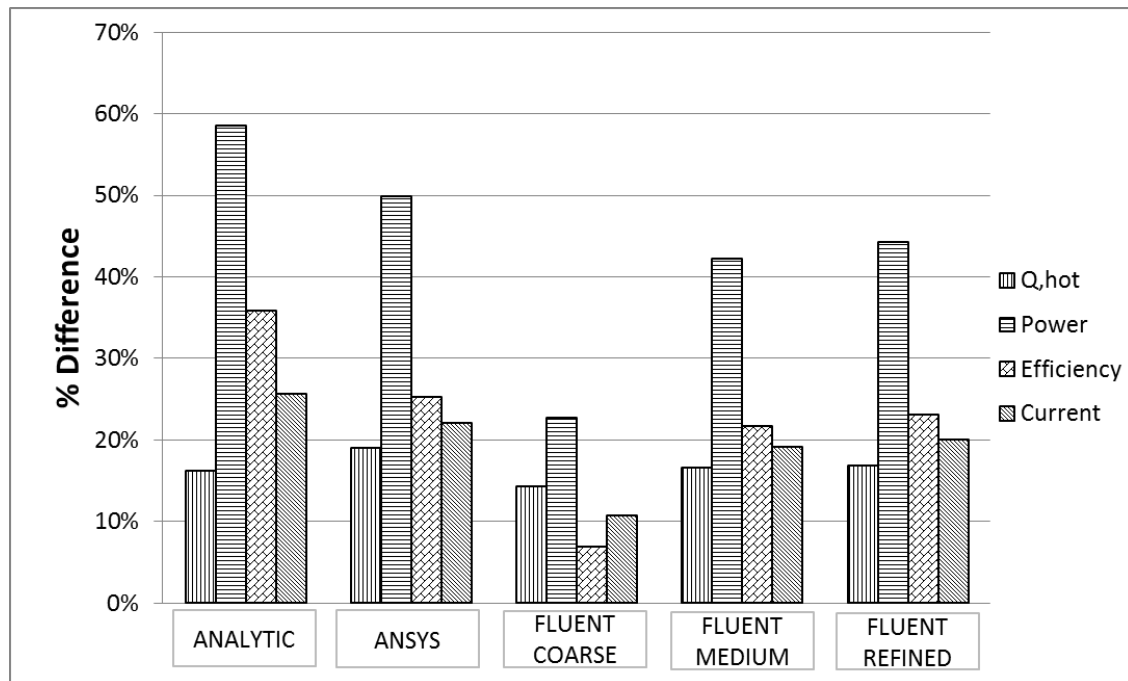


Figure 2.8 Chen [23] %Difference between Chen's commercial software models and measurements performed to qualify them. The five models used are a common simplified analytical model, a model used in the ANSYS F.E.A. software and three different Fluent C.F.D. models of differing mesh density: Coarse, Medium and Refined.

From Figure 2.8 it can be seen that Chen's model despite its complexity fails to accurately predict the output of the generators with an average difference of 43.5% and a minimum of 22.7% error in the power output of the generator as predicted by the model to that of a generator experimentally measured for comparison.

Modelling also proves difficult in accounting for variability in the thermoelectric generator performance. The manufacturing processes for common commercial generators are difficult to standardize and as thermoelectric properties are so sensitive the power and thermal characteristics of the generator can vary significantly. Rosado [24] began addressing this variability in his paper on finite element modelling for thermoelectric modules. Rosado dealt with a number of issues in modelling thermoelectric generators including the change in performance with solder thickness and relative position of thermoelectric elements. According to the results presented the power of a thermoelectric module can vary by almost 10% due to solder thickness and up to 1.5% due to the positioning of the thermoelectric elements.

Table 2.1 provides a review of some of the many models that attempt to predict the performance of a thermoelectric generator. It lists the assumptions and simplifications that researchers are using in their models to make them easier or more robust. However none of these, nor has any single model, had such success to be universally accepted. None of the models are created to predict the electrical output and the corresponding thermal properties of a TEG either tending to focus on one or the other.

Table 2.1 Review of assumptions and methodologies used in TEG performance models

	Thermoelectric Material Properties	Thomson Effect	Electrical Load	TEG Thermal Conductivity	TEG Electrical Conductivity	Heat Transfer Hot Side	Heat Transfer Cold Side
Hsiao 2010 [25]	Constant, evaluated from open circuit test.	Ignored	Full range of electrical resistances considered	Evaluated from $\frac{T_H - T_C}{Q_H - Q_C}$	Evaluated experimentally	Heat Transfer fin correlations	Heat Transfer channel flow correlations
Xuan 2002 [26]	Constant values factored by thermal conductivity	Ignored	Reported only at specific current values	Effective Value including interfaces	Effective Value including interfaces	Specified temperatures	Specified temperatures
Yu 2007 [22]	Constant	Ignored	Matched load resistance only	Constant	Constant	Heat Transfer channel flow correlations	Heat Transfer channel flow correlations
Kumar 2013 [27]	Averaged between Th&Tc	Ignored	Matched load resistance only	Only considers pellets, uses averaged conductivity	Only considers pellets, uses averaged conductivity	Heat transfer fin correlations	Heat transfer fin correlations
Chen 2011 [24]	Dependant on temperature	Based on 3D variation of Seebeck combined with joule	Single load resistance reported 3.4Ω	Elements are a function of temperature, includes copper and ceramic	Elements are a function of temperature, includes copper connectors	Single value heat transfer coefficients	Single Value heat transfer coefficients
Sandoz-Rosado 2010 [24]	Constant	Averaged values put into a bulk heating term	Reported over a wide range of current values	Based on elements, factor used to include ceramic & connectors	Based on elements, factor used to account for connectors	Specified temperatures	Specified temperatures
Kim 2013 [28]	Constant experimentally evaluated for models	Ignored	Wide range of resistances reported	Constant experimentally evaluated for models	Constant experimentally evaluated for models	Specified temperatures	Specified temperatures

2.8 A Review of Experimental TEG Characterisation Methodologies

As explained in section 2.7 the modelling of thermoelectric generators proves extremely difficult, either giving inaccurate results when simplifying assumptions of the material properties are made or requiring too many inputs when including all the thermoelectric effects. This leaves the most viable option to determine the characteristics of a thermoelectric generator as experimental. Experimental testing will also allow for the variance of the parameters introduced by material variability of manufacturing processes to be quantified and will capture all the real physics of the system. However a comprehensive repeatable test method needs to be established.

To experimentally capture the thermal and electrical characteristics of a thermoelectric generator there are certain parameters that are necessary to measure:

- Heat flowing in to the thermoelectric generator.
- Heat flowing out of the thermoelectric generator.
- Temperature on the hot side of the thermoelectric generator.
- Temperature on the cold side of the thermoelectric generator.
- Output voltage of the thermoelectric generator.
- Output current of the thermoelectric generator.

One such testing apparatus is that of Carmo [29] presented in his paper on the characterization of thermoelectric generators by their load dependent behaviour. The testing apparatus used by Carmo for these experiments was an electric hot plate to supply the heat and an aluminium heat sink under forced convection to extract it. The testing procedure, using LabView to control the power to the hot plate and fan thereby controlling the temperatures on the generator worked quite well but the precision was hampered by the capabilities of the apparatus he employed. The problem with Carmo's facility is that no energy balance could be accurately established given the large losses in the system.



Figure 2.9 Experimental Facility used to characterize the performance of thermoelectric generators Carmo[29]

Considering the inaccuracies of many facilities that are used to characterize the performance of thermoelectric generators, many papers have been written proposing testing facilities that be adopted as a standard method for reporting characterization data. One such paper was released in 2012 by Ahiska [19] detailing the T.E.P.A.S. (Thermoelectric Performance Analysis System). His facility is fully automated making for a high amount of control over the testing parameters and making for extreme ease of use. However it fails to address some fundamental issues that need to be taken into account when dealing with thermoelectric generators.

- The temperatures of the hot and cold sides of thermoelectric generators are measured directly using thermocouples embedded into copper plates directly in the heat flow path to and from the generator. This practice is avoided in general as the thermocouple can lead to a non-uniform temperature at the generator surfaces which leads to poor performance.
- The heater providing heat to the system is sandwiched by two thermoelectric generators to minimize its losses. The knowledge from the heat flow through the

TEGs can only be known if both TEGs are of exactly equal properties when in actual fact the thermal properties of TEGs can vary quite significantly.

- The thermal conductivity of a thermoelectric generator can also change in terms of the load resistance applied to the generator and thus both TEGs need to be subject to the same electrical load conditions for the heat flow to be attributed to each TEG correctly.
- The pressure on the TEG is not accounted for in the set up as can be seen in the figure 2.10. This leaves Ahsika unable to quantify the thermal contact resistance.
- The paper fails to address whether or not the power from both TEGs were measured or was it a single TEG.
- The system is not very well insulated from the ambient and as such the reported values for the heat flow from the TEG measured from the change in water temperature cannot be totally attributed to the heat from the heaters as it will be subject to the ambient temperatures.

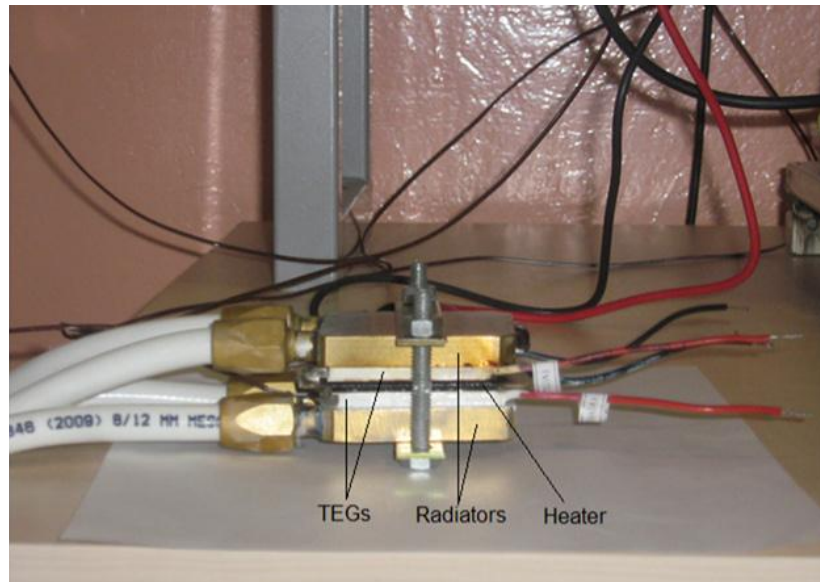


Figure 2.10 Image of Ahsika's T.E.P.A.S. facility.

There is no testing facility yet put forward that accurately meets the needs of designers for predicting the performance, both thermally and electrically, of thermoelectric

generators. Some of the facilities that have been proposed as benchmark devices for the purpose in characterizing TEG performance have been summarised in Table 2.2. None of the testing facilities have all the advantages of that used for this thesis which are described in full in section 3. The benefits of the different testing methods are reviewed in the experimental facility of this thesis.

Table 2.2 Review of a selection of TEG characterization facilities

	Capability of Measurements	Heat source measurement	Heat sink measurements	Hot and cold side temperatures measurement	Pressure loading measurement	Vacuum
Rauscher 2006 [30]	$T_h < 275$	Electric Heater	No	Thermopiles attached to the surfaces	Yes	No
Takazawa et al. 2006 [31]	$\Delta T_{max} = 57^\circ\text{C}$	No	Temperature gradient through copper block	Measuring the temperature of an aluminium nitride plate attached to each side of the module	No	Yes
Sandoz-Rosado & Stevens 2009 [32]	$Q_{max} = 1.3\text{kW}$	Not available	Not available	Not available	Yes	No
Ahiska 2012 [19]	$Q_{max} = 500\text{W}$	Electric Heater	Temperature change in cooling fluid	Thermocouples embedded in copper plates either side of TEG	No	No
Carmo 2011 [29]	Not available	No	No	Thermistors embedded in copper plates either side of TEG	No	No
Rodriguez et al 2009 [33]	50W max	Temperature gradient through material of known thermal conductivity	Temperature gradient through material of known thermal conductivity	Thermopiles attached to the surfaces	No	No
Tanji et al 1999 [34]	$\Delta T_{max} = 227^\circ\text{C}$	Temperature gradient through nickel block	Temperature gradient through nickel block	Extrapolation of thermal gradient through nickel blocks	Yes	No
Current Facility	$Q_{max} = 450\text{W}$	Temperature gradient through copper block	Temperature gradient through copper block	Extrapolation of thermal gradient through copper blocks	Yes	Yes

3 Experimental Facility

The basic operation concept of a thermoelectric generator, a TEG, is thermal energy is transferred from an external heat source to the hot surface of the TEG module and extracted at the cold surface into an external heat sink. This establishes a temperature difference across the TEG and an electrical power output can then be observed. In the design of facilities to characterize the performance of thermoelectric generators there are certain design features that are necessary. The most fundamental of those being: Isothermal surfaces at the TEG interface, one dimensional heat flow to and from the TEG, minimal heat losses from the facility, accurate determination of the interface temperatures, fine resolution of thermal energy supplied, minimal contact resistance and a variable electrical load to be applied to the TEG.

3.1 The Experimental Facility

The primary purpose of the thermoelectric module test apparatus, TEM Tester, was to supply a known quantity of thermal energy to a TEG module at a specified temperature difference to measure the performance / electrical power generated. Figure 3.1 shows a schematic of the testing facility which is comprised of four main parts: the TEG testing area, the heat supply, the heat extraction loop and the electrical measurement apparatus. The testing area is placed inside a vacuum chamber indicated in the figure as a dashed line. This consists of the copper blocks used to direct the heat flow, the TEG being tested and the heat delivery and removal methods.

To accurately measure the thermal energy across the TEG module it is secured between two copper blocks of similar cross sectional area to the TEG as shown in figure 3.2. Heat is supplied to the system by resistance heaters that are embedded into the bottom copper block. Heat flows up this “hot” copper block through the TEG and then directed from the TEG through a “cold” copper block that has fins machined on the opposite end of the TEG. Heat is extracted from the system via chilled water passing over these fins.

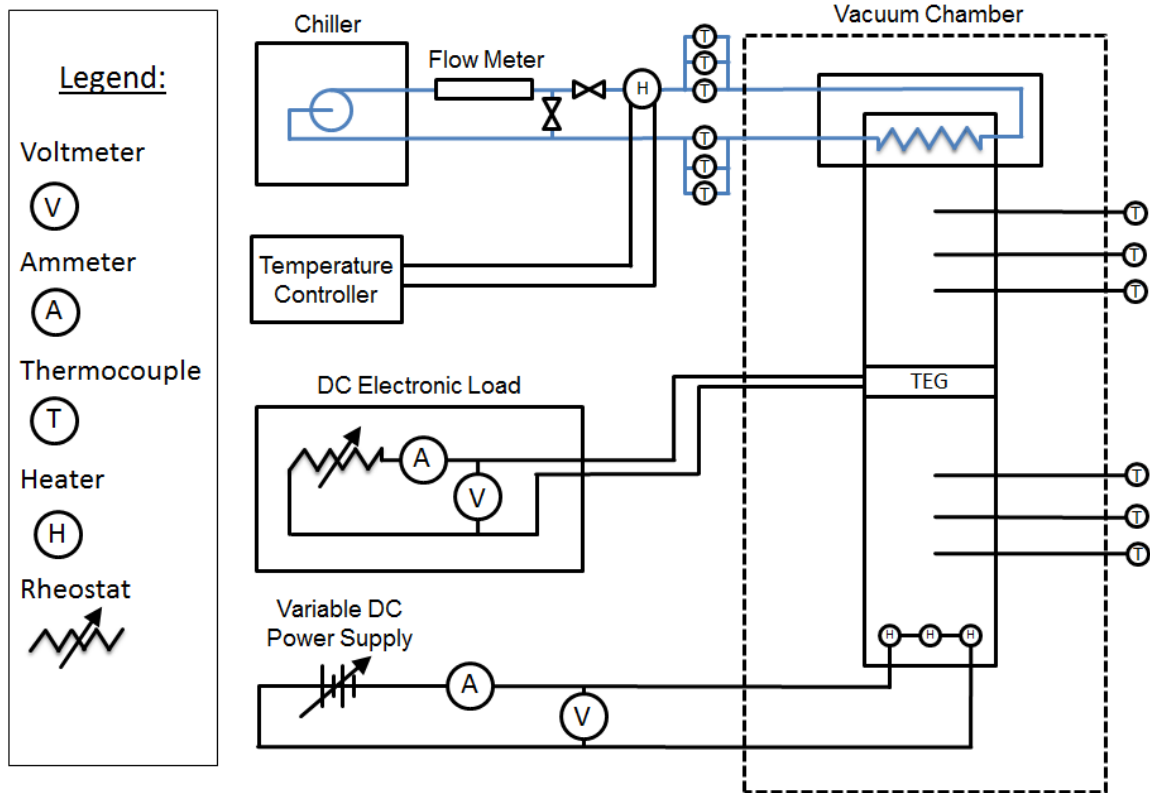


Figure 3.1 Schematic representation of the TEMTester

The heat delivery method is the loop at the bottom of the schematic which consists of resistance heaters being powered by a variable dc power supply with the input power measured using a voltmeter and ammeter. The heat extraction system is the top loop of the schematic and deals with the flow of water into the testing area. The water temperature is controlled using the chiller and in-line heater in conjunction and is delivered to the testing system at a certain flow rate by the chiller’s internal pump controlled via throttling valves. The thermocouples located on the loop either side of the testing area measure the temperature of the water as it enters and exits while the flow rate is measured as it leaves the chiller with a flow meter. The DC Electronic Load is essentially a programmable resistor used to apply a variable electrical load to the system and measure the power generated by the thermoelectric generator using a voltmeter and ammeter.

The testing area of the apparatus is placed inside a vacuumed chamber which minimizes heat losses to the surroundings serving two functions: it helps to ensure the heat delivered to and removed from the TEG is one dimensional as it removes other possible paths for the heat to flow and secondly it also ensures that the energy balance for the system is as accurate as possible.

Thermoelectrics as a subject is dependent on the temperatures at either junction of the thermocouple and the difference between them. To accurately capture this parameter, the temperature gradient through the copper blocks is measured using thermocouples placed at axial locations along the length of the block as specified in figure 3.2. The measurement of these temperatures and their positions relative to the surface in contact with the TEG the temperature at this surface can be extrapolated. The reason that this method was chosen over directly measuring the temperature with a sensor is that the presence of a sensor would adversely affect the one dimensional heat flow.

The “hot” copper block is supported by a ceramic of a low thermal conductivity (0.088W/mK) to reduce the heat flowing vertically downwards while providing support. To prevent heat flowing from the side surfaces of the copper blocks the whole system is placed inside a vacuum chamber preventing convection heat transfer.

The high conductivity of copper and the one dimensional heat flow combined created an isothermal surface on either side of the TEG. It is possible that if one of the thermoelectric couples experienced a lower temperature difference it would compromise the performance of the TEG as a whole.

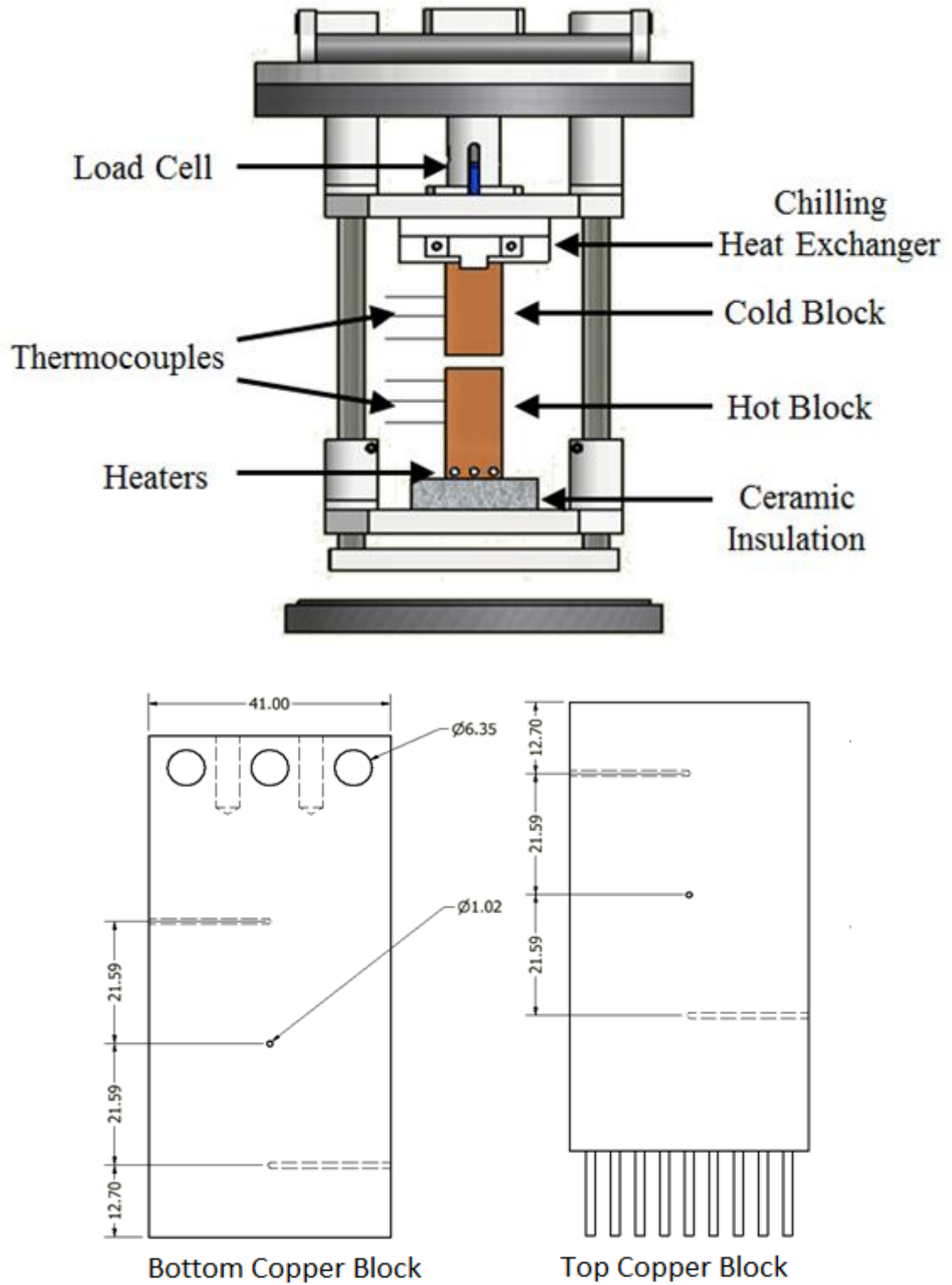


Figure 3.2 Simplified sketch of the TEMTester. Specified dimensions in mm.

3.2 The Energy Balance

An accurate energy balance is needed for the testing of thermoelectric generators in order to quantify the conversion efficiency of the TEG. An accurate energy balance also provides a check on the quality of the one dimensional heat flow as all losses in the system cause deviations from the path of one dimensional heat transfer. The heat flowing through the system is calculated at four points through the TEMTester to accurately track heat flow and losses.

3.2.1. $Q_{HEATERS}$

The heat energy enters the system via three 100W cartridge heaters (Omega CSH-101100/120) and is referred to as $Q_{HEATERS}$. This allows for an estimation of the heat supplied to the system by measuring the current and voltage to the heaters.

$$Q_{Heaters} = V_{Heaters} \times I_{Heaters} \quad 3.1$$

The power is supplied to the heaters using a HP 6655A Power Supply, chosen for use with the TEMTester because of its high resolution for power output (0.0003W). This resolution allows for precise control of the heat flowing through the generator which is essential for controlling the temperature differences across the TEG. As the power supply provides a fine resolution of power output, it was necessary that the small variations could be accurately measured. The power input to the system was measured using an Agilent U 1253B Multimeter (accuracy of 0.03% of the reading + 5 LSD) and a BK 2831D Multimeter (accuracy of 1.0% of the reading + 10 LSD) to measure the voltage across and current through the heaters respectively.

3.2.2. Q_{HOT}

The heaters supplying the heat are embedded in a copper block with the dimensions 41mm x 41mm to match the TEG dimensions (40mm x 40mm) with allowance for tolerances. The heat flow through the copper is calculated using three thermocouples inserted into the centre of the block positioned along its length as described in Fig. 3.2. This heat flow is referred to as Q_{HOT} .

$$Q_{HOT} = k_{C110} \times A \times \left(\frac{dT}{dx}\right)_{HOT} \quad 3.2$$

Copper C110 was chosen as the material for the blocks as its conductivity is well known as a function of temperature allowing for the calculation to be as accurate as possible with the large range of temperatures experienced of the system. The length of the block and the spacing of the thermocouples were determined to provide a measurable temperature difference within the expected error of the thermocouples.

3.2.3. Q_{COLD}

The heat flow from the TEG through the copper block is one dimensional due to the vacuum in the same manner as the “hot” copper block. This heat flow is calculated in the same manner as that of the block supplying the heat.

$$Q_{COLD} = k_{C110} \times A \times \left(\frac{dT}{dx}\right)_{COLD} \quad 3.3$$

3.2.4. Q_{WATER}

The thermal energy not converted to electrical energy is extracted via a water chilling loop. Fins are machined in the copper block in the surface opposite that of the TEG. Water flows across these fins absorbing the heat then flows from the vacuum chamber to a chiller that removes the heat and returns the now chilled water back to the copper block in a continuous cycle.

The temperature of the water entering the vacuum chamber is measured using three thermocouples. Two plastic blocks were manufactured specifically to measure the water temperatures. The blocks separate the flow into three individual channels to mix the flow eliminating any thermal gradient effect on the measurement. The temperatures of all three channels are measured individually before all the flows recombine and exit the block. The channel temperatures can be averaged increasing the accuracy of the temperature measurements. The heat rejected from the system, referred to as Q_{WATER} , is calculated using the formula:

$$Q_{WATER} = \dot{m}C_P(\bar{T}_{W,I} - \bar{T}_{W,O}) \quad 3.4$$

Two different chillers were used for the testing performed: A high capacity chiller, the Lytron RC045 and a low capacity chiller, the Lytron RC011. The water flow rate was measured using either an Exact Flow Dual Rotor Turbine Flow meter connected to an Omron K3NR rate meter, for the low capacity chiller, or the Proline Promass 80E, a Coriolis mass flow meter made by Endress & Hauser, for the high capacity chiller.

The inlet temperature to the system was limited by the chillers which had a maximum output temperature of 35°C. To overcome that limit on the cooling loop an inline heater was installed allowing for the water temperature and thus the cold side temperature of the TEG to be increased to 80°C.

3.2.5 Electrical Energy

To fully characterize a TEG, it must be tested over a range of temperature conditions and electrical conditions which will generate different thermal properties and electrical outputs. The variable electrical conditions were achieved using a BK 8500 Electronic DC Load as a load resistance across the TEG. The DC Load is a programmable load that allows for the power coming from a generator to be limited and controlled by various parameters (Voltage, Current, Resistance and Watts) while mimicking an electronic load.

As this energy is converted to electrical from thermal via the thermoelectric generator to account for the balance of energy of the system the electrical energy must be quantified. The DC Load reported the current through and voltage across the simulated electronic load allowing for the calculation of all the electronic properties and magnitudes of the power produced by the TEG.

3.2.6 Energy Balance

Figures 3.3 and 3.4 show the energy flowing through the system as a function of the heat input to the system via the heaters. There is a large drop between the heat input to the system and the heat flowing through the hot and cold blocks up to 33% for the TEG1 12610-5.1 and 23% for the TEG1B 12610-5.1. This large drop between the heaters and

the heat flowing through the hot blocks is due to losses in the system that could not be removed. The two most likely reasons for losses in our system are conduction through a path other than through the copper blocks or radiation from the copper blocks to the vacuum tank. A simple calculation for the magnitude of the radiation showed that at most it could account for 2.75W or 13.5% of the losses between the heaters and the heat through the hot block. Figures 3.3 and 3.4 show the energy balance of the TEMTester for all testing reported in this thesis. The large drop between the QHEATERS and QHOT is easily seen. The following figures of 3.5 and 3.6 show the comparison of both thermal and electrical energy going into the TEG and leaving the TEG.

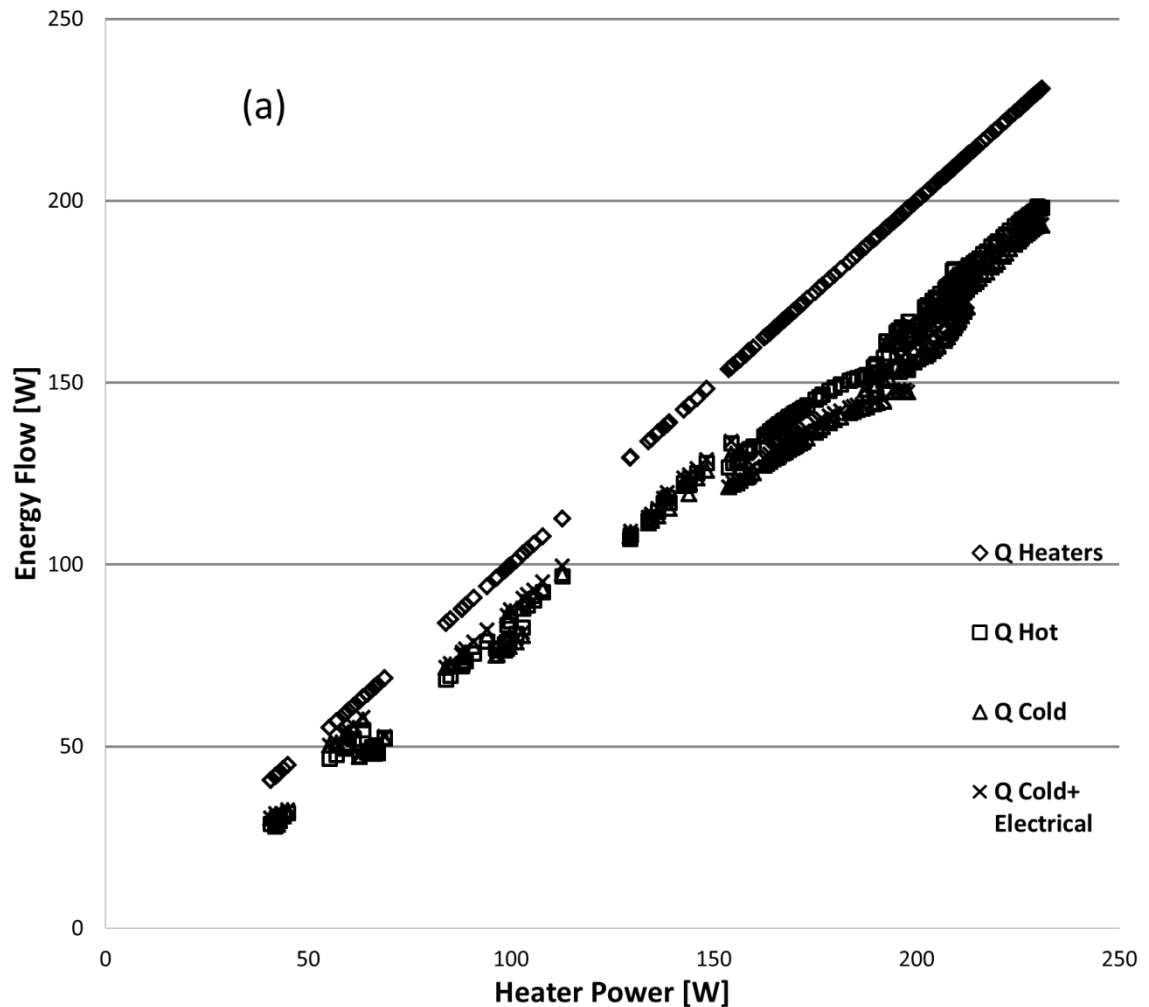


Figure 3.3 Energy balance for the experiments performed on the TEG1 12610-5.1.

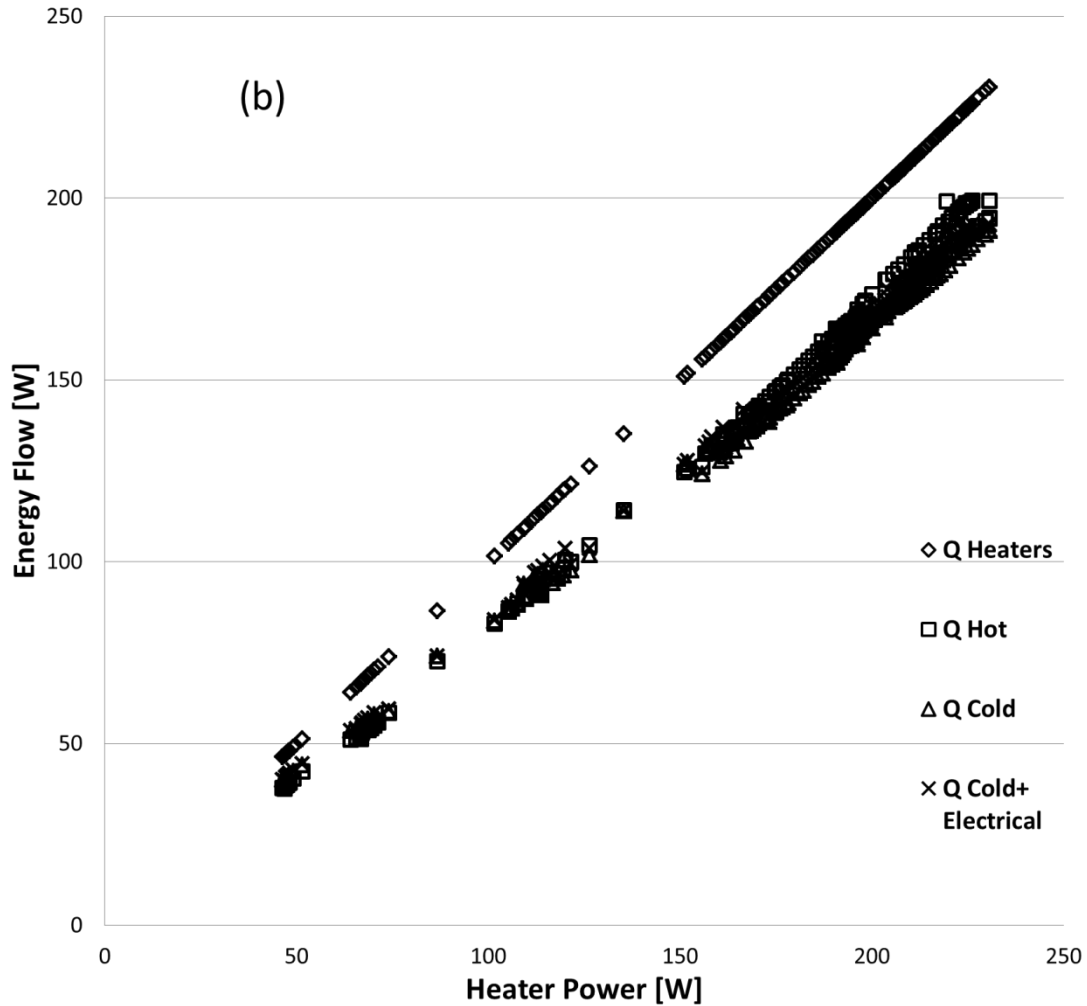


Figure 3.4 Energy balance for the experiments performed on the TEG1B 12610-5.1.

The comparison between the heat flowing into the TEG and the heat and electricity flowing out of the TEG are presented in Fig. 3.5 and 3.6. The average percentage difference between the energy in and out of a TEG is 2.85% for TEG1 and 2.23% for TEG1B with a maximum difference of 7.66% and 6.14% respectively. The 95% confidence interval for this data is defined as twice the standard deviation which is 3.06% for experiments on the TEG1 and 2.61% on the TEG1B encapsulating 95% of the data in $\pm 6.12\%$ and $\pm 5.22\%$.

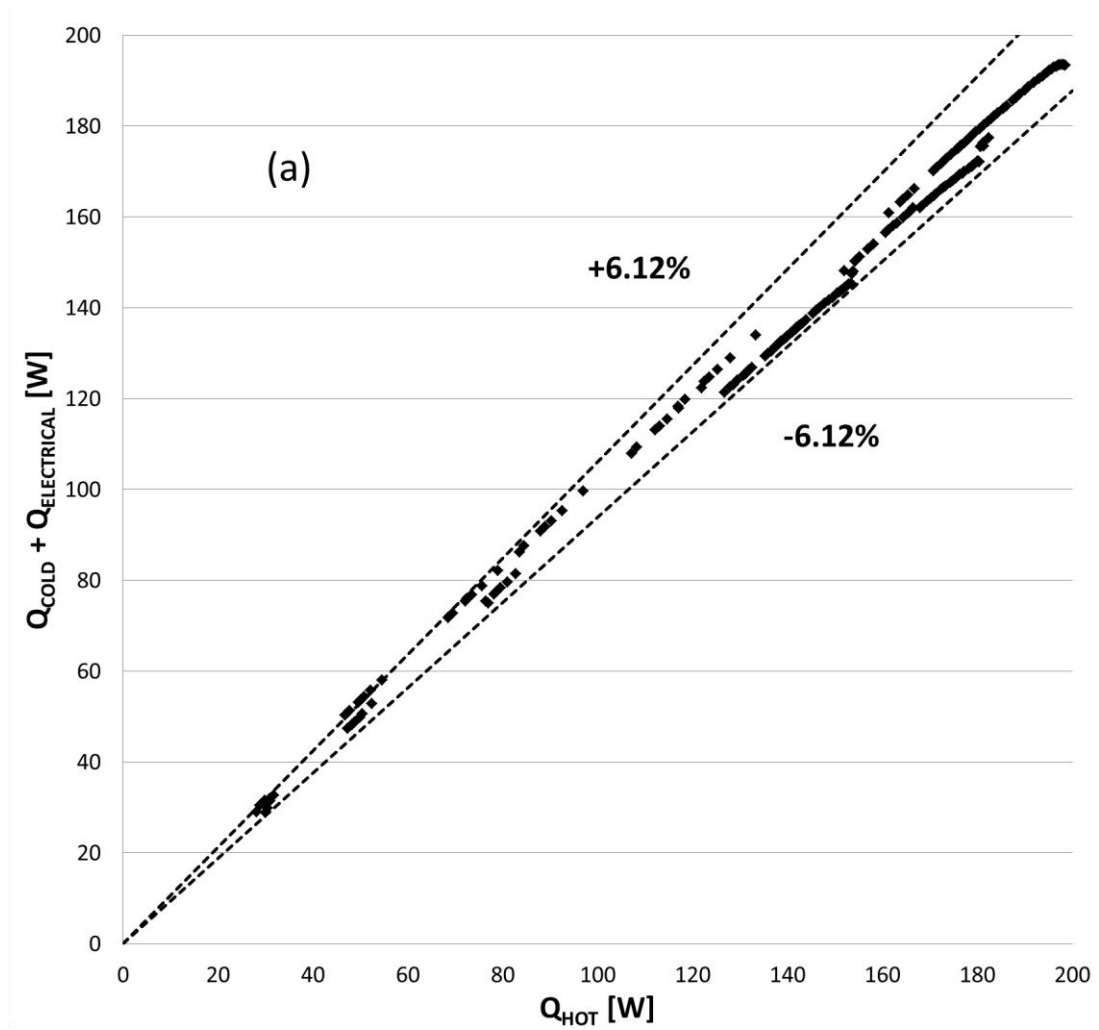


Figure 3.5 Energy into TEG (Q_{HOT}) vs energy out of the TEG (Q_{COLD} and $Q_{ELECTRICAL}$) with a 95% confidence envelope of 6.115%

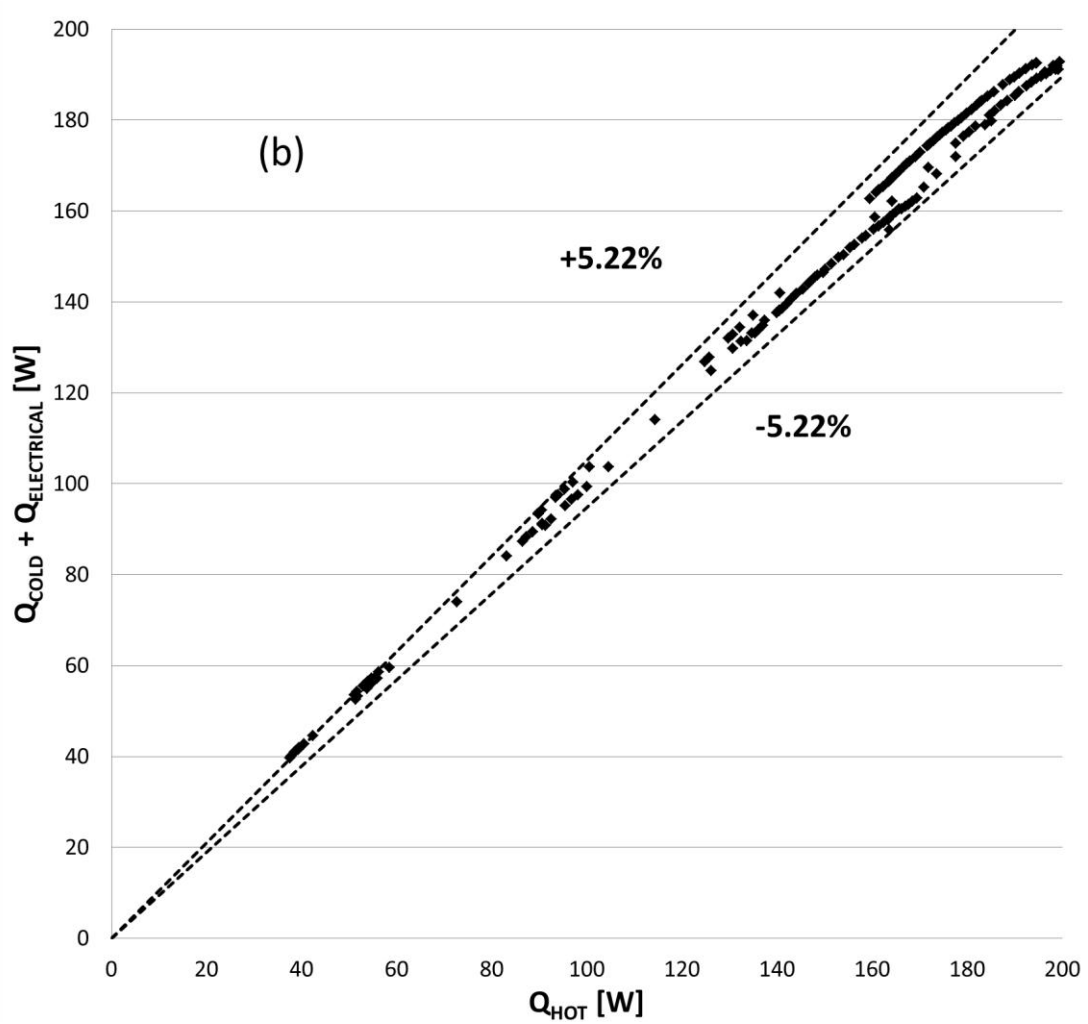


Figure 3.6 Energy into TEG (Q_{HOT}) vs energy out of the TEG (Q_{COLD} and $Q_{ELECTRICAL}$) with a 95% confidence envelope of 5.216%

3.3 Qualification

Validation of the capability of the TEMTester to measure the thermal conductivity of a material, a sample of known thermal conductivity was tested. The material used was MACOR machinable glass ceramic fabricated by Corning and compared against material properties provided by Corning. The comparison in Fig. 3.7 shows the thermal conductivity measured for two samples of different thicknesses, 1/8" and 1/4". Two samples were used for the qualification in order to allow for contact resistance to be

eliminated. The values obtained vary from 1.275 to 1.315W/mK which agrees well with Corning's data at the same average temperature which is 1.289 W/mK.

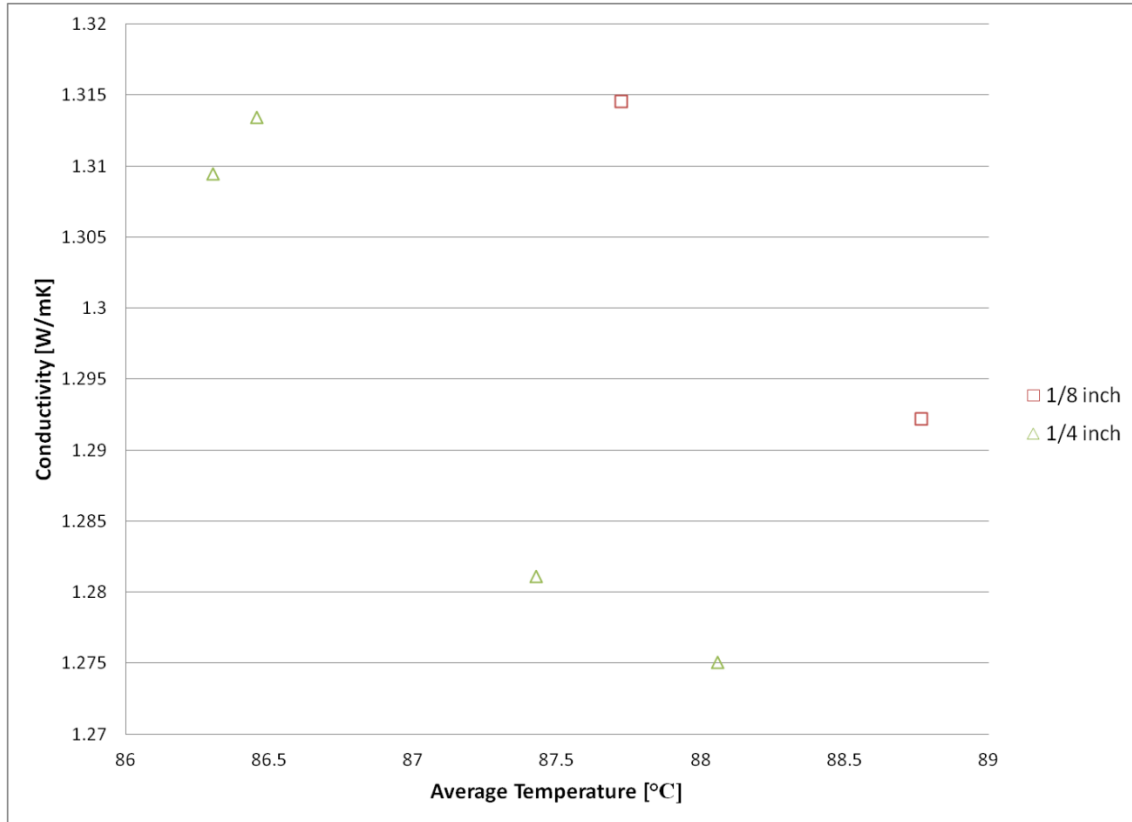
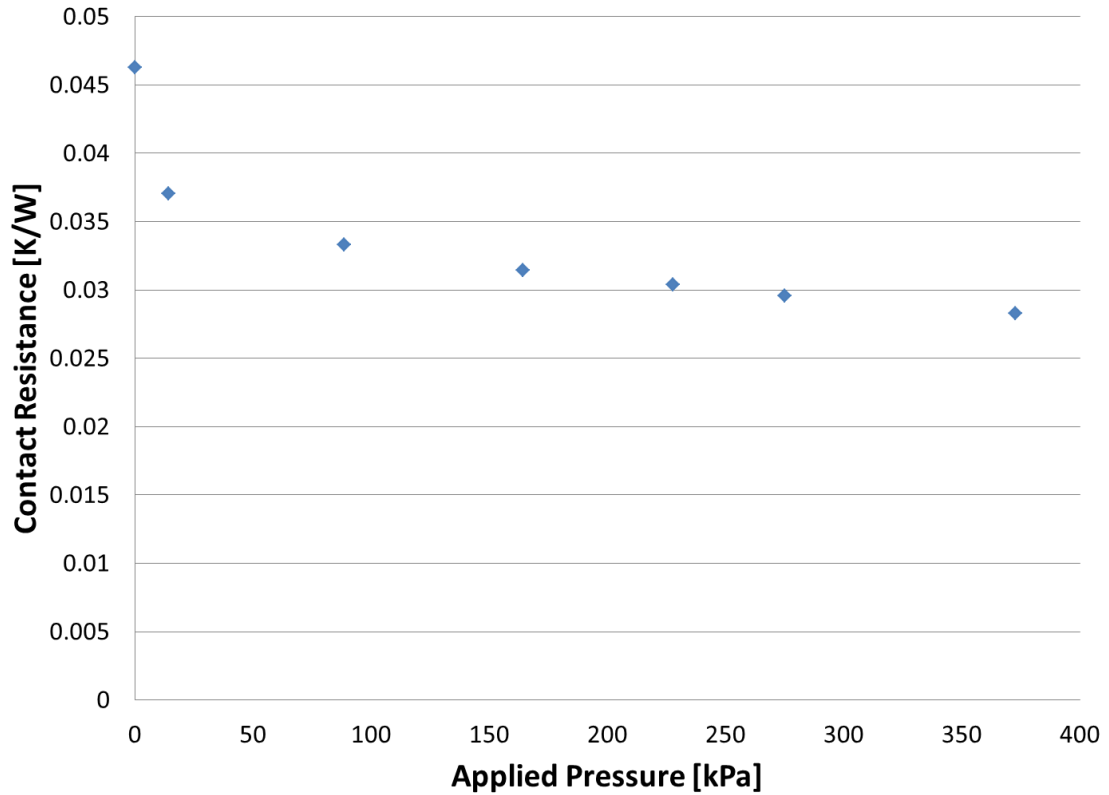


Figure 3.7 Thermal Conductivity results of MACOR machinable glass ceramic

It was found during testing that the contact resistance on the blocks was not significant enough to appreciably affect the results of the glass thermal conductivity tests. Fig. 3.8 shows an investigation into the relationship of thermal contact resistance and contact pressure for the TEMTester. A load cell measured the pressure applied to the TEG which was controlled by a pressure screw. The pressure screw could be manipulated outside of the vacuum chamber. With the increase in pressure on the system, the thermal resistance converges on a finite thermal contact resistance of 0.03 K/W. This value is approximately 3% of the typical thermal resistance for a TEG, which indicates that contact resistance is insignificant when measuring the thermal conductivity of a TEG using the TEMTester.



Repeatability tests were performed on the same TEG under the same conditions and the results were shown to be in agreement to 4% for power and 2% for both current and voltage.

Figure 3.8 Thermal contact resistances between the copper blocks with varying applied pressure.

3.4 Data Acquisition System

The data from the experiment is acquired using National Instruments cards:

- NI 9213 (16-Channel Thermocouple Input Module)
- NI 9201 (8-Ch, ± 10 V, 500 kS/s, 12-Bit Analogue Input Module)
- NI 9423 (8-Channel, Up to 30 V, 1 μ s, Sinking Digital Input Module)

These cards are all housed in a NI Compact DAQ 8-Slot USB Chassis which is connected via USB connection to a devoted Data Processing Computer. The computer uses LabVIEW software to display the measured data in real time. It is programmed to extrapolate the TEG surface temperatures and calculate the four values for the flow of heat through the system displaying them all in real time.

The heat balance was constantly reported via the four heat flow values allowing any fault in the system can be quickly identified. The extrapolated TEG surface temperatures were used to assess whether or not the system was thermally in steady state. For the purpose of the testing, steady state was defined as the TEG surface temperatures not fluctuating by more than 0.1°C over a period of 6 minutes. Once the system was at steady state the LabVIEW program recorded 120 samples of raw data to a text file over the next 6 minutes.

Table 3.1 Parameters measured in TEMTester apparatus

Symbol	Measured Data
$T_{HOT:1,2,3}$	Temperature in the Hot Block at position 1,2 and 3
$T_{COLD:1,2,3}$	Temperature in the Cold Block at position 1, 2 and 3
$x_{HOT:1,2,3}$	Position of a thermocouple in the Hot Block
$x_{COLD:1,2,3}$	Position of a thermocouple in the Cold Block
$T_{W,I: 1;2;3}$	Temperatures of the water entering the system
$T_{W,O: 1;2;3}$	Temperatures of the water exiting the system
V_{TEG}	Voltage difference generated by the TEG
I_{TEG}	Current generated by the TEG
V_{HEATER}	Voltage difference across the cartridge heaters
I_{HEATER}	Current flow through the cartridge heaters
Q	Volumetric flow rate of the water in the cooling loop
\dot{m}	Mass flow rate of the water in the cooling loop

3.5 Data Reduction

The first step in the data reduction process was applying the calibration curves to the raw data. The four heat balances were calculated using equations 3.1-3.4 and were used as the first check as to the validity of the data.

The voltage and current reported by the DC Load was used to calculate many characteristics of TEG. The most important of those is the power that the TEG produces which is simply the product of the Voltage and Current:

$$P_{TEG} = V_{TEG} \times I_{TEG} \quad 3.5$$

The resistance at which this power occurs at can also be calculated using the current and voltage values from the DC Load:

$$R_{TEG} = V_{TEG} \div I_{TEG} \quad 3.6$$

The efficiency of a TEG is calculated by comparing the amount of electrical power that was generated by the TEG the amount of heat energy that is supplied to the TEG. This efficiency is referred to the conversion efficiency of a TEG.

$$\eta_{TEG} = 100\% \times P_{TEG} \div Q_{HOT} \quad 3.7$$

In general, the thermal conductivity can be calculated from the relationship between the heat flow through a sample and the temperature difference caused by the heat flow. However, because of a TEGs ability to convert heat flow into electrical power the heat flow into a TEG is not equal to the heat flowing out of it i.e. $Q_{HOT} \neq Q_{COLD}$. To account for this discrepancy in the heat flow through a TEG, the thermal conductance and thermal resistance of a TEG were calculated using the following formulae respectively:

$$K_{TEG} = (Q_{HOT} + Q_{COLD})/[2 \times (T_{HOT} - T_{COLD})] \quad 3.8$$

$$R_{TEG,TH} = [2 \times (T_{HOT} - T_{COLD})]/(Q_{HOT} + Q_{COLD}) \quad 3.9$$

Using the voltage produced by a TEG under open circuit voltage conditions, a circuit containing an “infinite” electrical resistance, it is possible to infer an effective Seebeck coefficient of the materials in the TEG:

$$\alpha_{TEG} = V_{OC}/(T_{HOT} - T_{COLD}) \quad 3.10$$

To improve the accuracy of the TEMTester and to ensure that the heat flow from and to the TEG is one dimensional, three thermocouples embedded in the copper blocks track the temperature gradients. The temperature gradient in each block can be found from the following equations:

$$\left(\frac{dT}{dx}\right)_{HOT} = \frac{\sum_{i=1}^n (x_{HOT,i} - \bar{x}_{HOT}) \times (T_{HOT,i} - \bar{T}_{HOT})}{\sum_{i=1}^n (x_{HOT,i} - \bar{x}_{HOT})^2} \quad 3.11(a)$$

$$\left(\frac{dT}{dx}\right)_{COLD} = \frac{\sum_{i=1}^n (x_{COLD,i} - \bar{x}_{COLD}) \times (T_{COLD,i} - \bar{T}_{COLD})}{\sum_{i=1}^n (x_{COLD,i} - \bar{x}_{COLD})^2} \quad 3.11(b)$$

The above equations are used for the evaluation of the Q_{HOT} and Q_{COLD} where \bar{x} and \bar{T} are the average thermocouple positions and average temperatures respectively. The dominance of the beginning and the end temperatures over the middle on the gradient only changes minimally to that calculated from the two dominant temperatures alone. This slope term is quite relevant in the extrapolation of the TEG surface temperatures in the ‘hot’ and ‘cold’ blocks using the following formula:

$$T_{HOT,SURF} = \bar{T}_{HOT} - \frac{dT}{dx_{HOT}} \bar{x}_{HOT} \quad 3.12(a)$$

$$T_{COLD,SURF} = \bar{T}_{COLD} - \frac{dT}{dx_{COLD}} \bar{x}_{COLD} \quad 3.12(b)$$

3.6 Experimental Procedure

In each test, the temperature of the two surface temperatures on the TEG were maintained constant while varying the electrical parameters. There were two major types of tests performed for this thesis. The first type of test, test A, where the load resistance is varied in fine steps to identify the max power (matched) conditions

The second type of test, test B, makes use of the simplification that the maximum power occurs at a voltage value of half the open circuit voltage. For these tests, the outputs of the TEG are only measured at the open circuit and at different multiples of the matched load resistance.

In an effort to describe the experimental procedure for these experiments, a general procedure will be presented first followed by a more detailed account on how the electrical parameters of the system have to be varied to perform the different tests.

1. A thin uniform layer of thermal paste (0.05mm) was coated over the TEG.
2. The TEG was placed on the “hot” block and connected to the DC Load.
3. The bottom shelf was slid upwards to bring the TEG in contact with the ‘cold’ block and locked in place.
4. The pressure screw was adjusted to exert the desired pressure on the TEG, monitored using the load cell.
5. The TEMTester was placed inside the vacuum chamber.
6. Using a vacuum pump, the vacuum chamber was brought to the vacuum pressure.
7. The desired constraint magnitude was set using the DC Load.
8. The chiller was adjusted to desired temperature using the built in controller and the water flow rate was adjusted to the desired flow using the bypass and throttle valves in tandem.
9. If the desired water temperature was not achieved due to the 35°C limit on the chiller output the inline heater was adjusted to reach the temperature.
10. The cartridge power supply was adjusted to desired voltage for the heaters (the current drawn was dependent on the heaters resistance and not controlled directly)
11. The system was allowed to reach steady state which may involve multiple adjustments to the power supply, chiller temperature, water flow rate and inline heater power. (Steady state is defined as the extrapolated block surface

temperatures calculated by the DAQ not varying by 0.5°C over a period of 120 samples.)

12. With the system steady state at the desired temperature difference, 120 samples of data was recorded to a text file.
13. The electrical or thermal conditions on the TEG were then adjusted for the next desired data point which would cause the system to deviate from thermal stability and would require beginning this process at step 11.

To perform test A at step 7, the DC load was set to a short circuit condition and a resistance was applied via the DC load in small increments until the load resistance reaches $50\text{-}60\Omega$. This test results in a power curve similar to that in figure 3.9(a) below.

Test B begins with the DC load set to open circuit conditions at step 11 in the experimental procedure. The data was recorded once the system reached steady state. The voltage across the TEG measured from this test is the open circuit voltage. The DC Load is then set to a voltage limit of half the open circuit voltage which is where the TEG outputs its maximum power and a data point was taken under these conditions. The resistance at which the maximum power occurred is the matched load resistance and is calculated from the TEG current and voltage during the max power test. The next 5 data points were taken at multiples of that matched load resistance; 2, 3, 4,5,20. This test results in a power curve similar to that in figure 3.9 (b).

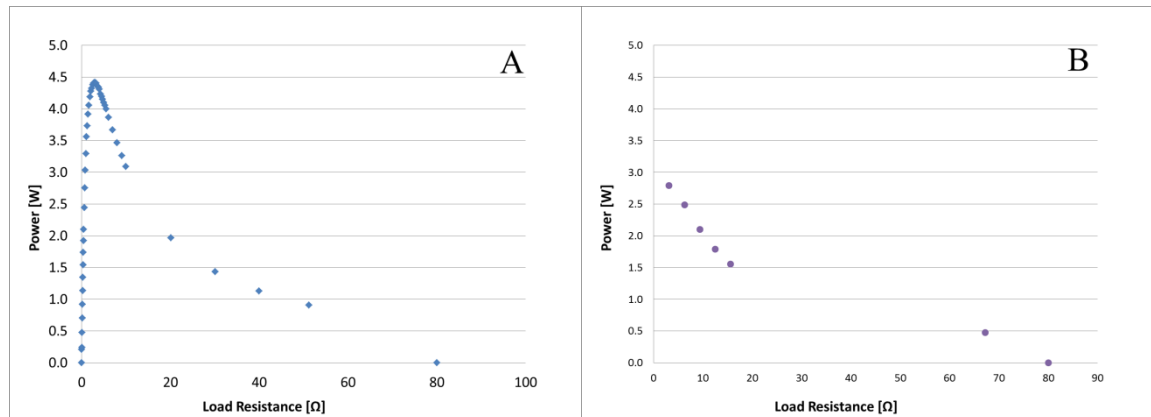


Figure 3.9 Examples of the power curves resultant from the testing for this thesis, on the left in (a) is the detailed test: “A” and on the right (b) the spot testing, “B”.

3.7 Uncertainty Analysis

The uncertainty of the measurement reported in this thesis is a product of two types of uncertainty, the biased uncertainty which is a property of the measurement device and the temporal uncertainty which is a function of the variations in the measurement over time.

The biased uncertainty is quantified by the calibration of the device which was either performed by the manufacturer/supplier or performed in house against a device of well-known accuracy. The temporal uncertainty of the devices is quantified by the standard deviation of the reading acquired by the DAQ over the 120 samples taken for each data point.

$$u(x) = \sqrt{u_{temporal}^2 + u_{bias}^2} \quad 3.13$$

With the uncertainty of the different device measurements known the uncertainty of the each calculated value is found by the following formula

$$u(R) = \sqrt{\sum_{i=1}^n \left(u(x_i) \frac{dR}{dx_i} \right)^2} \quad 3.14$$

where “R” is any function used to calculate a value which contains the arguments x_1 to x_n where $R = f(x_1, x_2, x_3, \dots, x_n)$

The following four tables, 3.2-3.5, document the uncertainties of the important calculated values for the testing. The first two tables document the maximum uncertainties of the values measured for the TEG1, table 3.2, and the TEG1B, table 3.3. The small magnitude of some values measured can cause the uncertainty to be relatively large percentage resulting in a large maximum percentage error. Due to this apparent high uncertainty, the uncertainties of a typical measurement, which occurs at the maximum power output and 250[°C] on the TEG hot side, are included in tables 3.4 and 3.5 for TEG1 and TEG1B respectively.

The uncertainty of $Q_{HEATERS}$ and Q_{WATER} can be relatively low when compared to Q_{HOT} to Q_{COLD} . It should be noted that while the uncertainty of the measurement of these parameters are small they are not necessarily reliable. The heat from the heaters can travel through the system by other paths rather than through the copper block. The heat measured as extracted by the water is sensitive to the ambient temperature.

Table 3.2 Maximum Uncertainty of measured and calculated values of the TEG1-12610-5.1

			V	I	R	P	T_{HOT}	T_{COLD}
			[V]	[A]	[Ω]	[W]	[$^{\circ}C$]	[$^{\circ}C$]
TEG1 12615- 5.1	%	$T_c=30$	3.3227	5.9708	13.7275	4.2398	0.2794	0.9914
		$T_c=50$	4.2360	10.1671	18.2873	10.9648	0.2750	0.6229
		$T_c=80$	5.7643	8.4333	16.6088	6.1073	0.3099	0.6886
	Value	$T_c=30$	0.0074	0.0054	0.0080	0.0080	0.3537	0.3143
		$T_c=50$	0.0072	0.0054	0.0078	0.0078	0.3080	0.3105
		$T_c=80$	0.0065	0.0048	0.0071	0.0071	0.1917	0.8625

			T_{avg}	Q_{HOT}	Q_{COLD}	$Q_{HEATERS}$	Q_{WATER}	K_{TEG}
			[$^{\circ}C$]	[W]	[W]	[W]	[W]	[W/K]
TEG1 12615- 5.1	%	$T_c=30$	0.6141	10.1084	10.0142	1.7841	27.6517	10.2775
		$T_c=50$	0.5413	16.5565	17.6705	1.9013	64.2265	14.723
		$T_c=80$	0.6497	10.3106	22.6763	1.7292	1543.8586	15.657
	Value	$T_c=30$	0.4621	6.2026	5.8449	2.9815	41.9115	0.1474
		$T_c=50$	0.4330	5.6785	5.8696	3.2054	12.0798	0.2573
		$T_c=80$	0.7456	5.5007	11.8417	2.8200	15.7750	0.2091

Table 3.3 Maximum Uncertainty of measured and calculated values of the TEG1B-12610-5.1

		[°C]	V	I	R	P	T _{HOT}	T _{COLD}
			[V]	[A]	[Ω]	[W]	[°C]	[°C]
TEG1B 12615- 5.1	%	Tc=30	0.7847	5.7285	4.3630	5.7232	0.2731	1.0241
		Tc=50	3.3227	7.2942	144.2922	15.0828	0.2718	0.7308
		Tc=80	4.0500	5.9252	17.6198	5.2921	0.1843	1.1244
	Value	Tc=30	0.0068	0.0060	0.0074	0.0074	0.3214	0.3469
		Tc=50	0.0068	0.0512	0.0514	0.0514	0.3225	0.3650
		Tc=80	0.0063	0.0054	0.0070	0.0070	0.2863	0.8968

		[°C]	T _{avg}	Q _{HOT}	Q _{COLD}	Q _{HEATERS}	Q _{WATER}	K _{TEG}
			[°C]	[W]	[W]	[W]	[W]	[W/K]
TEG1B 12615- 5.1	%	Tc=30	0.6122	9.1768	9.5981	1.7157	0.0000	10.0549
		Tc=50	0.6070	12.3543	15.9386	1.8522	0.0000	13.6899
		Tc=80	0.6720	9.0076	17.3168	1.7066	0.0000	12.479
	Value	Tc=30	0.4666	5.7202	6.5079	3.1930	0.0000	0.1338
		Tc=50	0.4577	5.6850	6.5981	3.1402	0.0000	0.1756
		Tc=80	0.9382	5.1893	15.7361	2.7880	0.0000	0.164

Table 3.4 Uncertainty of measured and calculated values of the TEG1-12610-5.1 at the matched load condition

			V	I	R	P	T _{HOT}	T _{COLD}
			[V]	[A]	[Ω]	[W]	[°C]	[°C]
TEG1 12615- 5.1	%	Tc=30	0.1447	0.3481	0.2204	0.1507	0.1152	0.9308
		Tc=50	0.1488	0.3475	0.2283	0.1554	0.1146	0.5959
		Tc=80	0.172	0.4456	0.1876	0.2491	0.1126	0.3667
	Value	Tc=30	0.0055	0.0042	0.0069	0.0069	0.2872	0.2986
		Tc=50	0.0054	0.0042	0.0069	0.0069	0.2858	0.2969
		Tc=80	0.0051	0.0039	0.0064	0.0064	0.2806	0.2925

			T _{avg}	Q _{HOT}	Q _{COLD}	Q _{HEATERS}	Q _{WATER}	K _{TEG}
			[°C]	[W]	[W]	[W]	[W]	[W/K]
TEG1 12615- 5.1	%	Tc=30	0.2945	3.0793	3.5142	1.4086	10.4043	5.7361
		Tc=50	0.2756	2.8982	3.1813	1.4001	1.1186	6.1895
		Tc=80	0.2463	3.5218	3.9791	1.4473	3.771	6.3057
	Value	Tc=30	0.4143	5.2162	5.5795	2.8739	14.8892	0.0759
		Tc=50	0.4121	5.2560	5.5914	2.9737	2.1368	0.0691
		Tc=80	0.4053	4.9900	5.2807	2.4607	3.6076	0.0778

Table 3.5 Uncertainty of measured and calculated values of the TEG1B-12610-5.1 at the matched load condition

		[°C]	V	I	R	P	T _{HOT}	T _{COLD}
			[V]	[A]	[Ω]	[W]	[°C]	[°C]
TEG1B 12615- 5.1	%	T _c =30	0.1625	0.2848	0.3529	0.134	0.1149	0.8868
		T _c =50	0.1621	0.2873	0.3467	0.1351	0.1146	0.6078
		T _c =80	0.1885	0.3329	0.3226	0.1944	0.1127	0.7423
	Value	T _c =30	0.0052	0.0046	0.0070	0.0070	0.2864	0.2995
		T _c =50	0.0052	0.0046	0.0069	0.0069	0.2856	0.3047
		T _c =80	0.0049	0.0043	0.0065	0.0065	0.2808	0.5922
		[°C]	T _{avg}	Q _{HOT}	Q _{COLD}	Q _{HEATERS}	Q _{WATER}	K _{TEG}
			[°C]	[W]	[W]	[W]	[W]	[W/K]
TEG1B 12615- 5.1	%	T _c =30	0.2928	2.9225	3.2173	1.3986	12.8826	6.1179
		T _c =50	0.2789	2.8486	3.2705	1.4032	6.8749	6.2415
		T _c =80	0.3984	3.2974	7.1365	1.4339	97.5023	7.0686
	Value	T _c =30	0.4144	5.2566	5.6703	2.9959	0.4175	0.0714
		T _c =50	0.4177	5.2728	5.7121	2.9625	12.6254	0.0690
		T _c =80	0.6554	5.0420	10.4489	2.5963	20.727	0.0891

4 Results and Discussion

In this chapter, the results of the characterisation experiments performed on two TEGs (TEG1 12610-5.1 and TEG1B 12610-5.1) are presented. The manufacturer's data was extrapolated to allow for a thorough comparison with the experimental results. The experimental data is used in the derivation of a mechanistic model which can predict the performance of a TEG in a waste heat recovery system.

4.1 Manufacturer's Data

The manufacturer provides data in the form of five graphs: maximum power (the power at matched load resistance condition), voltage at matched resistance, current at matched resistance, matched load resistance and open circuit voltage. Those five graphs contain three data sets for three specified cold side temperatures 30, 50 and 80°C with hot side temperatures ranging between 80-300°C. Another graph is also provided detailing the current and power as a function of voltage at a specified temperature difference of 300°C hot and 30°C cold along with a table for this single temperature condition detailing the values from the charts and the heat flow across the TEG.

Using graph digitizing software, the data from the graphs of varying temperature conditions were extracted. This data was used to recreate the manufacturer's graphs and those of max power, matched resistance voltage, matched resistance current and open circuit voltage for a TEG1 12610-5.1 are presented in figure 4.1. The extrapolated data and tables of the important parameters for both TEG1B 12616-5.1 and TEG1B 12616-5.1 are provided in Appendix A

The data extracted from the manufacturer's graphs gives the voltage and current of the generator at two points for any temperature difference reported: the matched load condition and open circuit voltage. These two points can be used to extrapolate for the current through the TEG at any voltage. The current and voltage allow for any power produced by a TEG at any load resistance to be determined.

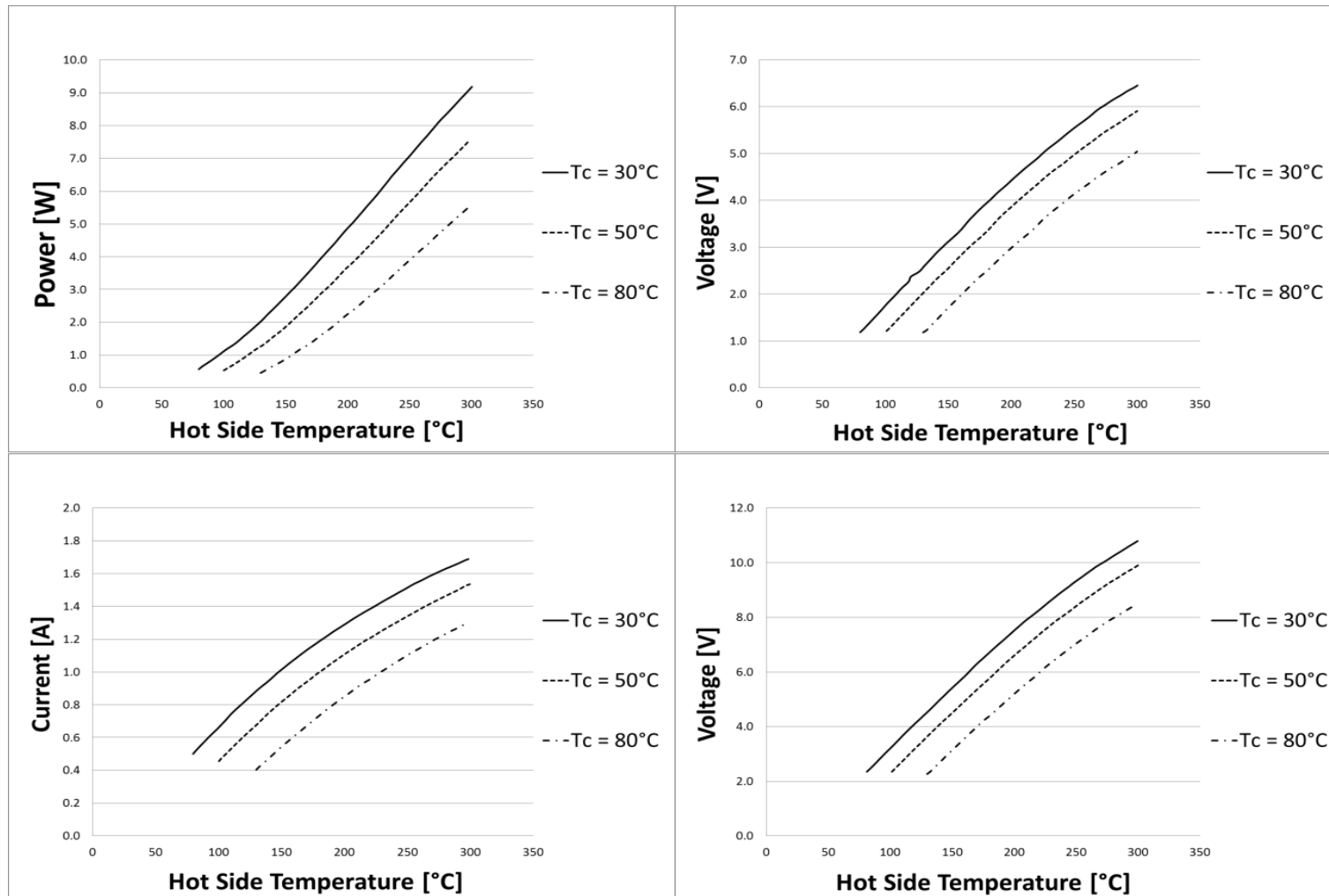


Figure 4.1 Performance data for a TEG1 12610-5.1 digitized from the manufacturer’s specifications. Top Left: Matched resistance power, Top Right: Voltage at matched resistance, Bottom Left: Current at matched resistance, Bottom Right: Open circuit voltage.

The extrapolation performed is possible due to the linear relationship between the current and voltage of a TEG via the internal resistance as stated by Ohm's law.

Figure 4.2 shows the extrapolated Voltage vs. Current data for a TEG1 12610-5.1 available from the manufacturer at a cold side temperature of 30°C at varying hot side temperatures. The symbols in figure 4.2 represent the available data from the manufacturer and the solid lines the extrapolated V-I curve for the generator calculated from Ohm's law as stated in section 2.5.2 of the literature review

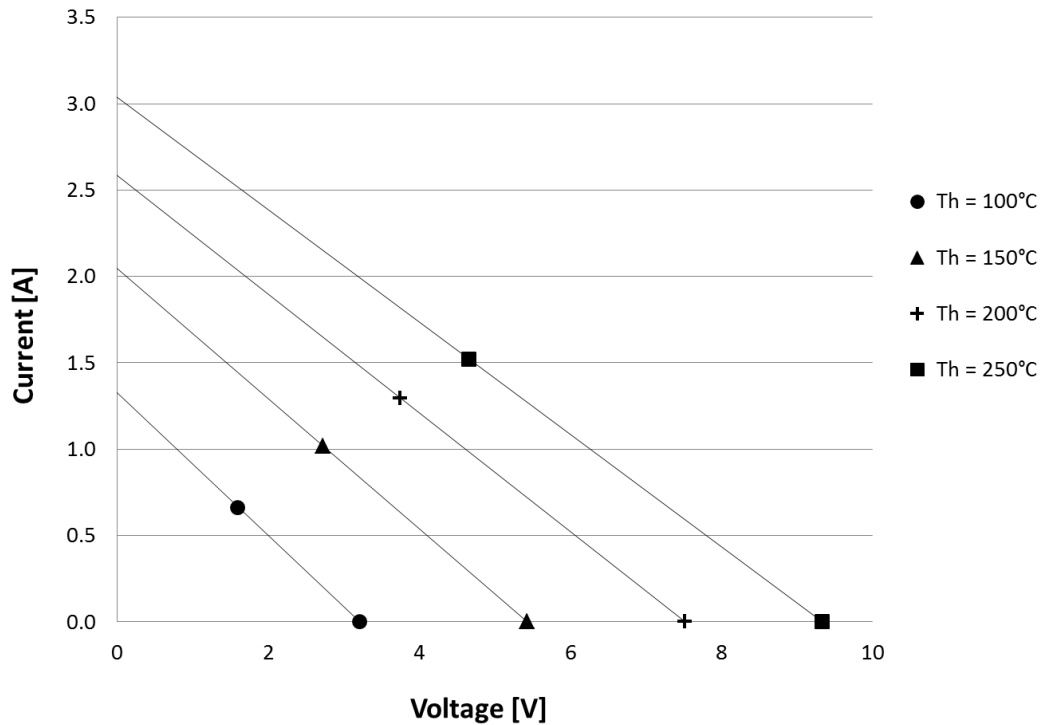


Figure 4.2 Current and voltage adopted from manufacturer's data for a cold side temperature, T_c , of 30°C.

The slope of the lines in figure 4.2 is the internal resistance of the generator at that temperature difference. The Seebeck coefficient can also be determined from this graph as the voltage differential at zero current is the open circuit voltage which is a function of the known temperature difference and the Seebeck coefficient. The power and load

resistance can be calculated at all voltage values and plotted easily using Joule's and Ohm's laws i.e. equation 3.5 and 3.6 respectively.

The power curves generated from the data in Fig. 4.2 is presented in Fig. 4.3. The matched load resistance is evident in the graph with a large peak in the power output at a relatively low resistance which corresponds to the internal resistance of the generator found from the slope of the V-I Curve in Fig 4.2. The internal resistance is usually calculated from the short circuit current which occurs at zero voltage and the open circuit voltage which occurs at zero current.

$$R_{TEG} = V_{OC} \times I_{SC} \quad 4.3$$

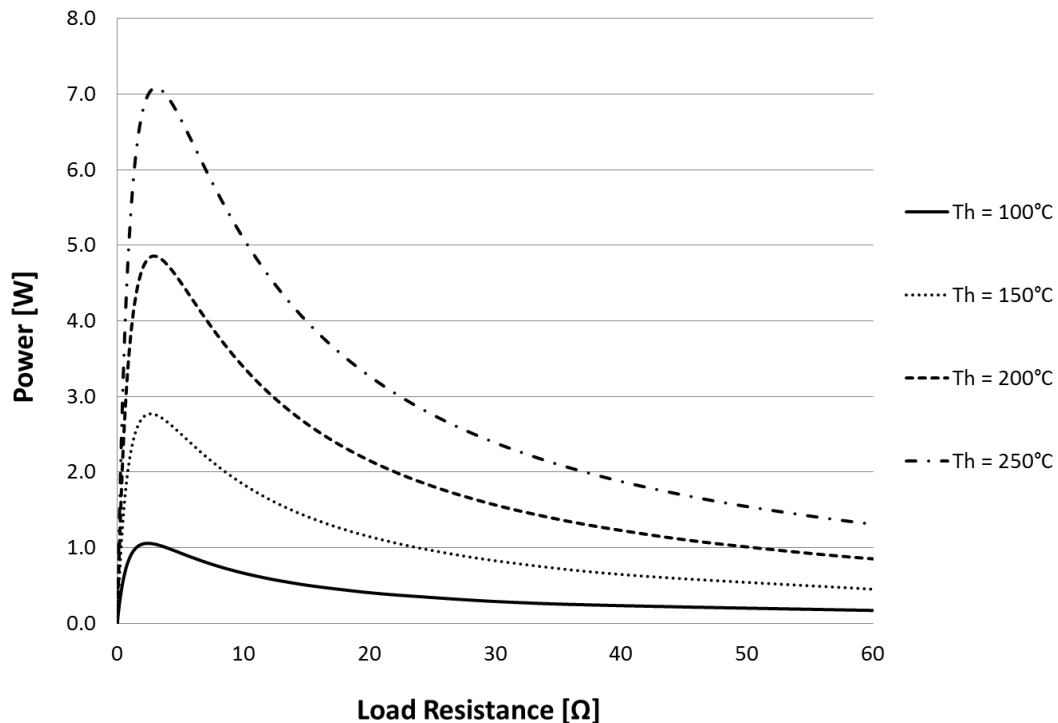


Figure 4.3 Curves of power output of a TEG1 12610-5.1 at different load resistances for a constant cold side temperature, T_c , of 30°C and various hot side temperatures.

With these curves, comparisons can be made between the experimental results from the generators and the manufacturer's specifications. Similar data is also provided for the TEG1B 12610-5.1 and the same process yields the same graphs for comparison of that generator. The manufacturer's data can be found in full in Appendix A.

4.2 Test Parameters

The testing parameters for the experiments on the generators were chosen based on the specifications provided by the manufacturer in order to allow an easy comparison and also to capture the temperature range of the P.O.W.E.R. project.

The heat source for the P.O.W.E.R. project is exhaust gas from a pizza oven which has been measured to exit the oven at approximately 260°C under standard operating conditions. The project extracts thermal energy from the exhaust gas flow converting some to electrical energy using TEGs and storing the rest for use in the store. With the removal of heat from the system, the temperature of the gas decreases thus changing the heat source for any generator further along in the flow direction. With the POWER system it is expected that there will be multiple stages along the flow of the exhaust gases resulting in multiple hot side temperatures for the generators. Given the temperature range of the exhaust gases two TEGs were selected to be fully characterised for their potential use in the project: TEG1 12610-5.1 and TEG1B 12610-5.1. The two TEGs differ by thermoelectric material with the TEG1B material designed for higher temperatures.

Table 4.1 shows the experimental matrix for the current experiments used to characterise the TEG. In the table, test type A is conducted with a fine resolution of electrical load and test type B is conducted at only specific load resistances as outlined in section 3.6 of this thesis.

Table 4.1 Table of testing parameters for both TEG1 12610-5.1 and TEG1B 12610-5.1

No.	Type of Test	Cold Side Temperature	Hot Side Temperature
1	B	30°C	100°C
2	B		150°C
3	B		200°C
4	A		250°C
5	B	50°C	100°C
6	B		150°C
7	B		200°C
8	A		250°C
9	B	80°	150°C
10	B		200°C
11	A		250°C

4.3 TEG Variability

Due to the varying manufacturing quality of the generators and the inconsistency in the quality of thermoelectric materials TEGs exhibit a large amount of variance. To quantify this variance, four of each generator type, TEG1 and TEG1B, of the same manufacturing batch were tested at the open circuit voltage and short circuit current conditions. These points were chosen because of their independence to the electrical load resistance applied. Figure 4.4 shows the short circuit current and open circuit voltage measured experimentally for samples A, B1, C1 and D1 respectively. The maximum power of the four TEGs was calculated using equation 4.4, a reformulation of equation 2.14, and is presented in Fig. 4.5 along with the manufacturer's stated maximum power. The Seebeck coefficient is calculated from the temperature difference and the open circuit voltage

while the internal resistance is calculated from the quotient of the open circuit voltage and short circuit current and are presented in Fig. 4.6.

$$P_{MAX} = \frac{(N\alpha_{CIRCUIT})^2 (T_H - T_C)^2}{4 \times R_{TEG}} = \frac{N\alpha\Delta T}{4} \times \frac{N\alpha\Delta T}{R_{TEG}} = \frac{V_{OC} \times I_{SC}}{4} \quad 4.4$$

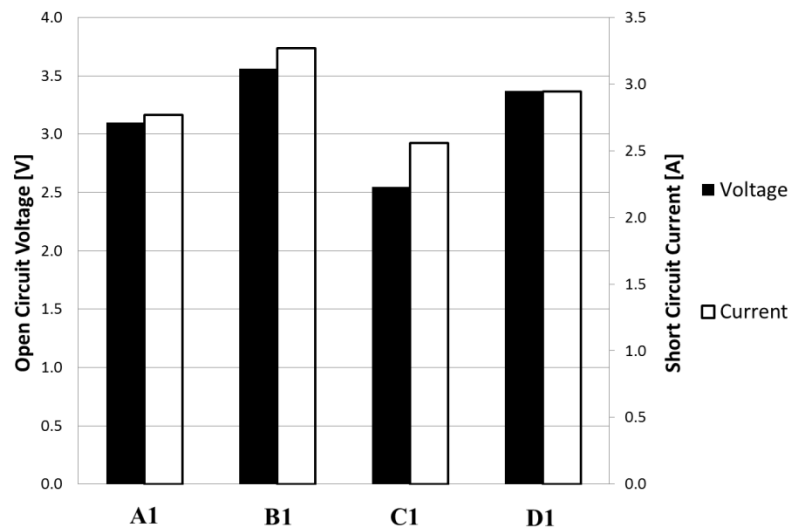


Figure 4.4 Experimental results for the short circuit current and open circuit voltage of four separate TEG1 12610-5.1 at a temperature difference of 200°C-50°C

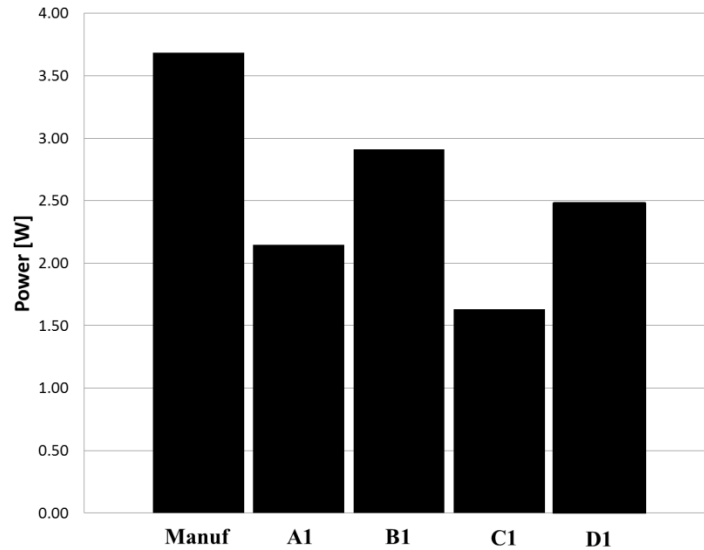


Figure 4.5 Results for the maximum power output of four separate TEG1 12610-5.1 at a temperature difference of 200°C-50°C.

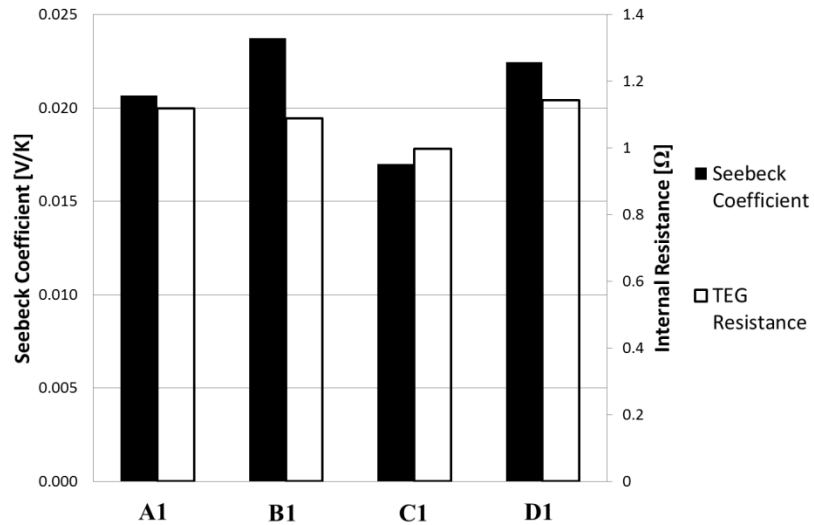


Figure 4.6 Values for the Seebeck coefficient and internal resistance of four separate TEG1 12610-5.1 at a temperature difference of 200°C-50°C.

For the TEG1 12610-5.1, the values for short circuit current and open circuit voltage vary significantly within the same batch. The percentage standard deviation of the experimentally measured short circuit current and open circuit voltage are 9% and 12% respectively. As the Seebeck coefficient is based on the open circuit voltage, it also has a percentage variance of 12%. Over the four generators tested, the internal resistance and matched power show a percentage variance of 5% and 20% respectively. In comparison with the manufacturer's data, the average maximum power is overestimated by 60%, the average open circuit voltage by almost 110% and the average matched resistance value by 170%.

The same tests were performed for the TEG1B 12510-5.1 and those results are presented in the following figures 4.7-4.9. The four sample TEGs are labelled A2,B2,C2 and D2.

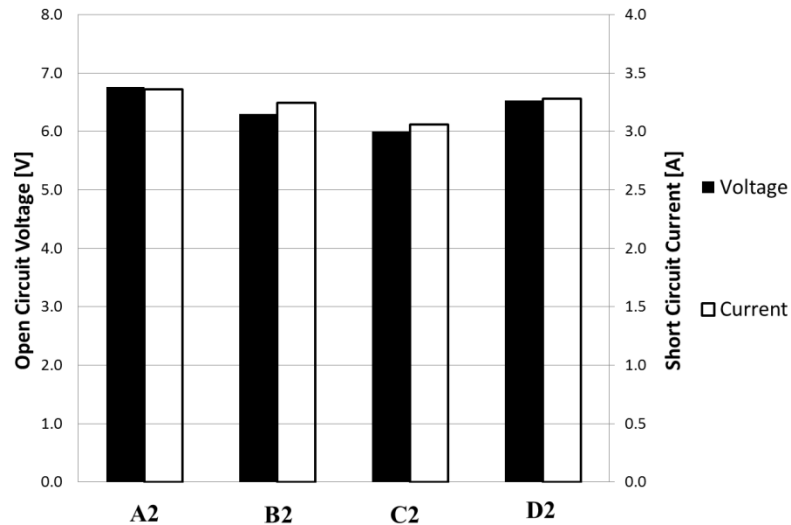


Figure 4.7 Experimental results for the open circuit voltage and short circuit current of four separate TEG1B 12610-5.1 at a temperature difference of 250°C-50°C

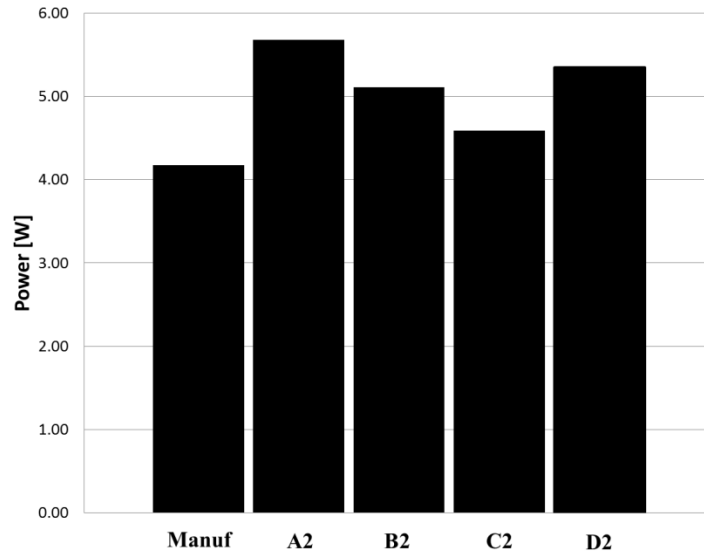


Figure 4.8 Results for the maximum power output of four separate TEG1B 12610-5.1 at a temperature difference of 250°C-50°C.

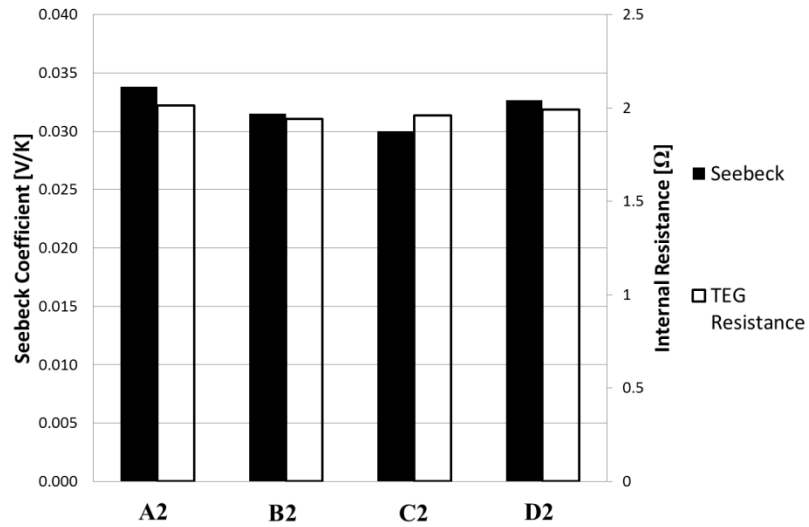


Figure 4.9 Values for the Seebeck coefficient and internal resistance of four separate TEG1B 12610-5.1 at a temperature difference of 250°C-50°C.

The measured values of this testing are presented in tables 4.2 and 4.3 for the TEG1 and TEG1B respectively. The tables also include the standard deviation and percentage standard deviation between the four TEGs. In the table the specified manufacturer data for this temperature difference is compared to the average value of the four TEGs tested.

Table 4.2 Measured values and calculated variance of TEG1-12610-5.1 along with a comparison to manufacturer’s data

	TEG1 12610-5.1				
	Open Circuit Voltage	Short Circuit Current	Maximum Power	Seebeck Coefficient	Matched Load Resistance
	[V]	[A]	[W]	[V/K]	[Ω]
A2	3.10	2.77	2.15	0.0207	1.12
B2	3.56	3.27	2.91	0.0237	1.09
C2	2.55	2.56	1.63	0.0170	1.00
D2	3.37	2.95	2.48	0.0225	1.14
Standard Deviation	0.38	0.26	0.47	0.0025	0.06
% Standard Deviation	12.10%	9.05%	20.43%	12.10%	5.11%
Manufacturer Data	4.17		5.40		1.77
Average Difference	1.01		1.00		0.21
% Average Difference	-15.81%		-30.87%		-12.99%

Table 4.3. Measured values and calculated variance of TEG1B-12610-5.1 along with a comparison to manufacturer's data

	TEG1B 12610-5.1				
	Open Circuit Voltage	Short Circuit Current	Maximum Power	Seebeck Coefficient	Matched Load Resistance
	[V]	[A]	[W]	[V/K]	[Ω]
A1	6.76	3.36	5.68	0.0338	2.01
B1	6.30	3.24	5.11	0.0315	1.94
C1	6.00	3.06	4.59	0.0300	1.96
D1	6.53	3.28	5.35	0.0327	1.99
Standard Deviation	0.28	0.11	0.40	0.0014	0.03
% Standard Deviation	4.42%	3.39%	7.68%	4.42%	1.38%
Manufacturer Data	3.68		6.59		2.96
Average Difference	3.45		1.39		1.88
% Average Difference	109.63%		60.74%		172.46%

The manufacturer's data underestimates the maximum power and the open circuit voltage of the TEG1B where it overestimated that of the TEG1. While the results for the TEG1B are much more uniform than the TEG1, the results still vary. The short circuit current and open circuit voltage have percentage standard deviations of 4.4% and 3.4% respectively. The calculated values of matched power output, Seebeck coefficient and internal resistance have a percentage variance of 7.7%, 4.4% and 1.4%. In terms of variance the TEG1B seems to be much more uniform than the TEG1 but it is still consistently deviated from the manufacturer's specifications. The average difference between the experiments and the manufacturer's data is 15% for the maximum power output, 30% for the open circuit voltage and 13% for the matched resistance value.

As the manufacturing process used in the fabrication of either the TEG1 or the TEG1B is not known, it cannot specifically be said what the reason for the much smaller variance of the TEG1B in comparison to TEG1. However, considering their relatively similar

construction, and thus most likely construction method, it would seem that the results are due to a more uniform material quality of the TEG1 thermoelectric pellets. The manufacturer's data fails to report on variance in any parameter of the TEG. This lack of data on the variance and on the testing method used by the manufacturer shows that there is a need for a standardised method (A.S.T.M. or equivalent) of testing and reporting the performance data of TEGs

This non-uniformity of TEGs presents a problem not only in the characterisation to be performed for this thesis but also more practically in the design of energy producing devices. This problem stems from the fact the performance of a TEG device containing multiple TEGs connected together will be limited by the least efficient in the system. With such a large difference between the TEGs it would be necessary to separate them based on their performance so that "good" TEGs are not used with and thus hampered by "bad" TEGs.

4.4 Typical Results

Under steady state thermal conditions, a thermoelectric generator has much the same power characteristics as a DC battery. Some of those characteristics are a maximum voltage at an infinite resistance and zero voltage under no load resistance. The current is a maximum when there is no load resistance across it and is zero when the resistance is infinite. Figures 4.10 and 4.11 show the voltage and current measured using the TEMTester as a function of load resistance under different thermal conditions. These characteristics are shown at the load resistance values of zero and 80 ohms (Infinite resistance case being plotted at 80 Ω for convenience).

The experimental power curves have the same shape as those generated from the manufacturer's data in figure 4.3. It can be seen from figure 4.12 that there is no power produced at either the open circuit or short circuit conditions with the maximum at a resistance corresponding to the internal resistance of the TEG.

Figure 4.13 shows the V-I curve of a thermoelectric generator which is similar in form to that extrapolated from the manufacturer's data in figure 4.2. This straight curve shows how the TEG at a constant temperature difference obeys Ohm's law with the voltage and current being related to each other by a constant, the slope, which represents the internal resistance of the generator. As previously mentioned, this encapsulates a range of data including the internal resistance, the Seebeck coefficient and the voltage and current characteristics of the generator at any load resistance applied. Due to the small amount of experimental data needed to create this graph and the amount of data that can be gathered from it, it could be used for a quick grading processes to assess the relative performance of TEGs before their use in a generation system.

The thermal resistance of the TEG as a function of the electrical resistance applied to it is presented in figure 4.14. While this graph does not show the clear cut trends of the four preceding graphs as a function of temperature it can be seen that it shows how the thermal resistance changes with different current flows through it. The thermal resistance of the TEG decreases by almost as much as 20% between the open circuit case and short circuit case. This change in thermal resistance is due to the flow of electrons in the TEG, which has implications for the thermal stability of a system with a fluctuating electronic load when it comes to design for an active system. The thermal resistance of the TEG is covered in more depth in section 4.7.

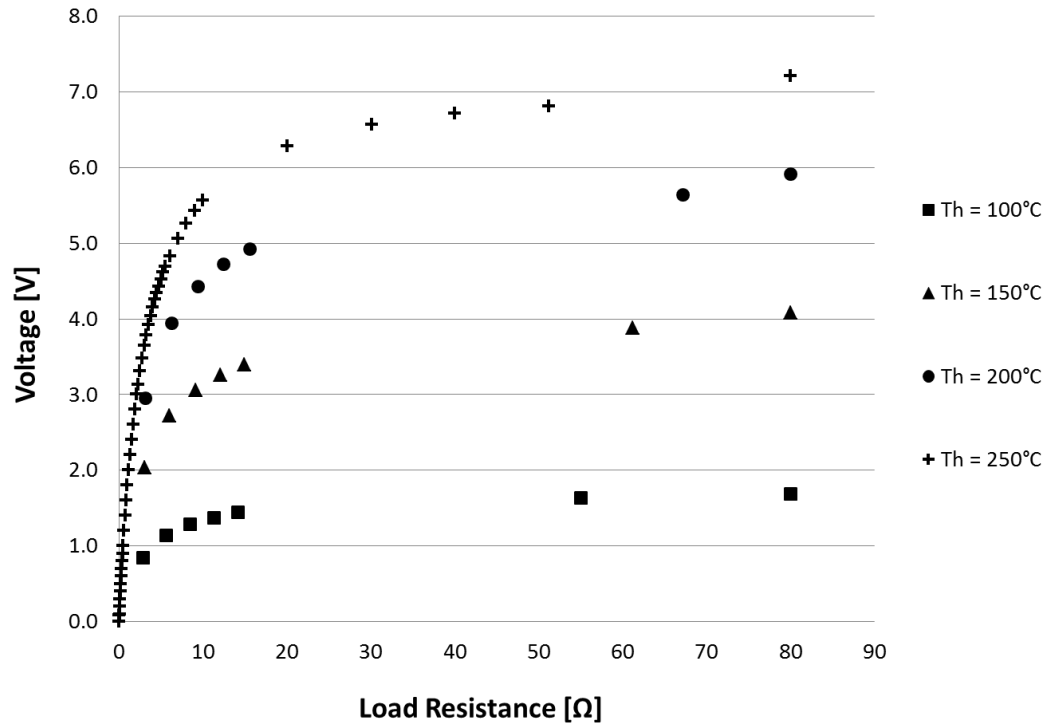


Figure 4.10 Experimentally measured voltage of a TEG5.1 12610-5.1 as a function of load resistance at a constant cold side temperature of 50°C and different hot side temperatures.

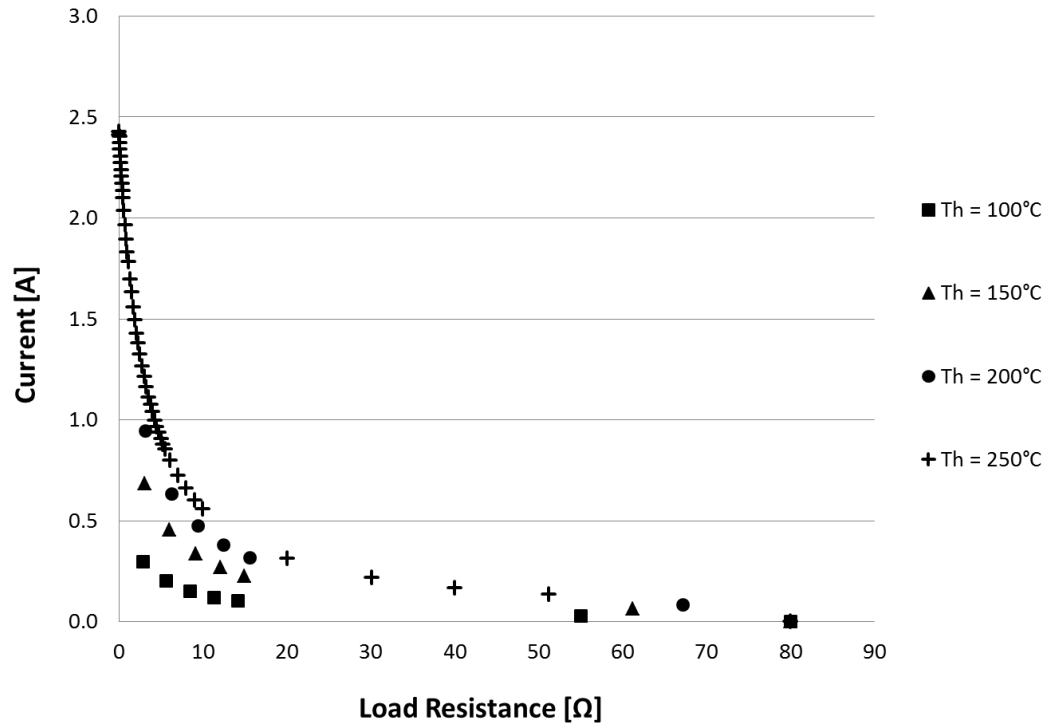


Figure 4.11 Experimentally measured current of a TEG5.1 12610-5.1 as a function of load resistance at a constant cold side temperature of 50°C and different hot side temperatures.

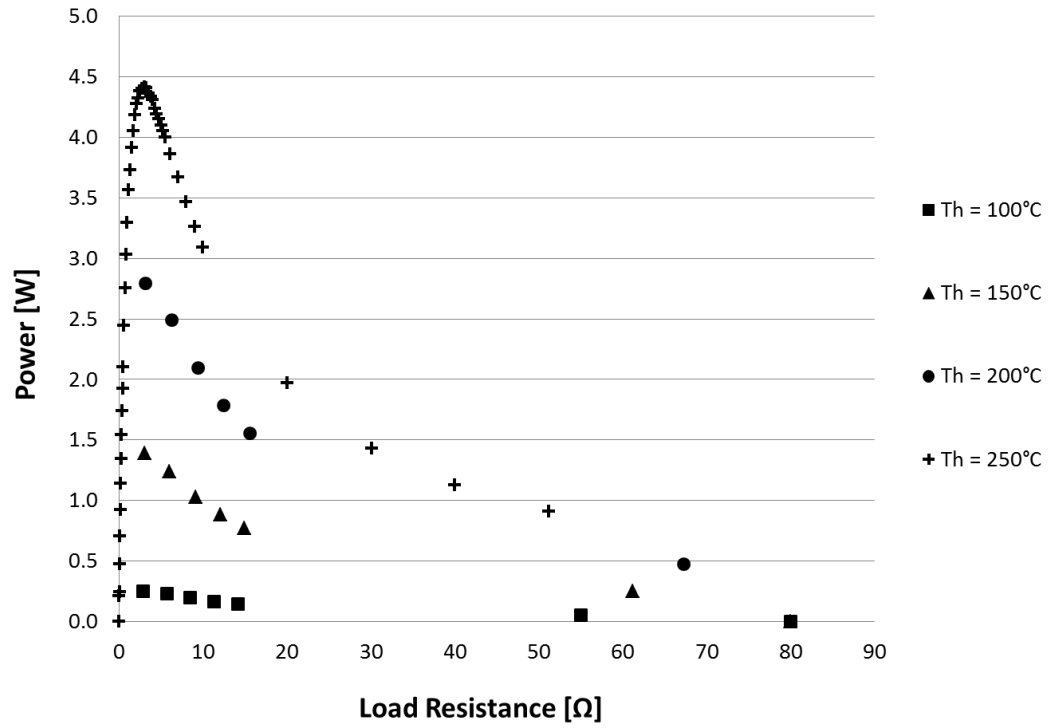


Figure 4.12 Experimentally measured power output of a TEG5.1 12610-5.1 as a function of load resistance at a constant cold side temperature of 50°C and different hot side temperatures.

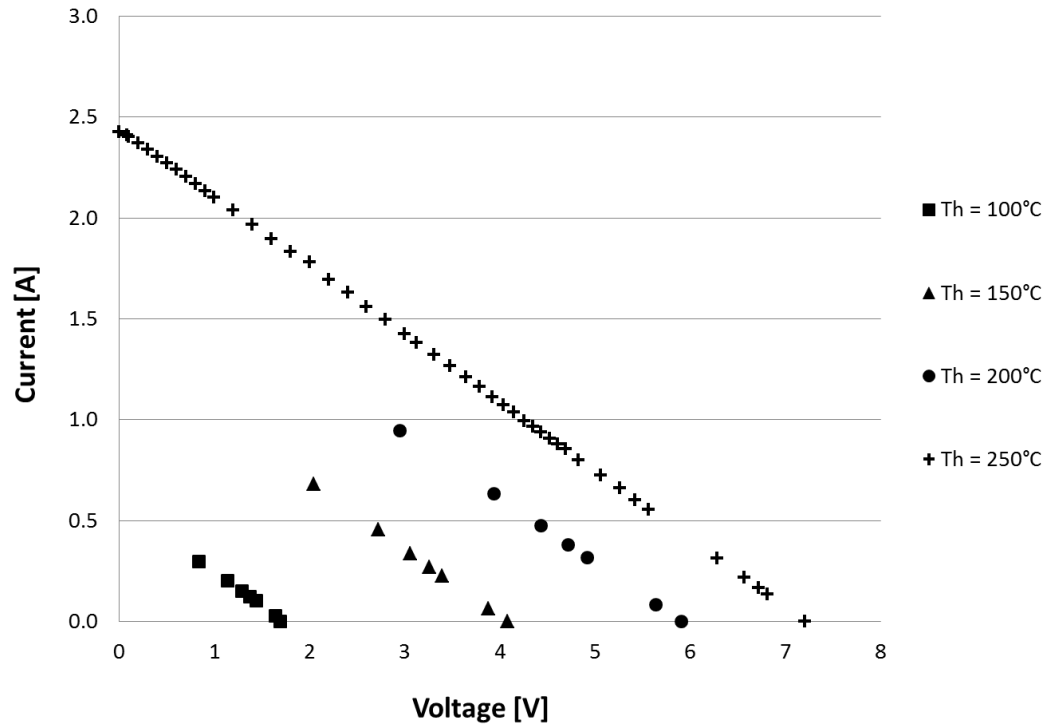


Figure 4.13 Experimentally measured V-I curve of a TEG1-12610-5.1 measured at a constant cold side temperature of 50°C and different hot side temperatures.

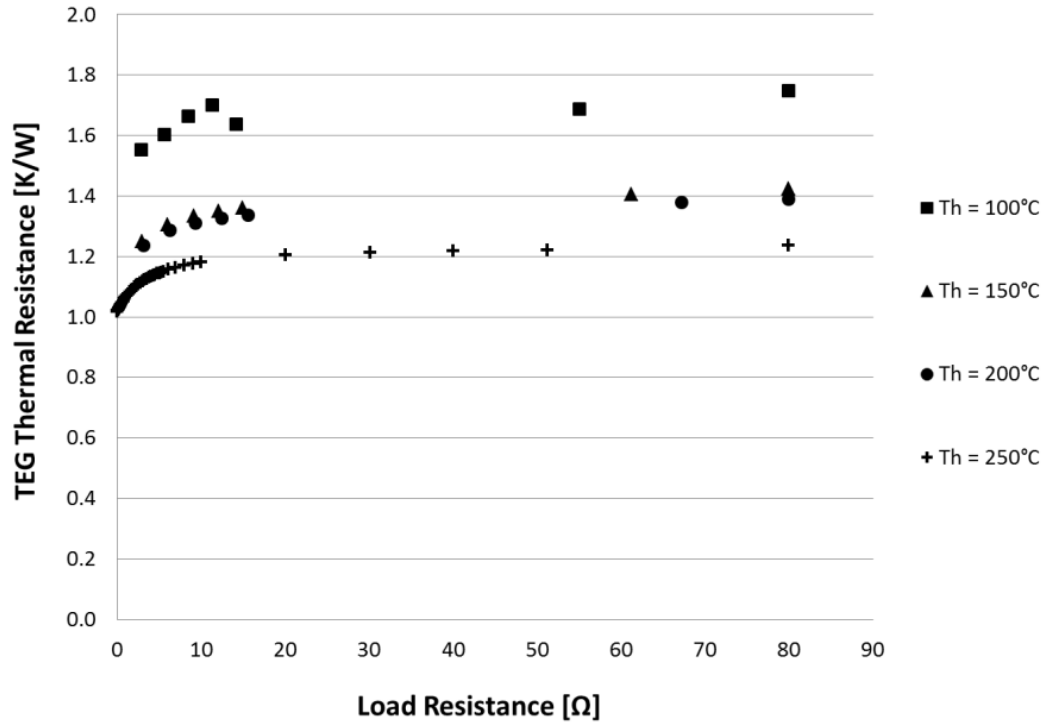


Figure 4.14 Experimentally measured curve of the thermal resistance of a TEG1-12610-5.1 measured at a constant cold side temperature of 50°C and different hot side temperatures.

4.5 Experimental and Manufacturer's Data Comparisons

The comparison between the experimental and manufacturer's data is shown in figures 4.15 to 4.17 which plot the power output of the TEG1 12610-5.1 and TEG1B 12610-5.1 as a function of load resistance at the different temperature conditions outlined in table 4.1.

The TEG performance specified by the manufacturer's data and that of the experiments performed do not agree well over the range of tested temperatures. The output of the TEG1-12610-5.1 is overestimated by the manufacturer's data. The manufacturer only supplies data for the power output at the matched load resistance. When the comparison is made between the maximum power measured experimentally and the power specified by

the manufacturer, the magnitude is overestimated by the manufacturer by a minimum of 28% for the tested temperature differences. The extrapolation of the manufacturer's data indicates that this overestimation of the power is consistent at all load resistances.

When the other power characteristics of the TEG1-12610-5.1, (the matched voltage, matched current, open circuit voltage and short circuit current) are compared to the given manufacturer's data, they are also all overestimated. However, the matched load resistance of the TEG is underestimated by the manufacturer. The power characteristics at the resistance stated by the manufacturer to be the matched load resistance still do not agree with the outputs in manufacturer's data (maximum percentage change of matched voltage: 3.48%, matched current: 3.44% and matched power: 0.38%).

The power of the TEG1B-12610-5.1 is overestimated by the manufacturer at a cold side temperature of the 30°C, Fig. 4.15(a), but out performs the manufacturer's specifications at the higher cold side temperatures of 50°C, Fig. 4.16(a), and 80°C, Fig. 4.17(a). This trend remains consistent over all electrical resistances according to the extrapolated manufacturer's data. In general the electrical characteristics of the TEG1B are underestimated by the manufacturer. Interpolating the data from the fine resolution tests to the manufacturer's matched resistance changes the agreement very little (maximum percentage change of matched voltage: 6.41%, matched current: 6.62% and matched power: 0.65%). This change according to the matched resistance improves the agreement of the values at 30°C on the cold side of the TEG to within 1.6% but the values at the other to cold side temperatures remain 10% off from the specifications of the manufacturer.

Tables 4.4 and 4.5 contain the percentage difference between the manufacturer's data and the experimentally measured results for both the TEG1 and TEG1B. The percentage difference is calculated using the following formula:

$$\%Difference = 100\% \times \frac{Manufacturer - Experimental}{Experimental} \quad 4.5$$

Table 4.4 Percentage difference between the prediction with the manufacturer’s data and the experimental data for a TEG1 12610-5.1.

	Cold Side Temp [°C]	Cold Side Temp [°C]	Matched Voltage [%]	Matched Current [%]	Matched Resistance [%]	Matched Power [%]	Open Circuit Voltage [%]	Short Circuit Current [%]
% Difference	30	100	32.9	23.5	-7.7	46.8	13.8	23.8
		150	30.5	17.8	-5.2	32.7	11.4	17.6
		200	36.6	21.3	-5.2	39.7	15.6	21.6
		250	46.1	25.8	-2.6	53.5	21.5	27.9
	50	100	54.6	52.5	-10.4	112.2	33.4	53.1
		150	29.1	20.4	-7.4	34.4	10.7	20.1
		200	32.3	17.7	-5.0	32.0	11.7	17.2
		250	36.9	11.0	3.4	28.0	15.5	10.4
	80	150	31.3	37.2	-16.4	61.6	15.0	39.1
		200	60.9	76.7	-22.1	147.3	37.4	72.8
		250	41.5	27.7	-6.6	51.4	22.3	24.6

Table 4.5 Percentage difference between the prediction with the manufacturer’s data and the experimental data for a TEG1B 12610-5.1

	Cold Side Temp [°C]	Cold Side Temp [°C]	Matched Voltage [V]	Matched Current [A]	Matched Resistance [W]	Matched Power [W]	Open Circuit Voltage [V]	Short Circuit Current [A]
% Difference	30	100	-2.5	27.2	-23.7	20.2	-3.8	26.8
		150	-6.5	16.2	-19.5	7.9	-6.7	15.2
		200	-5.4	10.6	-14.4	4.6	-5.4	10.5
		250	-5.7	7.3	-12.1	1.3	-5.6	7.1
	50	100	-11.5	4.2	-15.8	-9.9	-10.5	3.5
		150	-6.6	25.1	-25.2	16.2	-15.7	-5.3
		200	-11.7	-11.2	-0.3	-21.7	-16.9	-6.4
		250	-15.4	-4.0	-11.8	-18.8	-16.3	-3.1
	80	150	-76.0	-0.1	-11.7	-14.6	-76.1	0.1
		200	-50.4	-0.1	-13.7	-14.2	-50.1	-0.4
		250	-37.5	-7.5	-4.3	-18.4	-39.5	-3.8

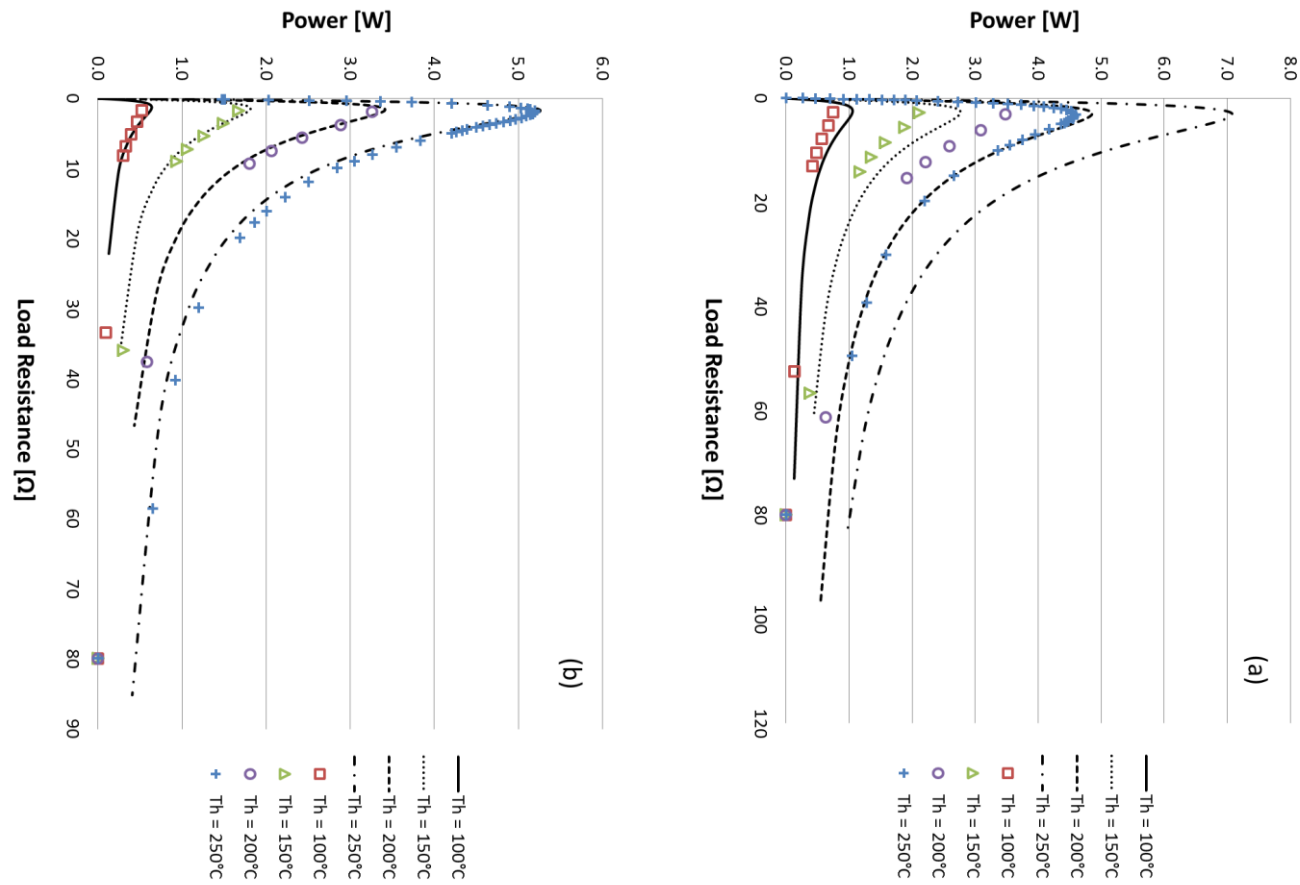


Figure 4.15 Manufacturer data and experimental results for a TEG1B 12610-5.1 (left) and TEG 12610-5.1 (right) at a constant cold side temperature of 30°C and varied hot side temperatures. Continuous lines are manufacturer specifications, symbols indicate experimental results.

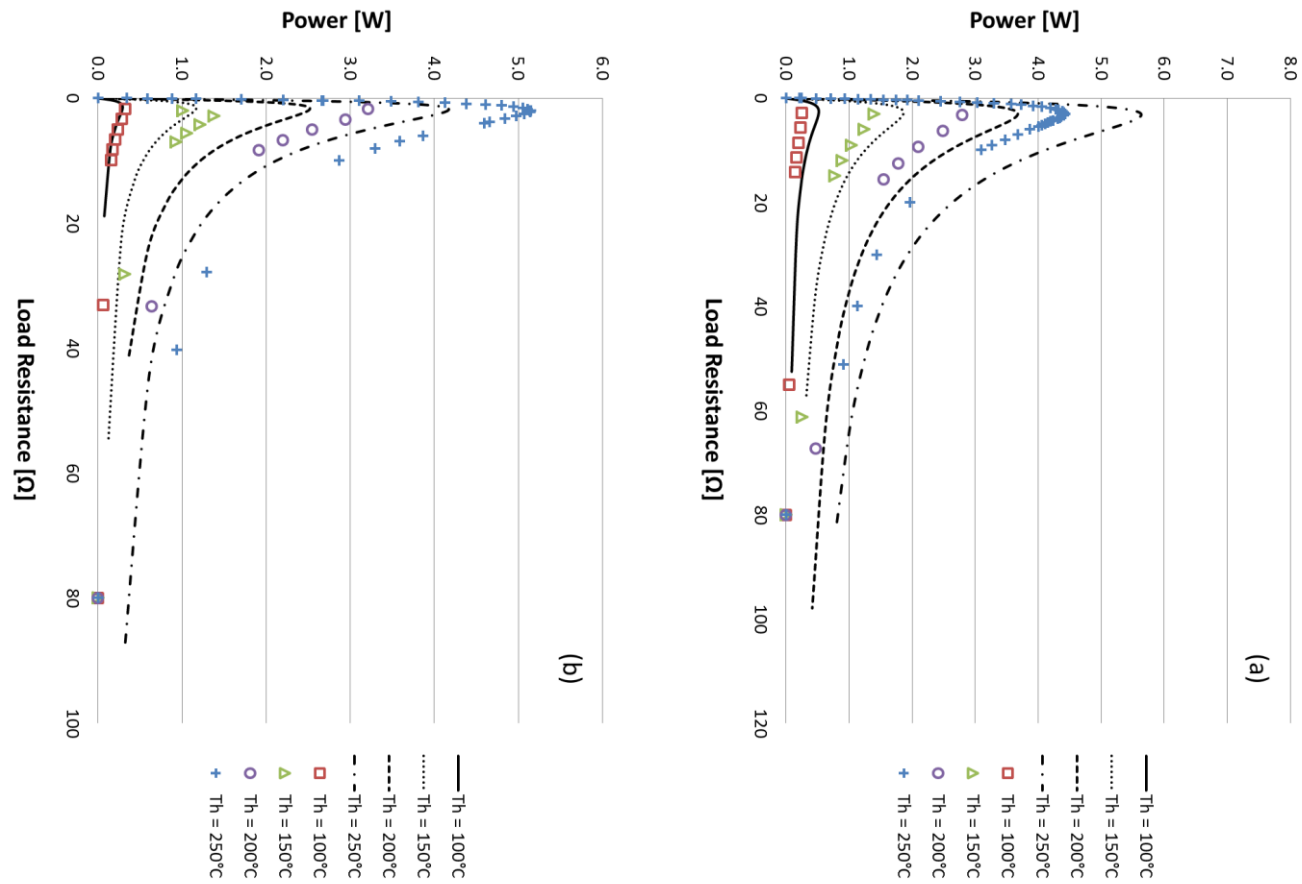


Figure 4.16 Manufacturer data and experimental results for a TEG1B 12610-5.1 (left) and TEG 12610-5.1 (right) at a constant cold side temperature of 50°C and varied hot side temperatures. Continuous lines are manufacturer specifications, symbols indicate experimental results.

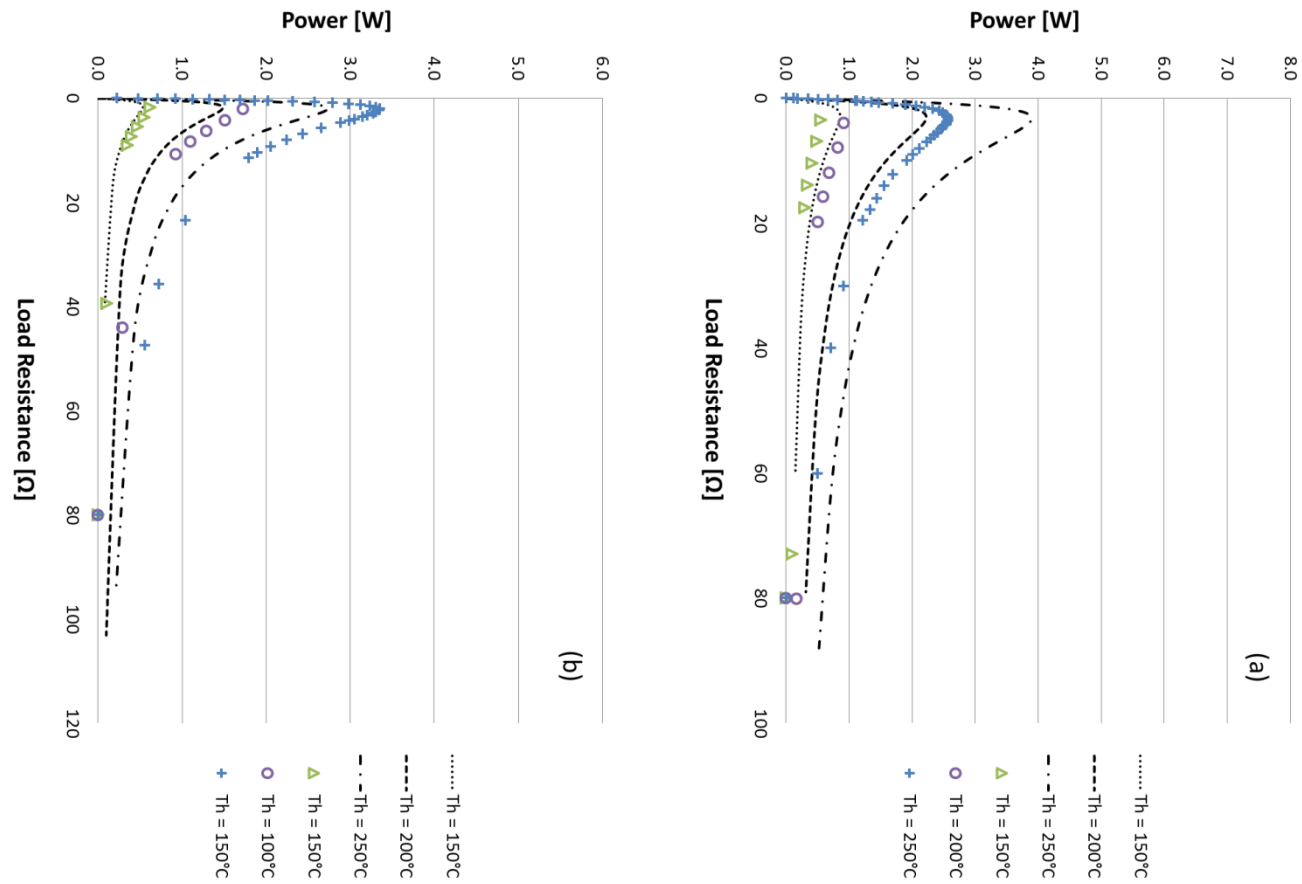


Figure 4.17 Manufacturer data and experimental results for a TEG1B 12610-5.1 (left) and TEG 12610-5.1 (right) at a constant cold side temperature of 80°C and varied hot side temperatures. Continuous lines are manufacturer specifications, symbols indicate experimental results.

4.6 TEG1 and TEG1B Comparisons

The following section outlines the detailed comparison of the two TEGs tested to evaluate the claim that the TEG1B-12610-5.1 is made of a thermoelectric material fabricated to perform better at higher temperatures.

The experiments prove the claim that TEG1B provides more power than its counterpart at higher temperatures. This is clearly seen in figure 4.18 as the higher the average temperature of the TEG, the more power is produced by the TEG1B compared to the TEG1. The data is plotted as a function of average temperature to make the trends clearer.

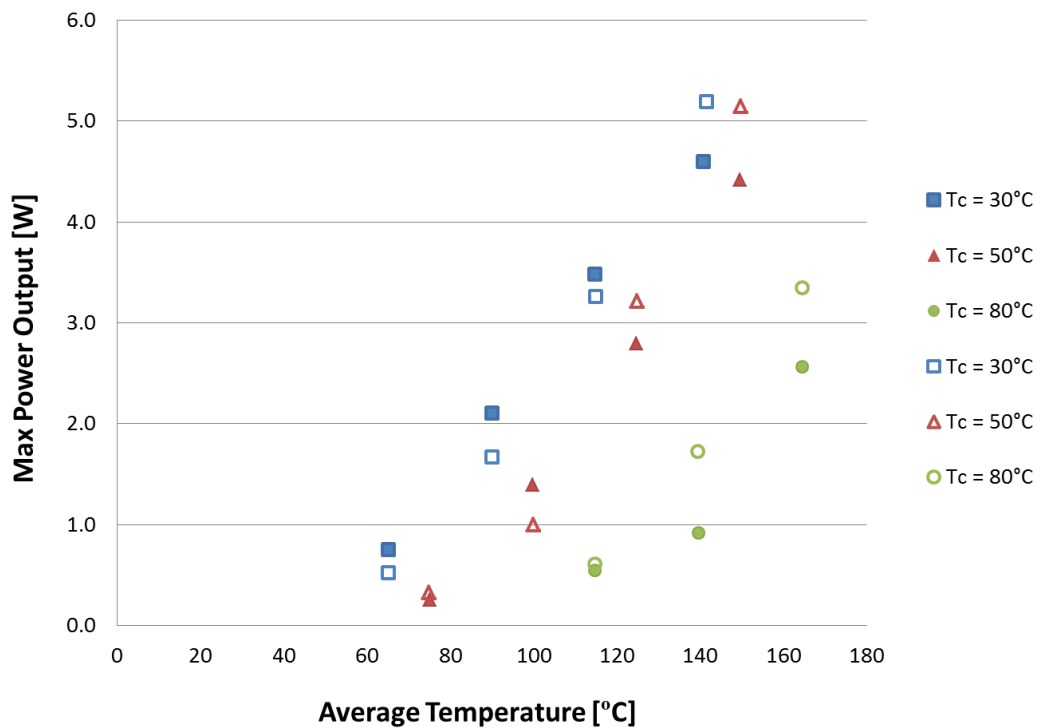


Figure 4.18 Experimentally measured maximum power output of the TEG1 12610-5.1 (filled symbols) and the TEG1B 12610-5.1 (hollow symbols).

The results of the open circuit voltage and the short circuit current, figs. 4.19 and 4.20, show that the TEG1B produces a higher voltage and a lower current than the TEG1. As the cold side temperature increases increasing the average temperature the open circuit voltage difference between them also increases and the gap between the short circuit current decreases.

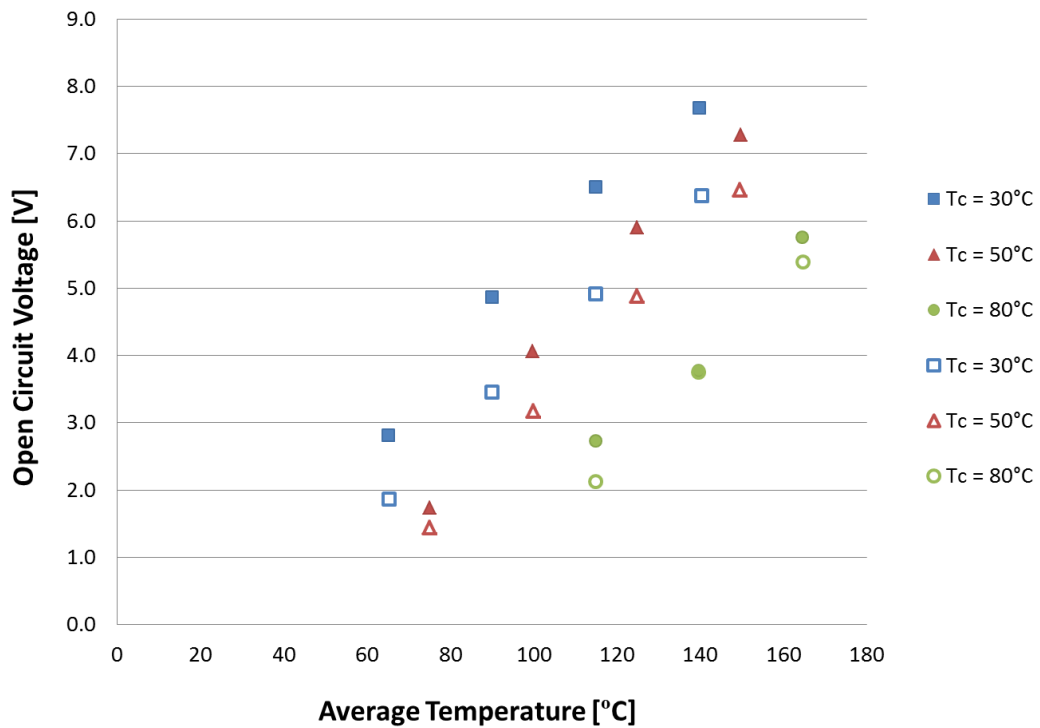


Figure 4.19 Experimentally measured open circuit voltage of the TEG1 12610-5.1 (filled symbols) and the TEG1B 12610-5.1 (hollow symbols).

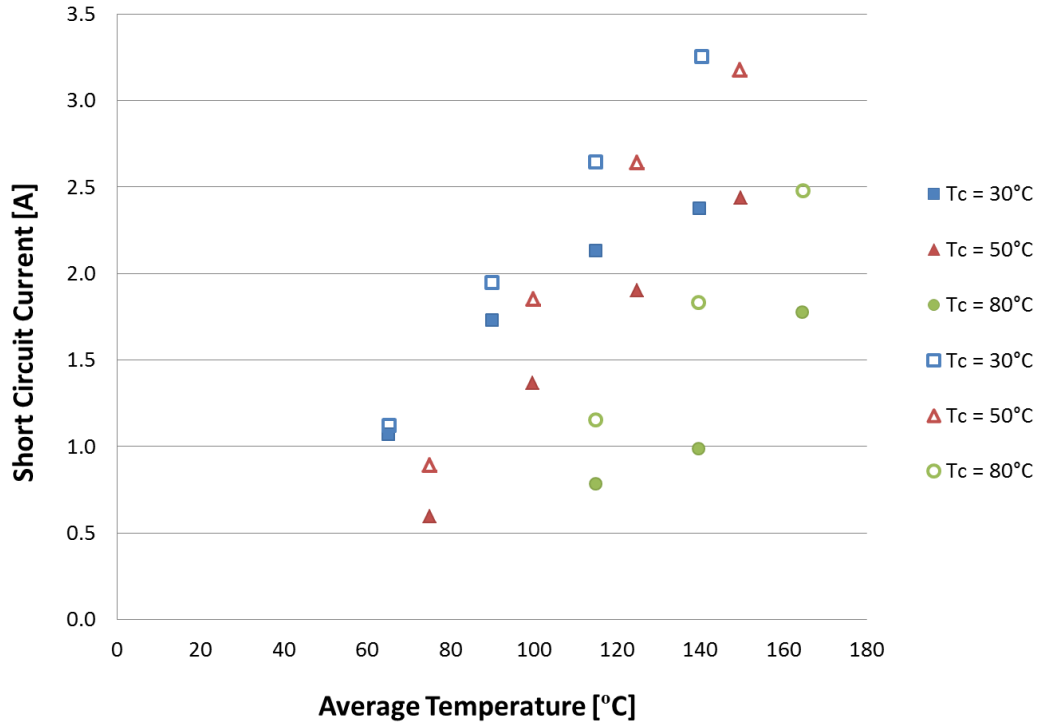


Figure 4.20 Experimentally measured short circuit current of the TEG1 12610-5.1 (filled symbols) and the TEG1B 12610-5.1 (hollow symbols).

The larger voltage and smaller current of the TEG1B is not only a characteristic at the extremes of the open circuit voltage and short circuit voltage. This can be seen in figures 4.21 and 4.22 which graph the voltage and current produced by both TEGs at the matched resistance current.

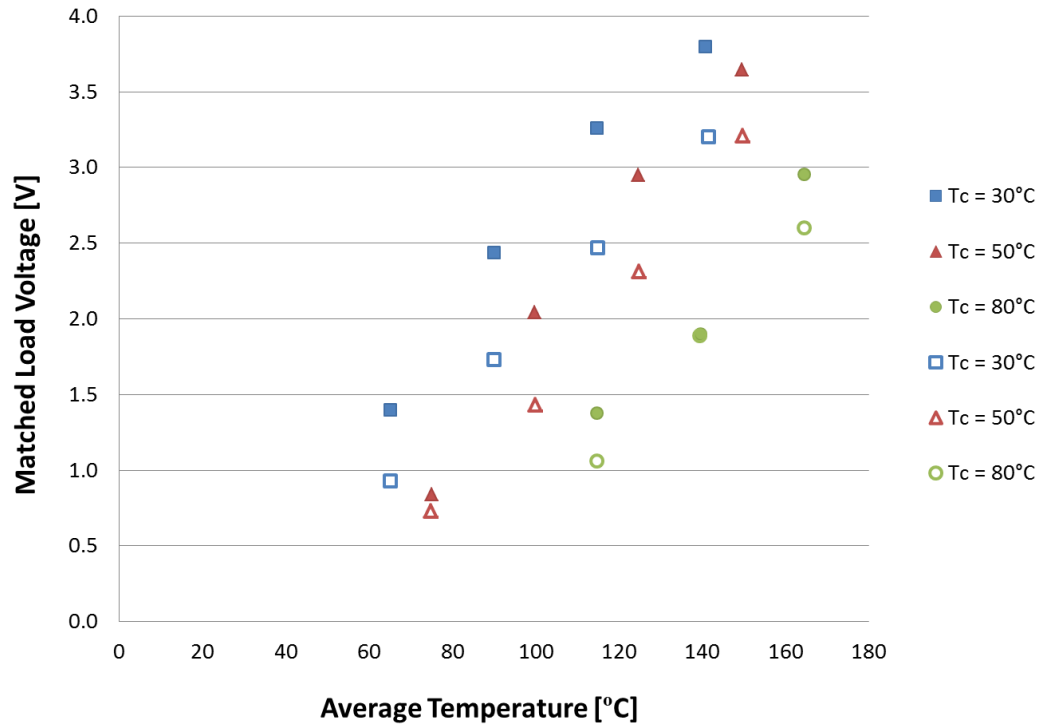


Figure 4.21 Experimentally measured voltage of the TEG1 12610-5.1 (filled symbols) and the TEG1B 12610-5.1 (hollow symbols) at the maximum power output.

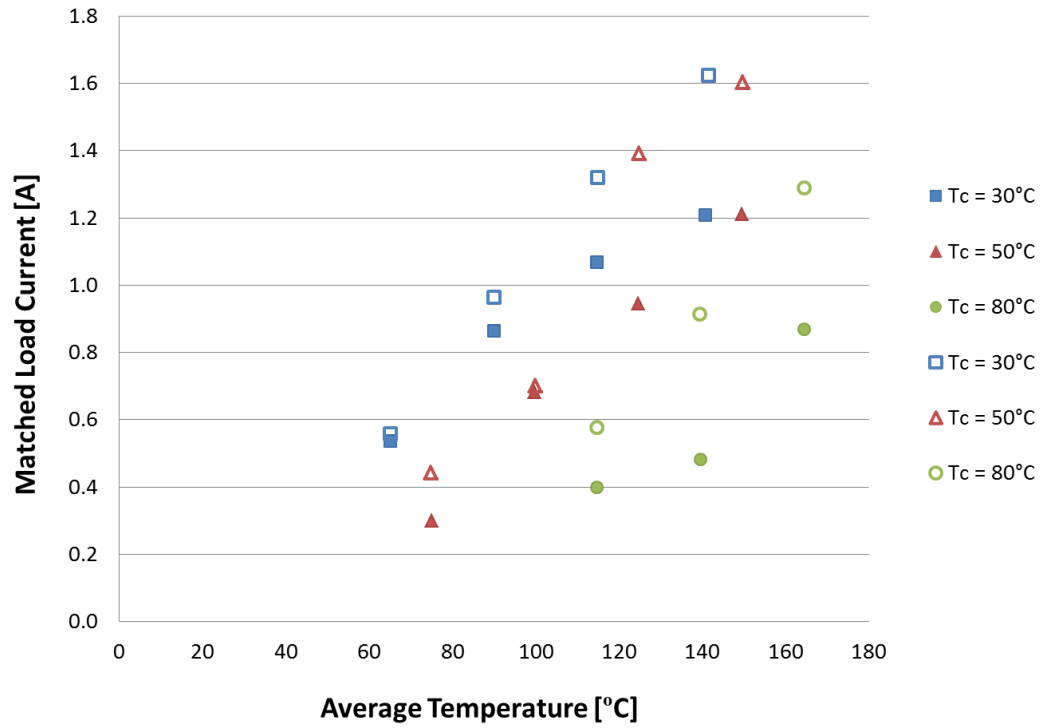


Figure 4.22 Experimentally measured current of the TEG1 12610-5.1 (filled symbols) and the TEG1B 12610-5.1 (hollow symbols) at the maximum power output.

The TEG1 has a much higher matched resistance than that of the TEG1B, both of which increase with average temperature, which can be seen in figure 4.23.

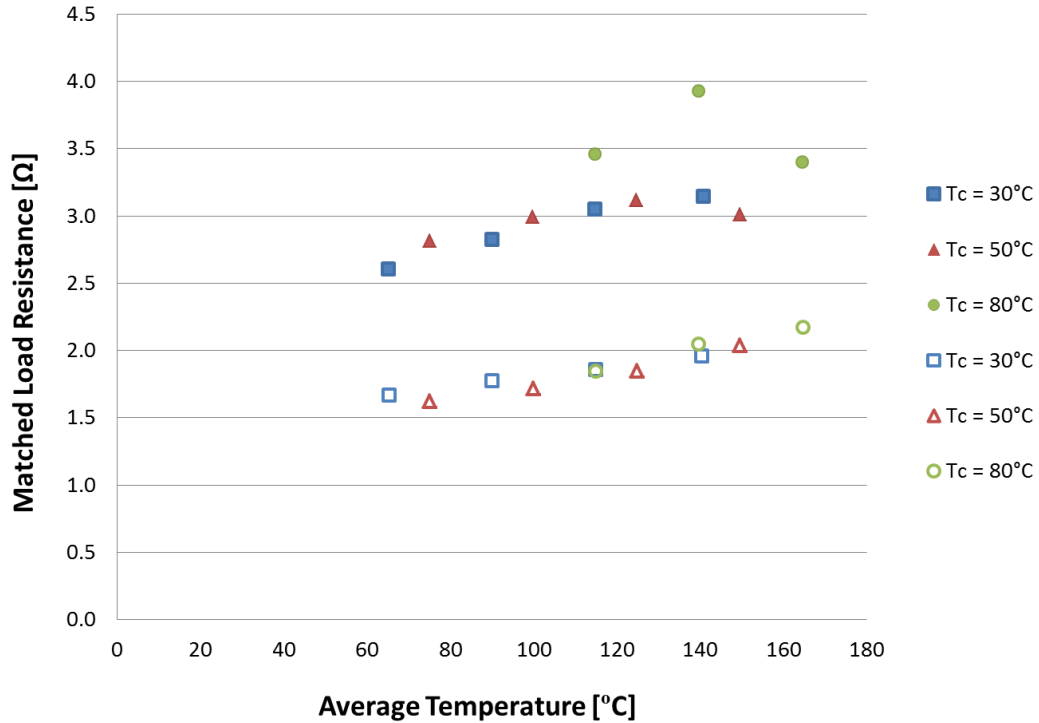


Figure 4.23 Experimentally measured resistance of the TEG1 12610-5.1 (filled symbols) and the TEG1B 12610-5.1 (hollow symbols) at which max power occurs.

Given the difference in the power output characteristics of the two TEG types, overlooking the difference in the magnitude of the power, a system can be designed with different electrical constraints in mind. For example, if the TEG system was to be used to charge a battery it would need a high enough voltage to charge the battery which would encourage the use of the TEG1-12610-5.1. However if both TEG1-12610-5.1 and TEG1B-12610-5.1 had a high enough voltage to charge the battery, then the TEG1B would be beneficial due to its high current providing faster recharging times. Similarly, if the TEG system is powering a device that has a high electrical resistance, then the TEG1 would make it easier to match the electrical resistance.

Tables 4.6 and 4.7 tabulate the data of the percentage increase or decrease in the electrical characteristics of the TEG1B over the TEG1 that was presented graphically in Fig. 4.18-4.23.

The current of the TEG1B consistently outperforms that of the TEG1 at all temperature differences at both the short circuit and matched resistance conditions. The fact that the TEG1B is a high temperature TEG is apparent at the matched load conditions where the TEG1B produces 48% more voltage than that of the TEG1 at a cold side temperature of 80°C. The voltage of the TEG1, however, is greater by as much as 33% at low cold side temperatures of 30 °C. As the average temperature increases, the TEG1B closes the gap in the magnitude of its voltage to as little as 0.3%.

The power produced by the TEGs perhaps shows that the TEG1B is a high temperature TEG where TEG1 is not. At the cold temperatures of 30°C, the power of the TEG1 is greater than that of the TEG1B by as much as 30%. As the cold side temperature rises to 80°C, the TEG1B produces 30% more power than the TEG1.

$$Difference = TEG1 - TEG1B \quad 4.6$$

$$\%Difference = 100 \times \frac{TEG1 - TEG1B}{TEG1} \quad 4.7$$

Table 4.6 Difference of the electrical characteristics of the TEG1B-12610-5.1 over the TEG1-12610-5.1

	Cold Side Temp [°C]	Cold Side Temp [°C]	Matched Voltage [V]	Matched Current [A]	Matched Resistance [Ω]	Matched Power [W]	Open Circuit Voltage [V]	Short Circuit Current [A]
Difference	30	100	0.47	-0.02	0.94	0.23	0.95	-0.05
		150	0.71	-0.10	1.03	0.44	1.41	-0.22
		200	0.79	-0.25	1.18	0.22	1.59	-0.51
		250	0.6	-0.41	1.17	-0.60	1.30	-0.87
	50	100	0.11	-0.14	1.16	-0.07	0.29	-0.29
		150	0.61	-0.02	0.94	0.39	0.89	-0.48
		200	0.64	-0.45	1.46	-0.42	1.02	-0.74
		250	0.44	-0.39	1.00	-0.72	0.82	-0.74
	80	150	0.32	-0.18	1.63	-0.06	0.61	-0.37
		200	0.01	-0.43	1.86	-0.81	0.02	-0.85
		250	0.035	-0.42	1.38	-0.79	0.37	-0.70

Table 4.7 Percentage difference of the electrical characteristics of the TEG1B-12610-5.1 over the TEG1-12610-5.

	Cold Side Temp [°C]	Cold Side Temp [°C]	Matched Voltage [V]	Matched Current [A]	Matched Resistance [Ω]	Matched Power [W]	Open Circuit Voltage [V]	Short Circuit Current [A]
% Difference	30	100	33.5	-4.1	36.1	30.8	33.6	-4.6
		150	29.1	-11.7	36.5	20.7	29.0	-12.5
		200	24.2	-23.6	38.7	6.2	24.3	-24.1
		250	15.7	-34.2	37.2	-13.0	16.9	-36.7
	50	100	13.1	-48.1	41.3	-28.7	16.5	-49.5
		150	29.9	-2.4	31.6	28.1	21.9	-35.2
		200	21.6	-47.1	46.7	-15.2	17.3	-38.9
		250	11.9	-32.1	33.3	-16.4	11.2	-30.2
	80	150	23.0	-45.2	47.0	-11.7	22.1	-46.8
		200	0.3	-89.3	47.3	-88.6	0.5	-85.7
		250	11.9	-48.3	40.6	-30.6	6.4	-39.3

4.7 Thermal conductivity

The thermal conductivity of a thermoelectric generator is composed of two distinct components: the thermal component and the electrical component. The thermal component refers specifically to the conductivity of the TEG when it is conducting no current so that it is not influenced by electricity flowing through the TEG. The electrical component arises due to the electrical and thermal coupling of the TEG that alters the conductivity depending on the magnitude of the current. This can be expressed in the following formula:

$$K_{TOTAL} = K_{ELECTRICAL} + K_{THERMAL} \quad 4.8$$

$$K_{ELECTRICAL} = \frac{\alpha^2 \bar{T}}{R_L + R_m} \quad 4.9$$

The thermal conductivity of a generator can be easily assessed at the open circuit voltage condition as there is no current flowing through the system so the electrical component of the system has no effect. The results for this are presented in figure 4.24 where they are presented as a thermal resistance calculated from the average of the generator's heat flux (Q_{HOT} and Q_{COLD}) and the temperature difference across it.

The thermal component of the generator is relatively stable for both the TEG1 and TEG1B with a percentage standard deviation of 8.4% and 2.5% respectively.

From equation 4.9 for a given TEG at a constant temperature difference, the maximum value for the electrical component occurs when the electrical load resistance is zero and the current is maximum. Using equation 4.9, the electrical component of the TEGs tested was calculated at the short circuit current condition using data obtained through experiments. The magnitude of the electrical component calculated was on average 9.6% for the TEG1 and 6.7% for the TEG1B. Both TEGs were tested for this change in thermal conductivity at three different temperature differences. The TEG thermal conductivity

was found to change in magnitude between the open circuit voltage, minimum thermal conductivity, and short

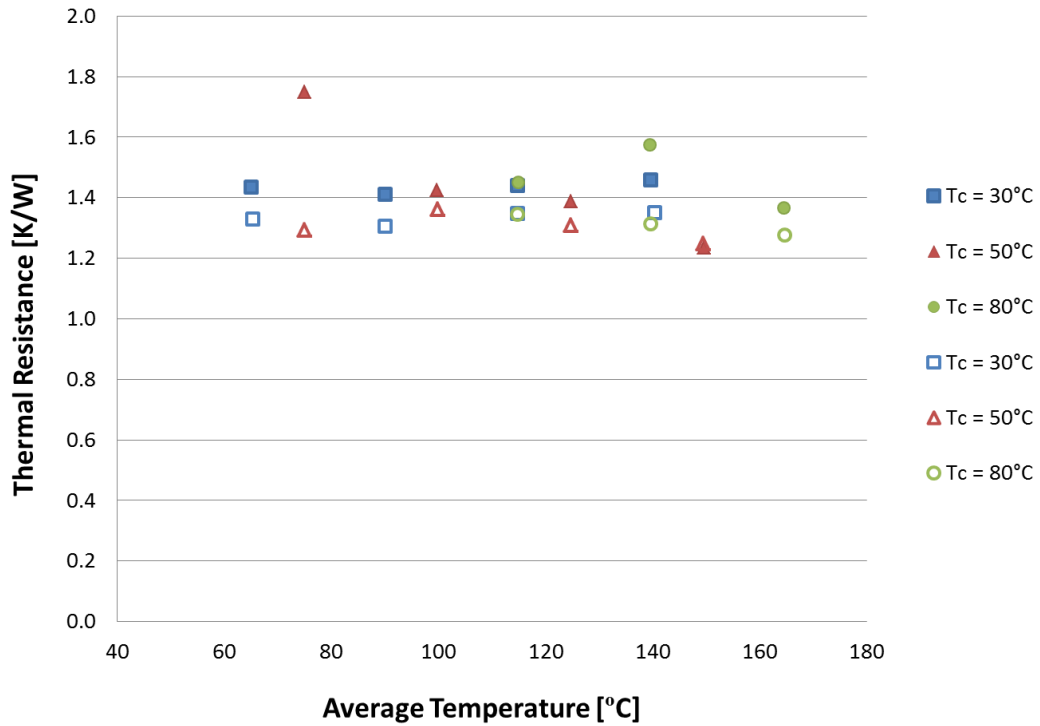


Figure 4.24 Thermal component of the overall thermal conductivity of a TEG1 (filled symbols) and a TEG1B (hollow symbols).

circuit current, maximum thermal conductivity, by 17.5% for the TEG1 and 18.5% for the TEG1B. This change in TEG thermal conductivity could only be a result of the electrical component as the thermal component only depends on the temperature difference which was constant for the experiments.

4.8 Mechanistic Model

With the linear relationship between the output of a thermoelectric generator and the temperatures, T_{HOT} and T_{COLD} , experienced by the generator, it is possible to create a mechanistic model to predict the performance of the TEG. Two linear relationships used

to create this mechanistic model are the open circuit voltage, equation 4.10, and short circuit current, equation 4.11.

$$I_{SC} = \frac{N\alpha_{CIRCUIT}(T_H - T_C)}{R_{TEG} + R_{LOAD}} \quad 4.10$$

$$V_{OC} = N\alpha_{CIRCUIT}(T_H - T_C) \quad 4.11$$

The mechanistic model is created by using a model reduction tool based on regression [36]. The result of the analysis are two equations for each TEG that predict the short circuit current and open circuit voltage at a single temperature difference which can be used to create the V-I curve at that temperature difference.

The equations generated for the TEG1 are:

$$V_{OC} = 0.9485 + 0.0338 T_H - 0.045 T_C \quad 4.12$$

$$I_{SC} = 0.6228 + 0.0102 T_H - 0.018 T_C \quad 4.13$$

These equations calculate the experimental data with an R^2 value of 0.9775 for the open circuit voltage and 0.9424 for the short circuit current.

The equations for the TEG1B are:

$$V_{OC} = -0.54 + 0.0316 T_H - 0.024 T_C \quad 4.14$$

$$I_{SC} = 0.2882 + 0.0143 T_H - 0.016 T_C \quad 4.15$$

These equations calculate the experimental data with an R^2 value of 0.989 for the open circuit voltage and 0.9714 for the short circuit current.

The outputs of the above equations of the mechanistic model are presented in figures 4.25-4.28 below:

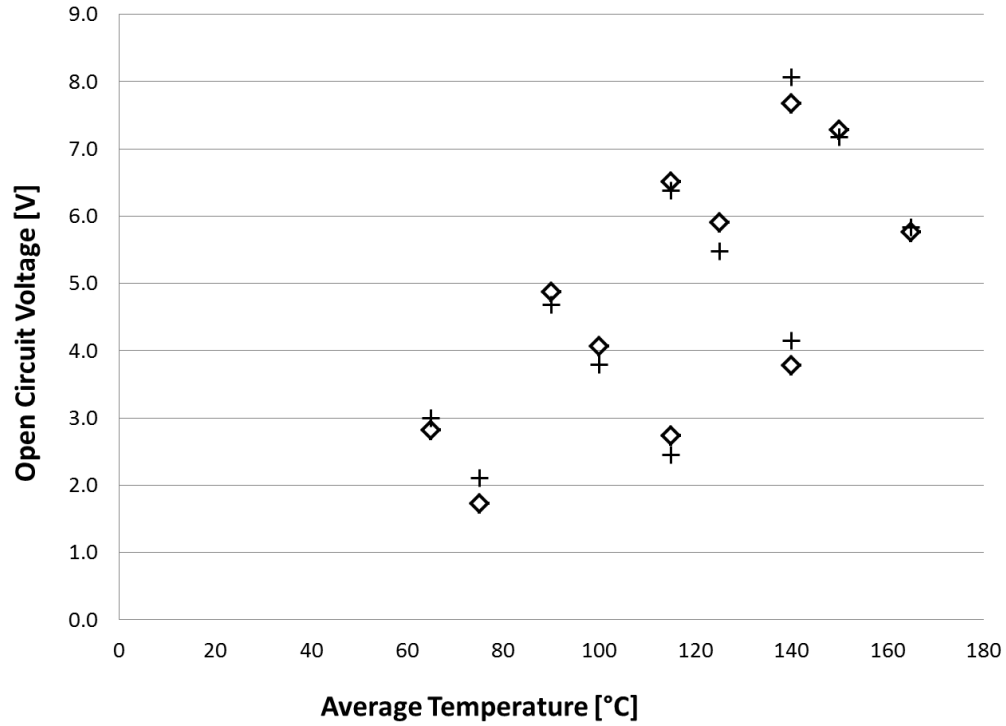


Figure 4.25 Open circuit voltage of the TEG1 12610-5.1. The diamonds are the experimentally measured values and the crosses the values predicted by equation 4.12

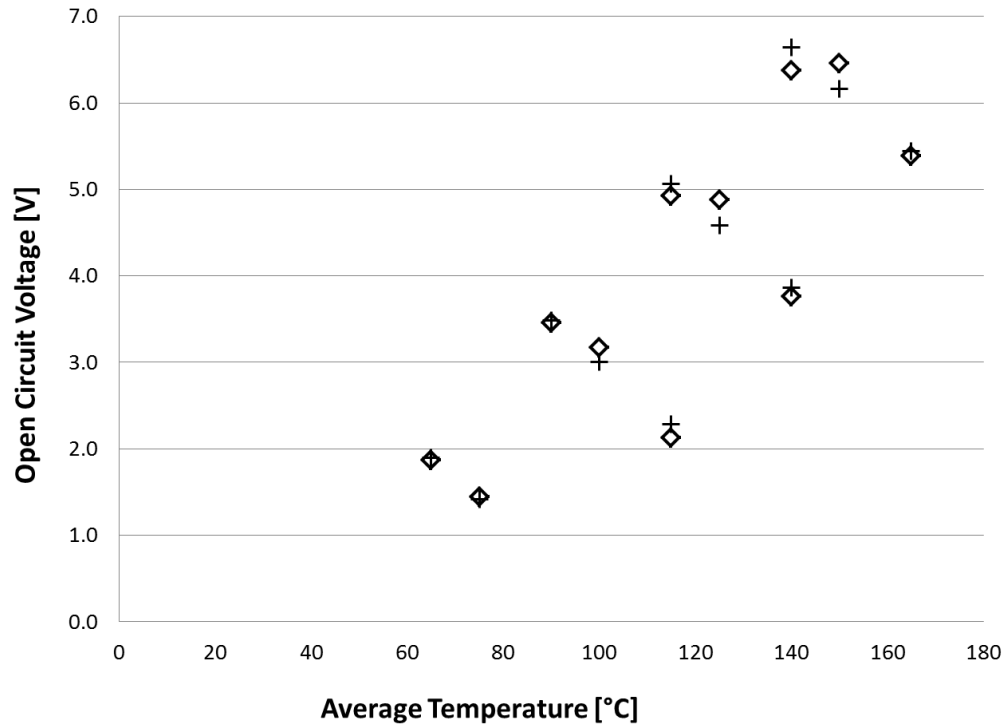


Figure 4.26 Open circuit voltage of the TEG1B 12610-5.1 The diamonds are the experimentally measured values and the crosses the values predicted by equation 4.14

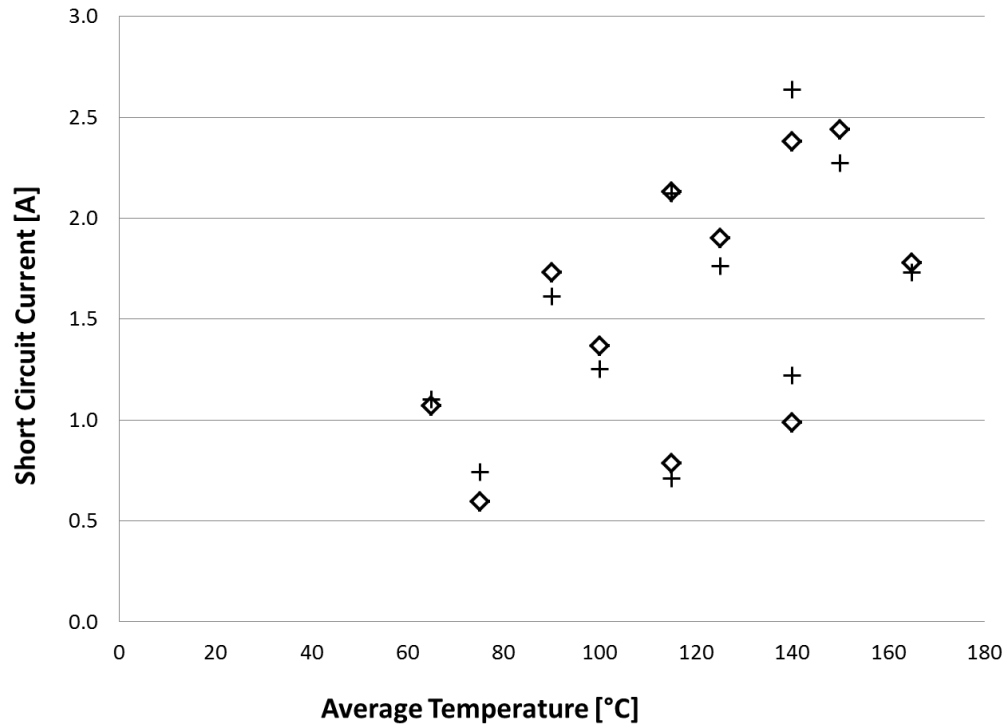


Figure 4.27 Short circuit current of the TEG1 12510-5.1. The diamonds are the experimentally measured values and the crosses the values predicted by equation 4.13

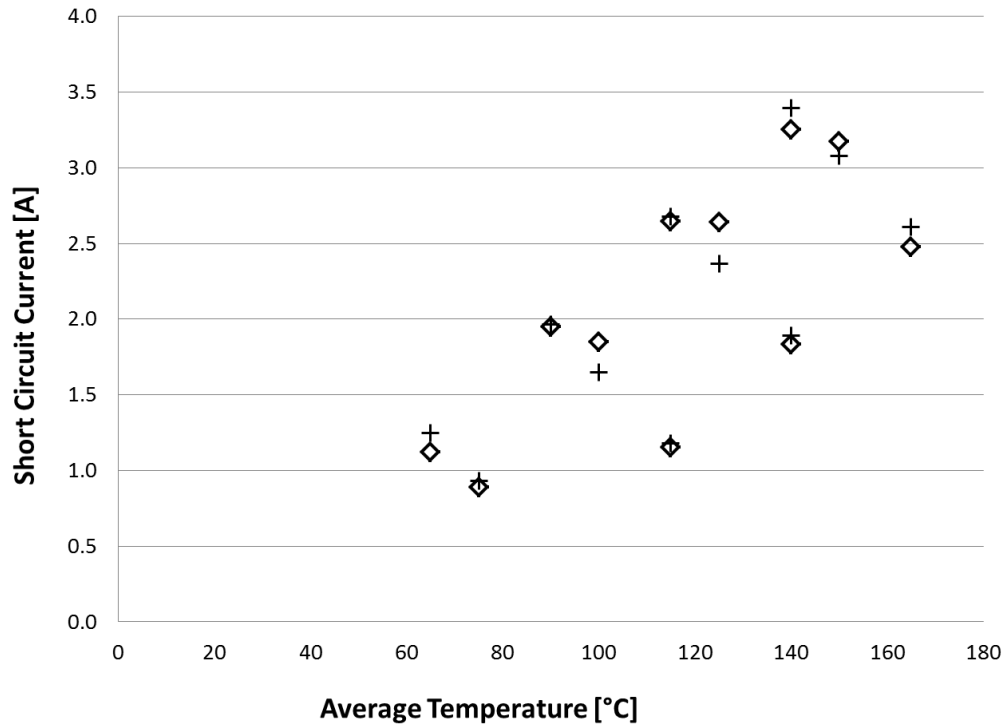


Figure 4.28 Short circuit current of the TEG1B 12610-5.1. The diamonds are the experimentally measured values and the crosses the values predicted by equation 4.15

With this mechanistic model predicting the short circuit current and open circuit voltage at any temperature difference, the power, current and voltage can be calculated for any applied electrical load. The Seebeck coefficient can also be calculated from the open circuit voltage and the internal resistance from the quotient of the open circuit voltage and short circuit current. This method of model creation allows for the accurate prediction of the power output from a TEG at any condition given a few experimental data points of any TEG.

The thermal conductivity of the TEG does not have a simple linear relationship that can be easily modelled using a mechanistic model. As stated in section 4.7, there is a relationship between the thermal conductivity and the current flowing through the TEG,

equation 4.9. This equation does not capture the change in thermal conductivity accurately as stated in that section being consistently 17-18% off. This indicates that the equation is overlooking something. The experimental results for thermal conductivity of the TEGS and that predicted using equation 4.9 are plotted in figure 4.29.

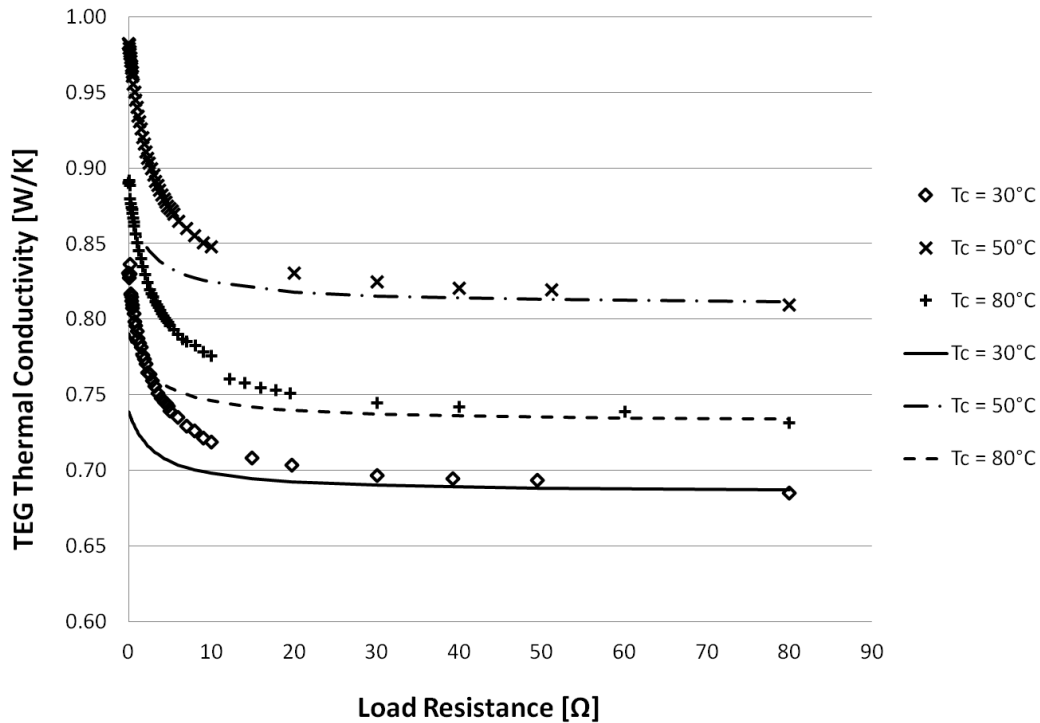


Figure 4.29 Thermal conductivity of a TEG1 12610-5.1 at a constant hot side temperature of 250°C and different cold side temperatures. The symbols are the experimental results and the lines the model.

The values for the model are obtained experimentally with the Seebeck coefficient calculated using the open circuit voltage and the internal resistance from the V-I curve. All the values of the electrical component can be seen to differ by a factor of 2.63 between the Eqn. 4.8 and experimental results. This factor itself varies by 5%. When this factor is included in the results the two lines agree very well as shown in figure 4.30.

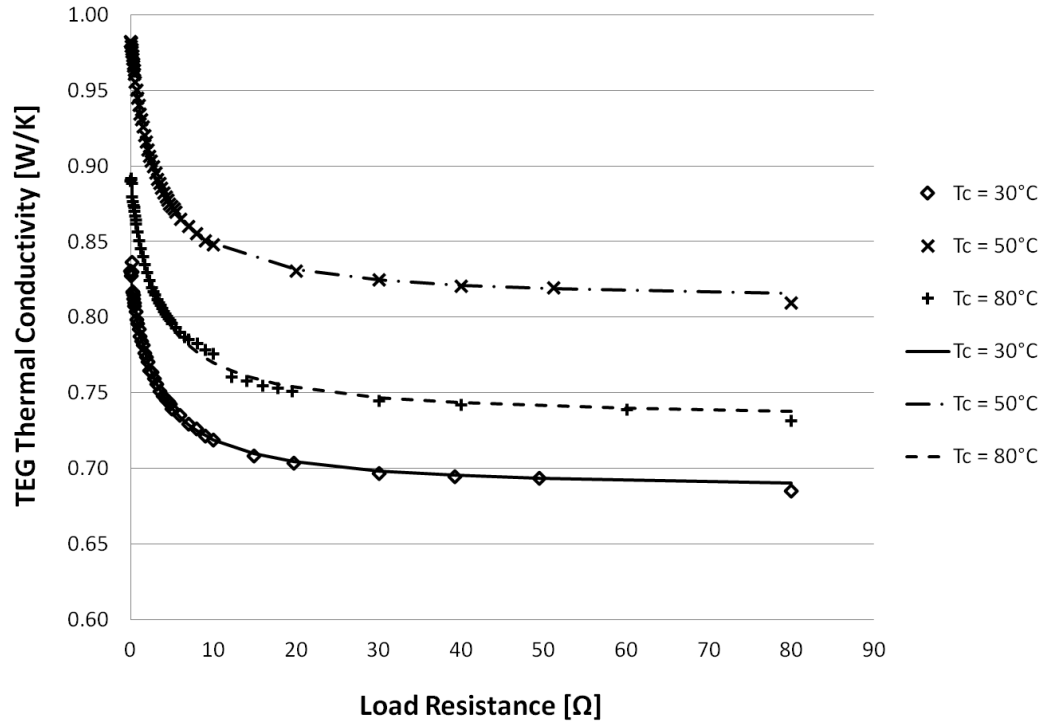


Figure 4.30 Thermal conductivity of a TEG1 12610-5.1 at a constant hot side temperature of 250°C and different cold side temperatures. The symbols are the experimental results and the lines are the modified model.

Calculated in the same fashion there is a factor of 2.61 for the TEG1B which varies by 13%. Equation 4.9 gives the correct trend as to how the thermal conductivity changes with current through a TEG but is consistently off by a factor of 2.6 for our experiments. With this factor of 2.6 incorporated to equation 4.8 as an empirical constant, a mechanistic model for the thermal conductivity of the thermoelectric generator can be calculated using the equation 4.16. The variables for this equation can be easily obtained from the same experiments that would be performed for the mechanistic models for current and voltage.

$$K_{TEG} = 2.6 \times \frac{\alpha^2 \bar{T}}{R_L + R_m} + K_{THERMAL} \quad 4.16$$

With these two models the performance of a thermoelectric generator can be accurately predicted over the range of temperatures at which the experimental data was performed.

- Given the temperature of the available heat source and sink for power generation and the resistance of the electrical load to be powered a thermal resistance network can be created using the mechanistic model for thermal conductivity and heat transfer correlations.
- This thermal resistance network allows for the predication of the temperature difference across the generators which involves an iterative process as the Seebeck coefficient and internal resistance change with temperature difference affecting the thermal resistance of the TEG.
- With the temperature difference across the TEG, a V-I curve can be created using the mechanistic models for open circuit voltage and short circuit current.
- This V-I curve and the known resistance of the load being powered by the generators allow for the power, voltage and current of the generator to be calculated.

5 Conclusion and Future Work

The objective of this research was the characterisation of thermoelectric generators both thermally and electrically and the coupling of these two aspects. This thesis is part of a larger research effort, the P.O.W.E.R. project, which is performing research into the waste heat recovery of pizza ovens in conjunction with Pizza Pizza. The reason this thesis focused on the thermoelectric aspect of the P.O.W.E.R. project was while there was a large amount of data reported both by industry and in research papers, much of it was contradictory, conflicting or insufficient. The contribution of this thesis to the P.O.W.E.R. project was to experimentally characterise the performance of the two commercial TEGs being considered for use in the P.O.W.E.R. project. These TEGs were to be characterised both thermally and electrically in conditions similar to those expected in the P.O.W.E.R. system. This characterisation also led to the development of a mechanistic model that can be used to predict the power output of a generator and the characteristics of that power output over a range of temperatures between 30-80°C on the cold side and 100-250°C on the hot.

The experiments performed have shown that the two TEGs studied for the use in the Pizza Pizza project deviate considerably from manufacturer's data supplied. The matched power output, one of the more significant parameters when considering thermal energy conversion, is overestimated by an average of 50% for the TEG1 and deviates from the manufacturer's results by an average of 13% for the TEG1B. Unfortunately, because of the lack of information about the manufacturer's testing methodologies it is unclear as to whether this inaccuracy is due to inconsistent manufacturing standards or material quality which leads to the production of inconsistently performing TEGs or it the inaccuracies of the testing methodology used to characterise their products.

There exists a need for a standard method of testing thermoelectric generators to prevent inaccuracies such as those associated with the manufacturer's data. The other objective of this thesis, which was independent of the P.O.W.E.R. project, was to test and validate an experimental facility designed for the specific purpose of characterising thermoelectric

generators. The TEMTester was designed to be a standardised testing apparatus for thermoelectric generators. This would eliminate the questionability associated with the manufacturer's data and would ensure that all data reported on thermoelectric generators, in industry and research, is consistent so that comparisons drawn between two sets of data are valid.

The results of this thesis have shown that the variance of the performance of TEGs is quite significant with the TEG max power found to vary by as much as 20% and 7.7% for TEG1 and TEG1B respectively. This variance has large implications for the design of thermoelectric systems as the power produced by linked TEGs is limited to the least efficient. With the sample size so small (4 TEGs tested of each model), it is impossible to say anything with any statistical certainty. However, considering the small batch used, the probability is that the variance is at least the value reported in this thesis or greater.

For the purpose of the design of the waste heat recovery system for the P.O.W.E.R. project, a comprehensive experimental comparison was made between the two TEGs proposed for its construction. It was found that the TEG1B, designed as a high temperature TEG, outperformed the TEG1 in terms of energy conversion at higher temperatures by as much as 10%. However, the TEG1B has a higher output current by almost 35% and the TEG1 has a higher output voltage by almost 20% meaning that given the requirements of the electrical load one TEG may be more beneficial even when it produces less power. The TEG best suited to the overall function of the P.O.W.E.R. project prototype has yet to be determined as more research has yet to be performed on other aspects but the results of this thesis give the project the full accounting it needs both thermally and electrically to optimize the system.

With the data collected in the characterisation of both TEG1 and TEG1B, two mechanistic models were created to predict the electrical output of these thermoelectric generators within the range of temperature differences tested at any applied electrical load. This model predicts the open circuit voltage and short circuit current of a generator for a given temperature difference which allows for the V-I curve to be generated giving

the power characteristics at all load resistance values. The models have excellent accuracy in recreating the experimental data with an R^2 value of 0.9775 and 0.9424 for the voltage and current of TEG1 respectively and 0.989 and 0.9714 for the voltage and current of TEG1B respectively.

5.1 Future work:

The testing done to investigate the variance of TEGs comprised of a very small sample size considering that TEG power generation devices could contain up to as many as 200 TEGs if not more. To truly be able to quantify the statistical variance of the different parameters of TEGs, many more of them must be tested under the same conditions. With this accurate and quantified variance, the variance can be included in different models to thermoelectric device design to give a more accurate idea of their output.

The literature review presented a critical review on the modelling methods of thermoelectric generators, both very complex models that include all thermoelectric phenomena and the more basic that simplify those different phenomena. It would seem that the only models that yield good results are those that experimentally extract the data from the TEG that they are modelling and use the result in the model as it already encompasses all the complex phenomena that others try to model. If accurate data were available about all the relevant parameters used in thermoelectric modelling (Seebeck coefficient, Thomson coefficient, electrical resistivity, thermal conductivity, and specific heat capacity), it is possible that the complexity of thermoelectrics can be accurately predicted.

While the TEMTester is an excellent device for the full characterisationh it is not a good method of testing TEGs quickly for the verification process proposed for grading TEGs on their performance prior to their inclusion in an energy producing device. It is possible that a more basic though less accurate testing system could be designed to quickly quantify the TEGs to be used in a thermoelectric system and provide a comparison to

other TEGs to be used eliminating the “weakest link” in a group of TEGs easily and efficiently.

References

- [1] James, S. R., (1989), "Hominid use of fire in the lower and middle Pleistocene. A review of the evidence", *Current Anthropology*, Vol. 30, pp. 1-26.
- [2] Benditt, J., (1989), "Cold water on the fire: a recent survey casts doubt on evidence for early use of fire", *Scientific American*, Vol. 260 (5), pp. 21-22.
- [3] Canadian Electricity Association (2012, March), "Key Canadian Electricity Statistics", Retrieved March 12th 2013 from:
http://www.electricity.ca/media/Industry%20Data%20and%20Electricity%20101%20May%202012/KeyCanadianElectricityStatistics_2012.pdf.
- [4] U.S. Energy Information Administration (2012, Sept), "Electricity Net Generation: Total (All Sectors), Selected Years, 1949-2011", *The Annual Energy Review*, pp. 224-225.
- [5] Majumdar, A., (2008, November), "Tapping America's Secret Power Source", Retrieved March 12th from: <http://www.greentechmedia.com/articles/read/tapping-americas-secret-power-source-5259/>.
- [6] Bédard, S., (2009), "Waste Heat to Power: A Process Integration Perspective", *Energy 2009: Lean and Green Conference*, CETC Number 2009-200 / 2010-02-26.
- [7] Chen, M., (2011), "A three-dimensional numerical model of thermoelectric generators in fluid power systems", *International Journal of Heat and Mass Transfer*, Vol. 54, pp.345-355.
- [8] Gao, J., et al., (2012), "A Thermoelectric Generation System and its Power Electronics Stage", *Journal of Electronic Material*, 10.1007/S11664-012-2034-5, pp. 1043-1050.
- [9] Kajikua, T., (2009), "Approach to the Practical Use of Thermoelectric Power Generation", *Journal of Electronic Materials*, Vol. 38 (7), pp.1083-1088.

- [10] Seebeck, TH. J. (1895), “Magnetische Polarisation der Metalle und Erze durch Temperatur-Differenz”, Leipzig, Germany, Wilhelm Engelmann.
- [11] Min, G., (2010), “Energy Harvesting for Autonomous Systems”, Norwood, MA, Artech House pp. 137.
- [12] MacDonald, D.K.C., (1966), “Thermoelectricity: An Introduction to the Principles”, Mineola, New York, Dover Publications Inc., pp. 17-18.
- [13] Snyder, G. J., (2004), “Disordered zinc in Zn_4Sb_3 with phonon-glass and electron-crystal thermoelectric properties”, *Nature*, Vol. 3, pp.458-463.
- [14] Min, G., Rowe, D. M., (1996), “Design theory of thermoelectric modules for electrical power generation”, *IEE Proc.-Sci. Meas. Technol.*, Vol. 143 (6), pp. 351-356.
- [15] Palacios, R. et al., (2009), “Analytical procedure to obtain internal parameters from performance curves of commercial thermoelectric modules”, *Applied Thermal Engineering*, Vol. 29 (17-18), pp. 3501–3505.
- [16] Hodes, M., (2004), “One-dimensional analysis of thermoelectric generation”, *IEEE Tran. Components and Packaging Technologies*, Vol. 28 (2), pp. 218-229.
- [17] Quan, R., et al., (2012), “Design of a Novel Heat Exchanger Using in Automobile Exhaust Thermoelectric Generator”, *Advanced Materials Research*, Vols. 430-432, pp. 1428-1432.
- [18] Ahiska, R et al. (2012) “A new method and computer-controlled system for measuring the time constant of real thermoelectric modules” *Energy Conversion and Management* Vol. 53, pp. 314–321
- [19] Ahiska, R., Mamur, H., (2012), “A test system and supervisory control and data acquisition application with programmable logic controller for thermoelectric generators”, *Energy Conversion and Management*, Vol. 64, pp. 15–22.

[20] Min, G., (2009), "A novel principle allowing rapid and accurate measurement of a dimensionless thermoelectric figure of merit", *Meas. Sci. Technol.*, Vol. 12, pp. 1261-1262.

[21] Lazard, M., (2009), "Heat Transfer in Thermoelectricity: Modelling, Optimization and Design" *Proceedings of the 7th IASME / WSEAS International Conference on heat transfer, thermal engineering and environment*, pp.129-134.

[22] Yu, J., Zhao H., (2007), "A numerical model for thermoelectric generator with the parallel-plate heat exchanger", *Journal of Power Sources*, Vol. 172, pp. 428–434.

[23] Chen, M., Rosendahl, L. A., Condra, T., (2011), "A three-dimensional numerical model of thermoelectric generators in fluid power systems", *International Journal of Heat and Mass Transfer*, Vol. 54, pp. 345–355

[24] Sandoz-Rosado, E., Stevens, R., (2010), "Robust Finite Element Model for the Design of Thermoelectric Modules", *Journal of Electronic Materials*, Vol. 39, No. 9, pp. 1848-1855.

[25] Hsiao, Y. Y., Chang, W.C., Chen, S. L., (2010), "A mathematic model of thermoelectric module with applications on waste heat recovery from automobile engine", *Energy*, Vol. 35, pp. 1447–1454.

[26] Xuan, X.C. et al., (2002), "A general model for studying effects of interface layers on thermoelectric devices performance", *International Journal of Heat and Mass Transfer*, Vol. 45, pp. 5159–5170.

[27] Kumar, S., et al., (2013), "Thermoelectric Generators for Automotive Waste Heat Recovery Systems Part I: Numerical Modeling and Baseline Model Analysis", *Journal of electronic materials*, 10.1007/S11664-013-2471-9, pp. 665-674.

[28] Kim, S., (2013), "Analysis and modeling of effective temperature differences and electrical parameters of thermoelectric generators", *Applied Energy*, Vol. 102, pp. 1458–1463.

[29] Carmo, J. P., (2011), “Characterization of thermoelectric generators by measuring the load-dependence behaviour”, *Measurement*, Vol.44, pp. 2194–2199.

[30] Rauscher, L., et al., (2006), “Efficiency determination and general characterization of thermoelectric generators using an absolute measurement of the heat flow”, *Meas. Sci. Technol.*, Vol. 16, pp. 1054–1060.

[31] Takazawa, H., et al., (2006), “Efficiency measurement of thermoelectric modules operating in the temperature difference of up to 550K”, *Proceedings International Conference on Thermoelectrics*, pp. 189-192.

[32] Sandoz-Rosado, E., Stevens, R., (2009), “Experimental Characterization of Thermoelectric Modules and Comparison with Theoretical Models for Power Generation”, *Journal of Electronic Materials*, Volume 39 (9), pp. 1848-1855.

[33] Rodriguez, J. G., et al., (2009), “Study of thermoelectric systems applied to electric power generation”, *Energy Conversion and Management*, Vol. 50, 1236–1243.

[34] Tanji, Y., et al., (1999), “Electric and Thermal Contact Resistances of the New Type Thermoelectric Module Assembled by a Screwing Method”, *Proceedings 18th International Conference on Thermoelectrics*, pp. 260-265.

[35] Adams, T. A., (2012), “Lecture 4-1: Model Reduction W/ Regression”, lecture notes distributed in *702X Advanced PSE Tools and Methods* at McMaster University, Hamilton, Ontario on 22nd of November 2012.

[36] Apertet, Y., et al., (2012), “Optimal working conditions for thermoelectric generators with realistic thermal coupling”, *Europhysics Letters*, 10.1209/0295-5075, Vol. 97 (2), 28001.

APPENDIX A

The manufacturer provides data for their products in two forms. The first being two tables that provide pertinent data for a TEG at a specific data point. The second is in the form of five charts detailing, the matched load power, matched load voltage, matched load current, matched load resistance and open circuit voltage under different temperature conditions all at matched load conditions. A final chart is also provided detailing power and voltage as a function of the current.

The manufacturer's data is at best questionable, a fact that is supported by the fact that the tables and charts directly contradict each other for the TEG1-12610-5.1. The table states the power at 300°C to 30°C is 5.1W and the charts represent them at 9.15W.

In this appendix, the Tables of data are presented along with the charts which have been digitized for both TEG1 and TEG1B. Alongside that data, data is presented that has been extrapolated from the given. Given the fact that the Voltage-Current curve for a TEG is a straight line the curve can be found using any two points on the curve. Those two points are provided at any temperature difference by the matched voltage, matched current and open circuit voltage charts.

Table A1 Data Table provided by Manufacturer for TEG1-12610-5.1

TEG1-12610-5.1			
Hot Side Temperature	Th	300	°C
Cold Side Temperature	Tc	30	°C
Open Circuit Voltage	Voc	7.8	V
Matched Load Resistance	Rm	3	Ω
Matched Load Voltage	Vm	3.9	V
Matched Load Current	Im	1.3	A
Matched Load Power	Pm	5.1	W
Heat Flow		113	W
Heat Flow		7	W/cm ²

Table A2 Data Table provided by Manufacturer for TEG1B-12610-5.1

TEG1B-12610-5.1			
Hot Side Temperature	Th	300	°C
Cold Side Temperature	Tc	30	°C
Open Circuit Voltage	Voc	7.2	V
Matched Load Resistance	Rm	1.8	Ω
Matched Load Voltage	Vm	3.6	V
Matched Load Current	Im	2	A
Matched Load Power	Pm	7.1	W
Heat Flow		148	W
Heat Flow		9.2	W/cm ²

The Voltage-Current charts gives the voltage and current values for the TEG for all temperature differences for the cold side temperatures of 30°C, 50°C and 80°C. This allows for the calculation of power and resistance to be calculated also.

Table A3 Data extracted from the Manufacturer’s Charts on TEG1-12610-5.1

TEG 5.1 A						
Cold Side Temperature T _c	Hot Side Temperature T _h	Matched Load Current I _m	Matched Load Voltage V _m	Matched Load Power P _m	Matched Load R _m	Open Circuit Voltage V _{oc}
[°C]	[°C]	[A]	[V]	[W]	[Ω]	[V]
30	100	0.663	1.862	1.103	2.408	3.203
30	150	1.018	3.185	2.798	2.675	5.429
30	200	1.296	4.455	4.867	2.892	7.520
30	250	1.522	5.555	7.054	3.059	9.332
50	100	0.455	1.299	0.532	2.521	2.307
50	150	0.821	2.635	1.872	2.767	4.501
50	200	1.114	3.905	3.685	2.962	6.593
50	250	1.346	4.992	5.655	3.112	8.404
80	150	0.546	1.810	0.887	2.892	3.143
80	200	0.854	3.054	2.266	3.057	5.191
80	250	1.109	4.180	3.882	3.174	7.046

Table A4 Data extracted from the Manufacturer's Charts on TEG1B-12610-5.1

TEG 5.1 B						
Cold Side Temperature T _c	Hot Side Temperature T _h	Matched Load Current I _m	Matched Load Voltage V _m	Matched Load Power P _m	Matched Load R _m	Open Circuit Voltage V _{oc}
[°C]	[°C]	[A]	[V]	[W]	[Ω]	[V]
30	100	0.711	0.907	0.625	1.269	1.797
30	150	1.122	1.618	1.802	1.442	3.225
30	200	1.462	2.336	3.416	1.599	4.653
30	250	1.743	3.017	5.262	1.733	6.019
50	100	0.461	0.646	0.291	1.390	1.290
50	150	0.875	1.335	1.163	1.529	2.672
50	200	1.235	2.038	2.515	1.653	4.054
50	250	1.537	2.713	4.172	1.767	5.405
80	150	0.577	0.936	0.523	1.617	1.873
80	200	0.913	1.625	1.483	1.783	3.255
80	250	1.191	2.299	2.733	1.931	4.591

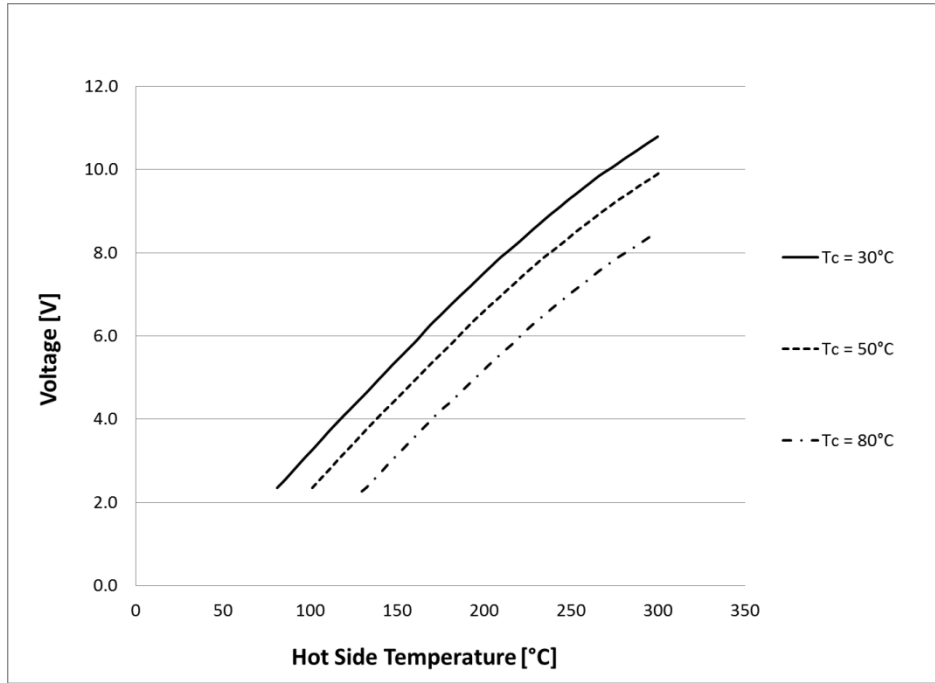


Figure A0.1 Manufacturer's Data for Open Circuit Voltage of the TEG1-12610-5.1A

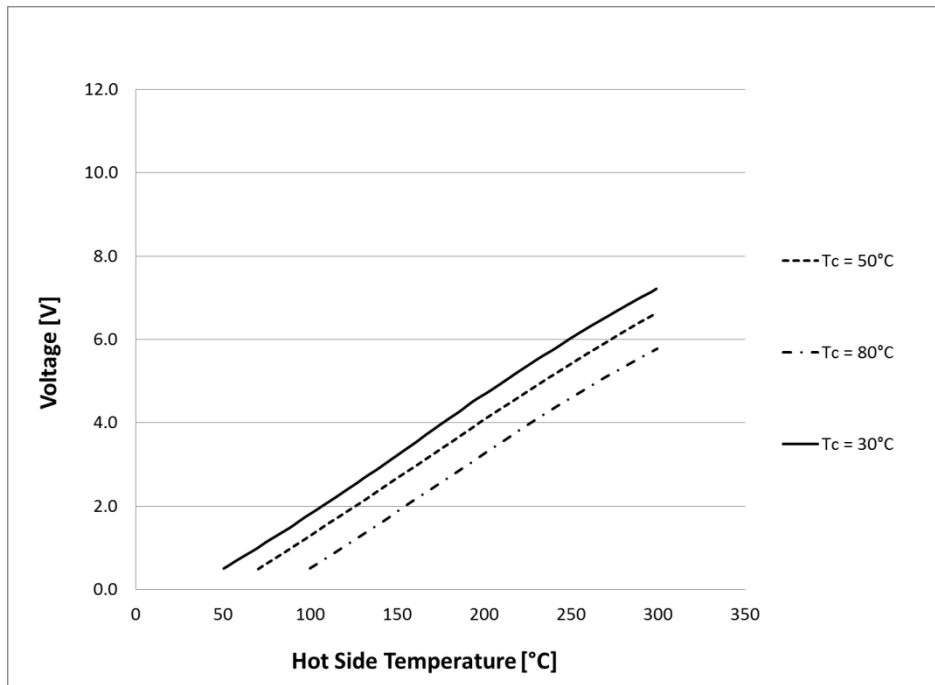


Figure A0.2 Manufacturer's Data for Open Circuit Voltage of the TEG1B-12610-5.1A

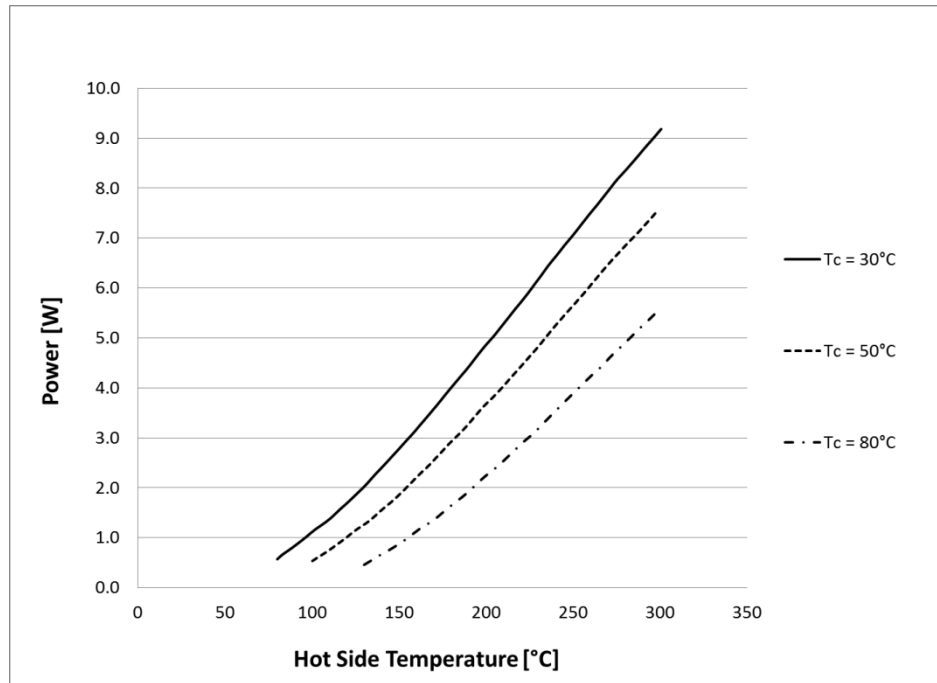


Figure A0.3 Manufacturer's Data for Matched Power Output of the TEG1-12610-5.1A

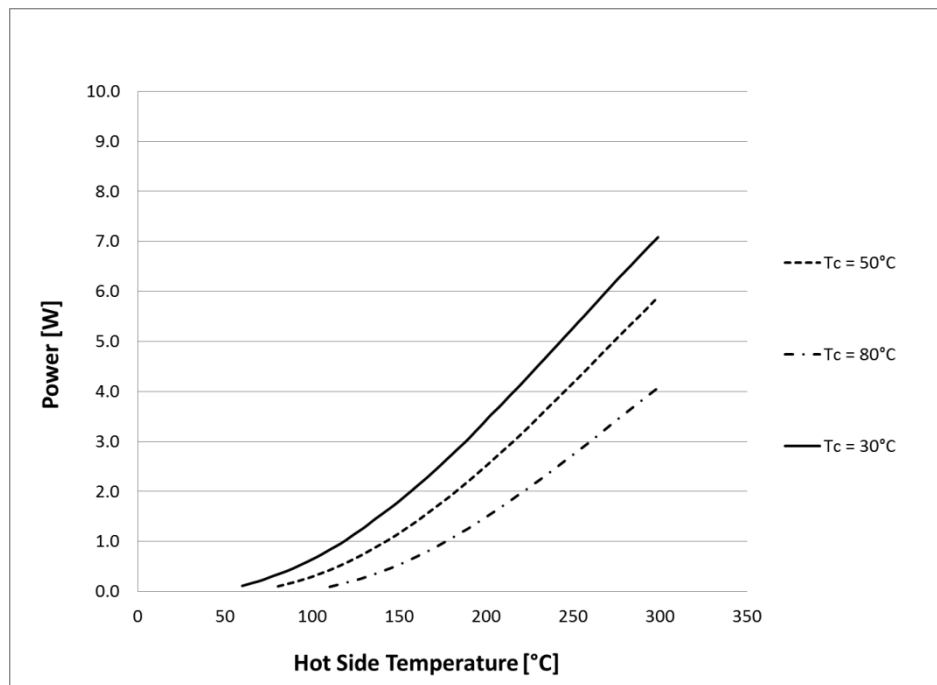


Figure A0.4 Manufacturer's Data for Matched Power Output of the TEG1B-12610-5.1A

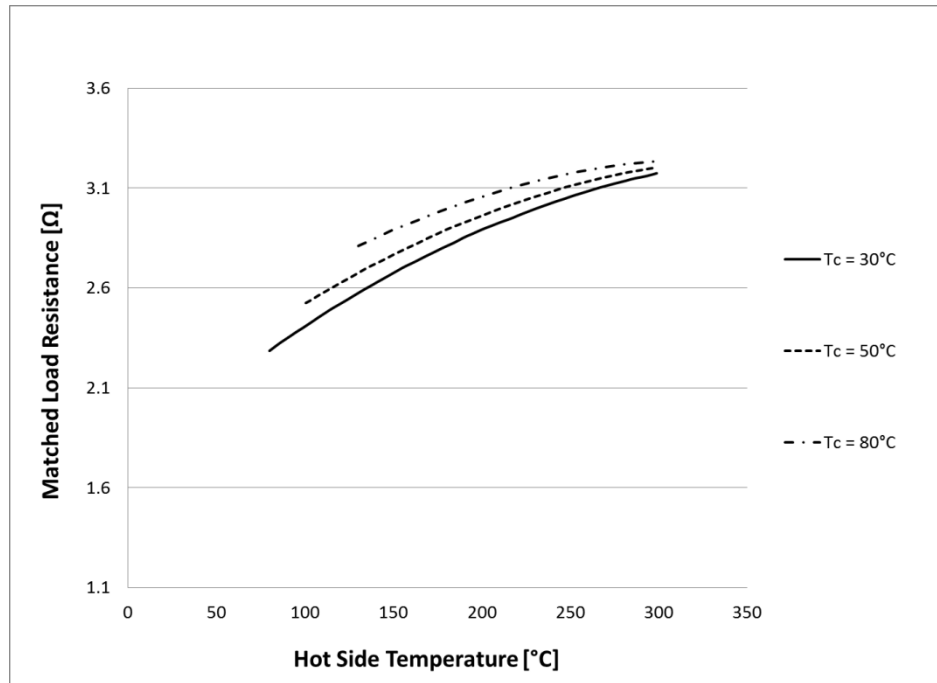


Figure A0.5 Manufacturer's Data for Matched Load Resistance of the TEG1-12610-5.1A

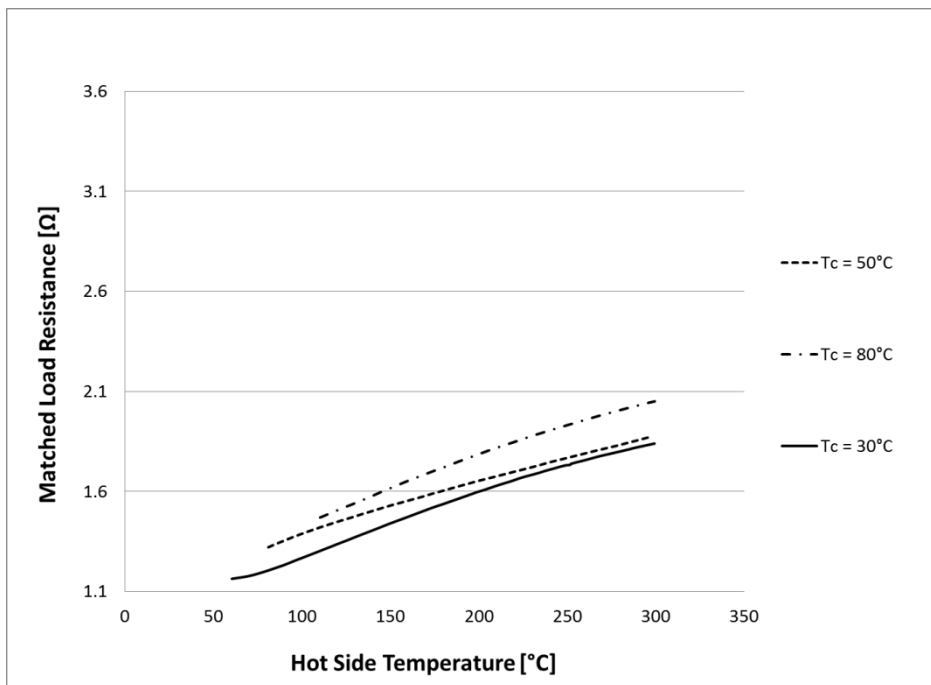


Figure A0.6 Manufacturer's Data for Matched Load Resistance of the TEG1B-12610-5.1A

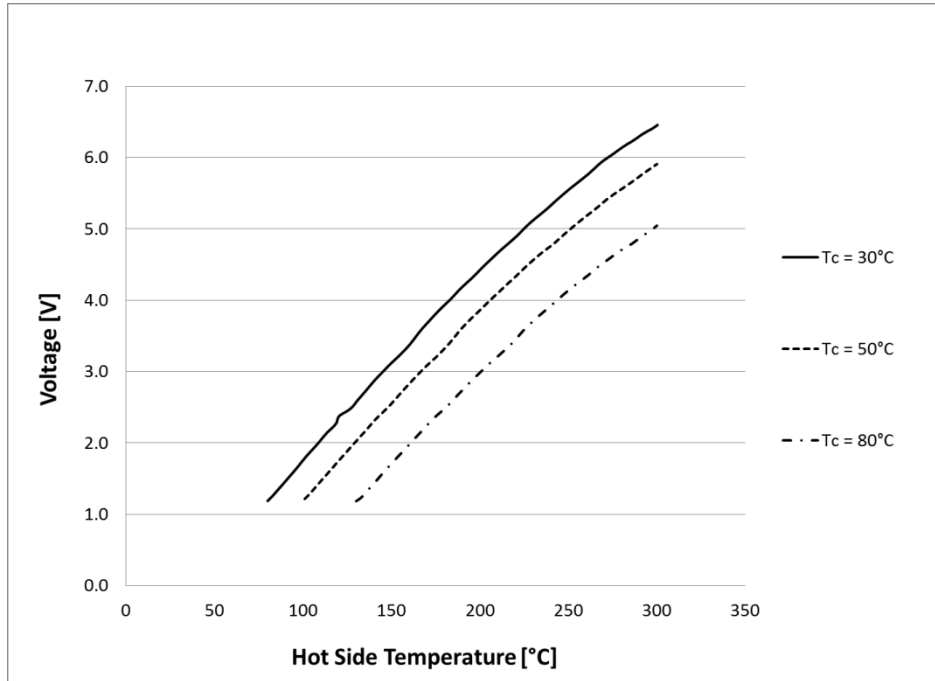


Figure A0.7 Manufacturer's Data for Matched Load Voltage of the TEG1-12610-5.1A

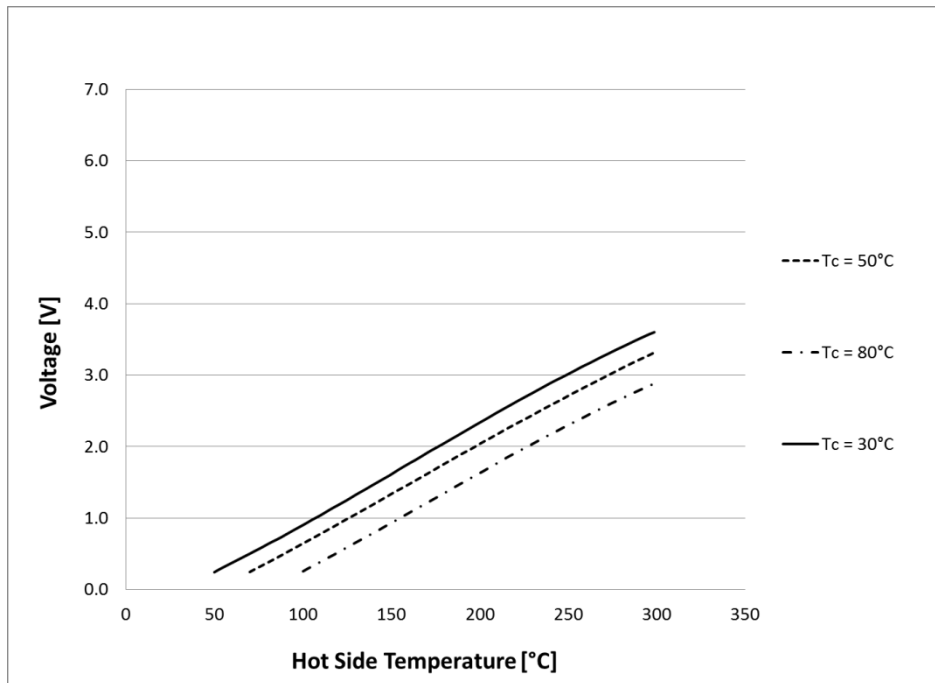


Figure A0.8 Manufacturer's Data for Matched Load Voltage of the TEG1B-12610-5.1A

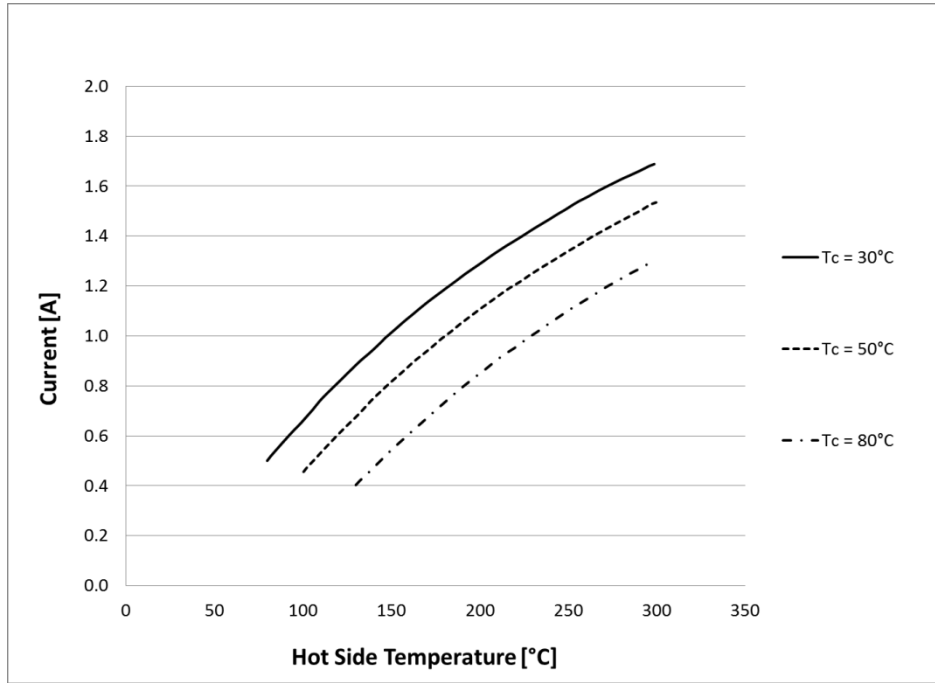


Figure A0.9 Manufacturer's Data for Matched Load Current of the TEG1-12610-5.1A

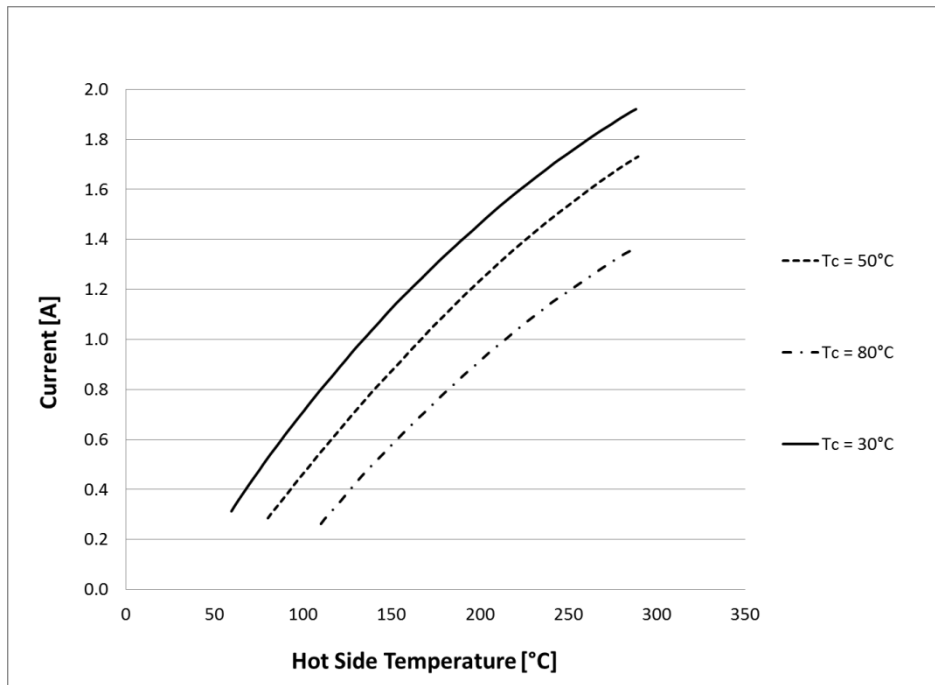


Figure A0.10 Manufacturer's Data for Matched Load Current of the TEG1B-12610-5.1A

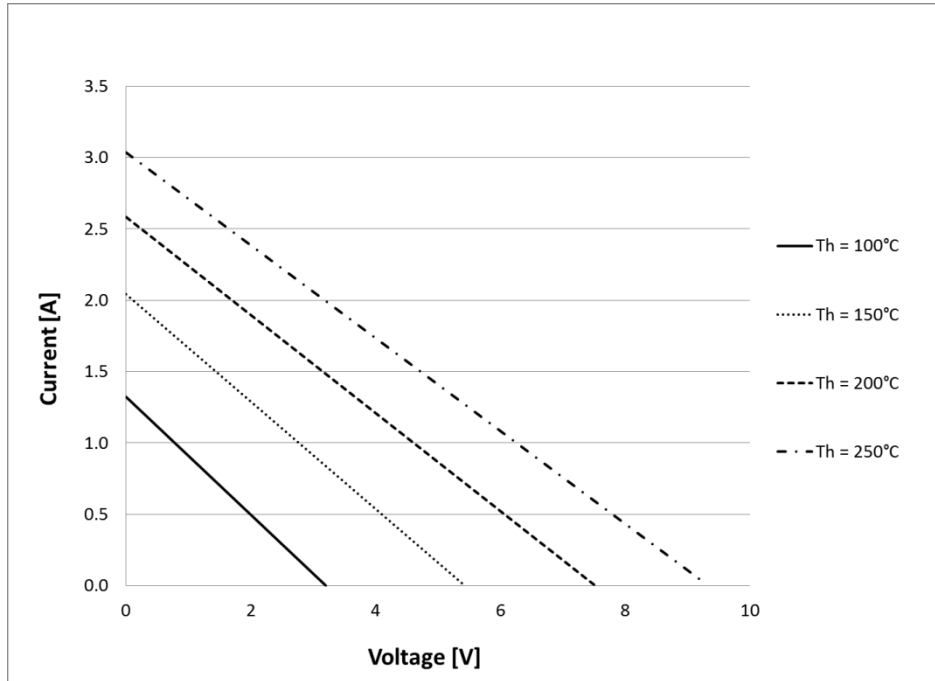


Figure A0.11 Extrapolated Manufacturer's V-I curve for TEG1-12610-5.1 with a constant cold side temperature, T_c , of 30°C at various hot side temperatures

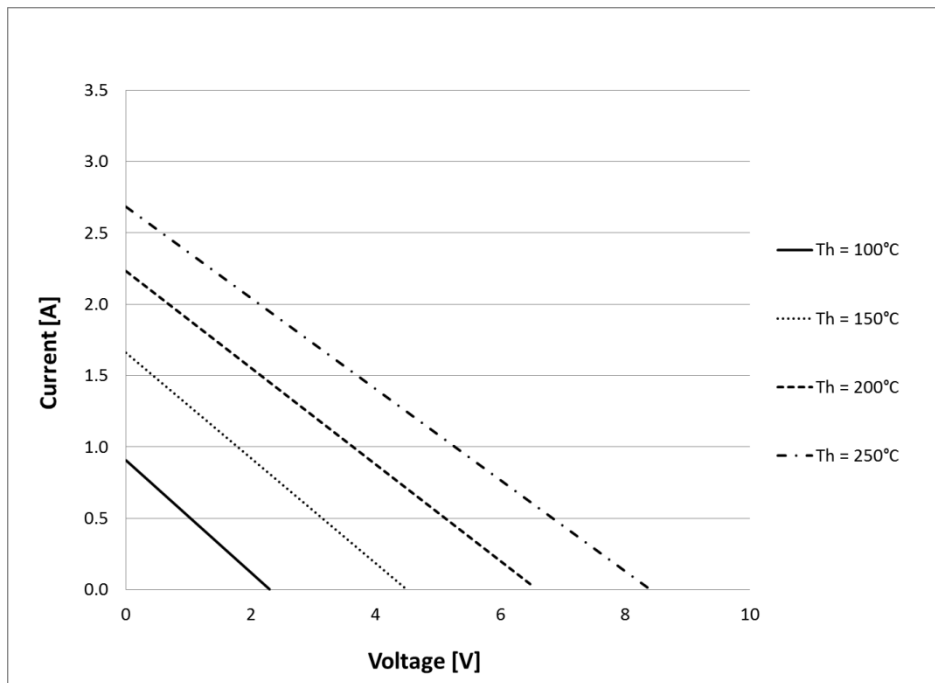


Figure A0.12 Extrapolated Manufacturer's V-I curve for TEG1-12610-5.1 with a constant cold side temperature, T_c , of 50°C at various hot side temperatures

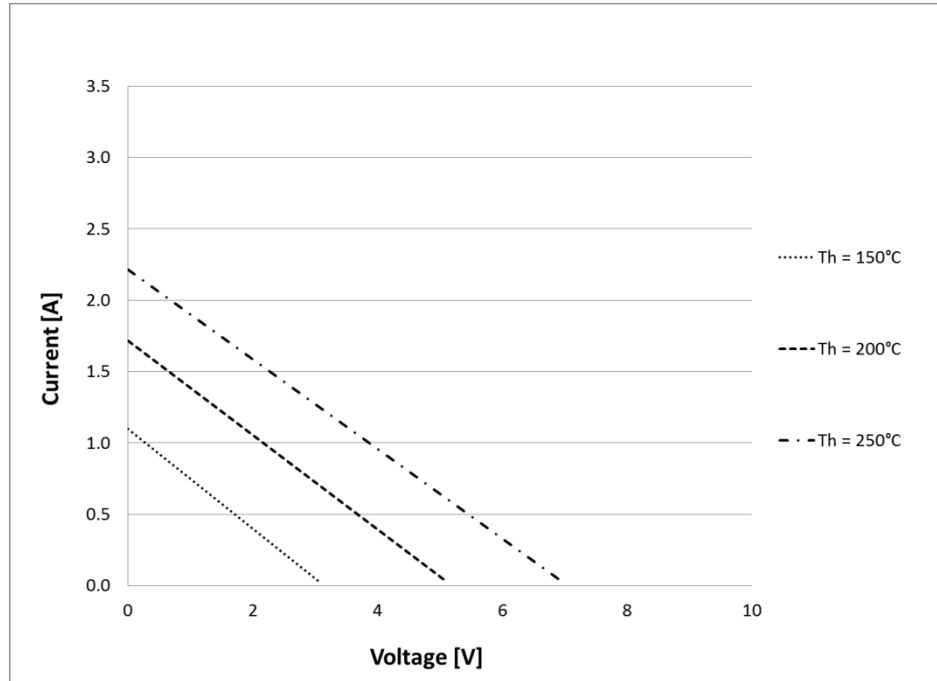


Figure A0.13 Extrapolated Manufacturer's V-I curve for TEG1-12610-5.1 with a constant cold side temperature, T_c , of 80°C at various hot side temperatures

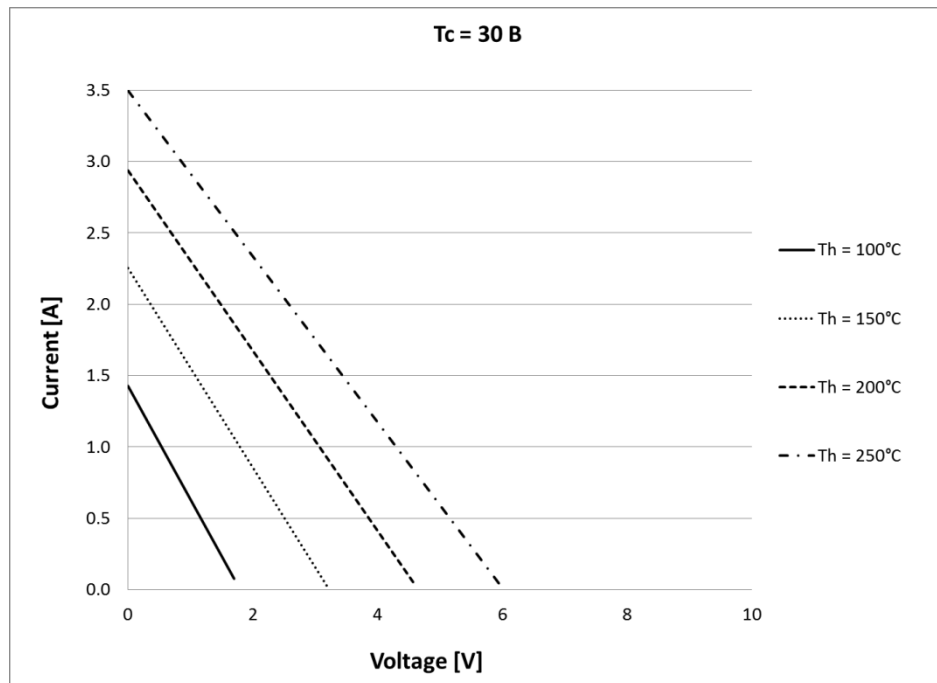


Figure A0.14 Extrapolated Manufacturer's V-I curve for TEG1B-12610-5.1 with a constant cold side temperature, T_c , of 30°C at various hot side temperatures

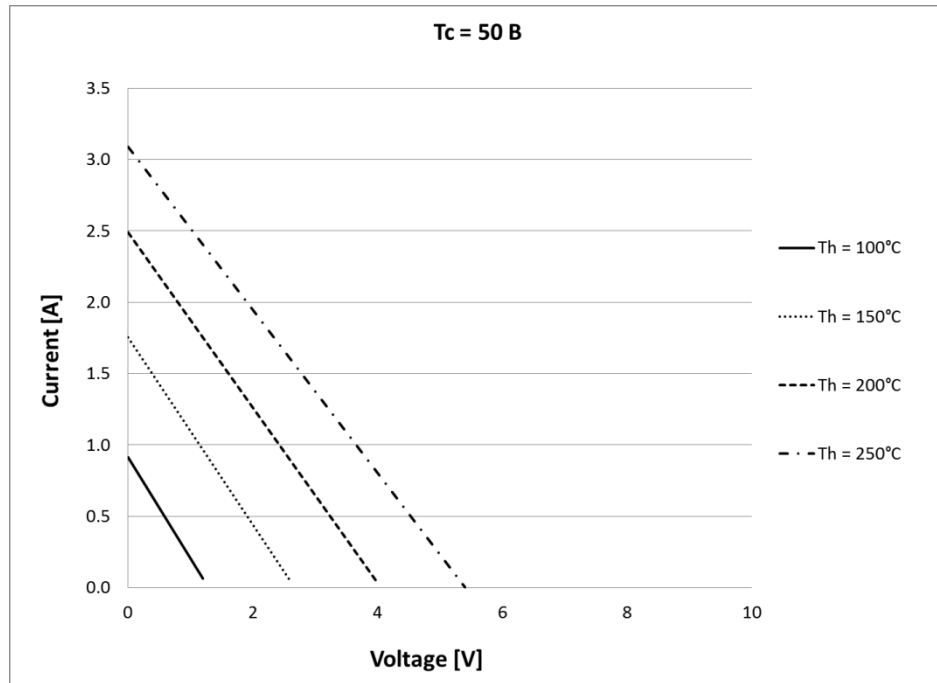


Figure A0.15 Extrapolated Manufacturer's V-I curve for TEG1B-12610-5.1 with a constant cold side temperature, T_c , of 50°C at various hot side temperatures

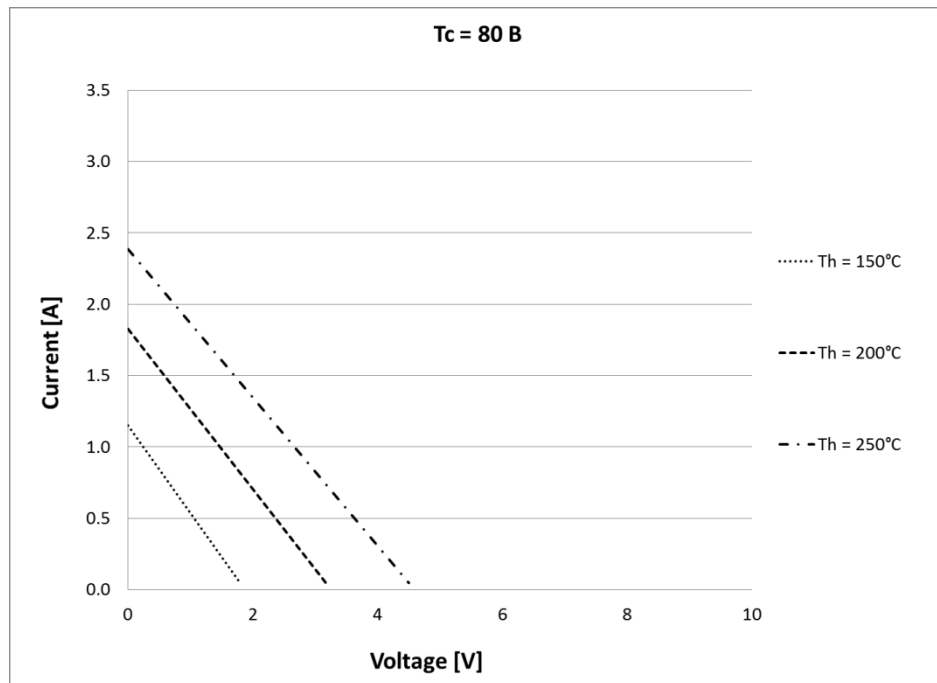


Figure A0.16 Extrapolated Manufacturer's V-I curve for TEG1B-12610-5.1 with a constant cold side temperature, T_c , of 80°C at various hot side temperatures

Given that the heat flow through the TEG is given by the charts, it is possible to extrapolate the thermal conductivity of the TEG as it varies with electrical load. The theory states that the thermal conductivity consists of a base thermal conductivity that occurs when there is no electron flow and another term that is dependent on the electron flow through the TEG, which is related to the Seebeck coefficient. Because the heat flow is only reported in the table of data only curves for the temperature difference of 30°C - 300°C can be generated.

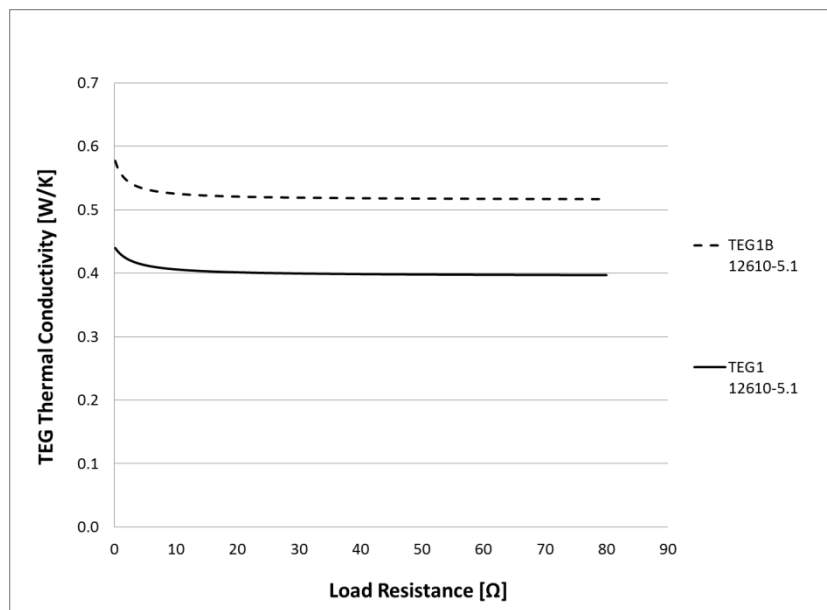


Figure A0.17 TEG thermal conductivity as a function of electrical load resistance for both TEG1-12610-5.1 and TEG1B-12610-5.1 under a temperature difference of 300°C - 30°C

The conductivity is calculated using the stated heat flow in the table and a Seebeck coefficient calculated from the open circuit voltage. The formula used is:

$$K_{TOTAL} = K_{ELECTRICAL} + K_{THERMAL}$$

$$K_{ELECTRICAL} = \frac{\alpha^2 \bar{T}}{R_L + R_m}$$

In the above formulae K_{THERMAL} is the thermal conductivity of the TEG under open circuit conditions and $K_{\text{ELECTRICAL}}$ the TEG conductivity aspect contributed by the thermoelectric effects.

APPENDIX B

There are quite a few measured and calculated values presented in this thesis. This appendix will provide a sample calculation of the error associated with all calculations and data on the error and uncertainty of the sensors used.

The sample calculations presented will be performed for the matched load condition of the TEG1 12612-5.1 at a temperature difference of 250°C - 50°C.

The uncertainty of the calculated values are calculated using the formula:

$$u(R) = \sqrt{\sum_{i=1}^n \left(u(x_i) \frac{dR}{dx_i} \right)^2}$$

where “R” is any function used to calculate a value which contains the arguments x_1 to x_n where $R = f(x_1, x_2, x_3, \dots, x_n)$.

TEG

The four parameters that are used to characterise the power from the TEG are the magnitude of the voltage, current and power produced and the load resistance at which these values are produced. The voltage and current of the TEG are measured by the BK 8500 Electronic DC Load. The uncertainty of those two measurements are:

- Voltage: In the range of 0-18V the accuracy of the measurement is 0.05% plus 0.02% of full scale.
- Current: In the range of 0-3A the accuracy of the measurement is 0.2% plus 0.15% of full scale. In the range of 3-30A the accuracy of the measurement is 0.1% plus 0.1% of full scale.

Voltage

$$u(V_{TEG}) = 0.05\% \times 3.645 + 0.02\% \times 18 = 0.00542[V]$$

Current

$$u(I_{TEG}) = 0.2\% \times 1.212 + 0.15\% \times 3 = 0.00421[A]$$

Power

$$P_{TEG} = V_{TEG} \times I_{TEG}$$

$$u(P_{TEG}) = \sqrt{\left(u(V_{TEG}) \frac{dP_{TEG}}{dV_{TEG}}\right)^2 + \left(u(I_{TEG}) \frac{dP_{TEG}}{dI_{TEG}}\right)^2}$$

$$u(P_{TEG}) = \sqrt{(0.00542 \times 1.212)^2 + (0.00421 \times 3.645)^2}$$

$$u(P_{TEG}) = 0.00687[W]$$

Resistance

$$R_{TEG} = V_{TEG} \div I_{TEG}$$

$$u(R_{TEG}) = \sqrt{\left(u(V_{TEG}) \frac{dR_{TEG}}{dV_{TEG}}\right)^2 + \left(u(I_{TEG}) \frac{dR_{TEG}}{dI_{TEG}}\right)^2}$$

$$u(R_{TEG}) = \sqrt{(0.00542 \times 1.212)^2 + (0.00421 \times 3.645)^2}$$

$$u(R_{TEG}) = 0.00687[\Omega]$$

Thermocouples

To calibrate the thermocouples used for this experiment they were placed in an isothermal block of copper. The temperature of the block of copper was monitored using a platinum resistance thermometer as a reference thermometer. The temperature of the thermocouples in the same block were then compared to the RTD to calibrate them.

There are many possible errors associated with this calibration method and the measurement of a temperature using a thermocouple. For the purpose of this thesis only what were considered the five major errors were calculated.

- RTD Bias: This is the bias uncertainty that is associated with the manufacture of the RTD temperature probe. It is stated as 0.01[°C].
- RTD Reader Bias: This is the bias uncertainty that is associated with the manufacture of the RTD reader that is used to read the temperature of the RTD. It is stated as 0.01[°C].
- RTD Drift: Over time the temperature measurement of the RTD drifts. According to Drnovsek et al. the drift can be estimated as 0.0075[°C] per year. Over the 9 years the drift would amount to 0.0675[°C] [B01].
- DAQ Bias: This is the bias uncertainty that is associated with the manufacture of the DAQ thermocouple card and chassis. It is stated as 0.2[°C].
- Calibration Error: The equation that maps the measured thermocouple readings during the calibration to the RTD has an associated error. The error for the calibration equations are found in table B0.1.

$$u(T) = \sqrt{\sum_{1}^{5} u(x_i)}$$

$$u(T1) = \sqrt{0.01^2 + 0.01^2 + 0.0675^2 + 0.2^2 + 0.073^2} = 0.224[°C]$$

Table B0.1 Errors associated with thermocouple measurements.

Uncertainty of Thermocouples						
	Top Cold Block	Middle Cold Block	Bottom Cold Block	Top Hot Block	Middle Hot Block	Bottom Hot Block
	T1	T2	T3	T4	T5	T6
	[°C]	[°C]	[°C]	[°C]	[°C]	[°C]
RTD Bias	0.01	0.01	0.01	0.01	0.01	0.01
RTD Reader Bias	0.01	0.01	0.01	0.01	0.01	0.01
RTD Drift	0.0675	0.0675	0.0675	0.0675	0.0675	0.0675
DAQ Bias	0.2	0.2	0.2	0.2	0.2	0.2
Calibration Error	0.073	0.078	0.077	0.027	0.027	0.035
Thermocouple Uncertainty	0.224	0.225	0.225	0.213	0.213	0.214

Temperature Gradient

The two main heat flows in this experiment and the extrapolations for the surface temperatures depend on the temperature gradient in the block. This temperature gradient is calculated using the following formula:

$$\left(\frac{dT}{dx}\right) = \frac{\sum_{i=1}^n (x_i - \bar{x}) \times (T_i - \bar{T})}{\sum_{i=1}^n (x_i - \bar{x})^2}$$

In the above formula the variable x refers to the position of the thermocouple from the surface and \bar{x} is the average of the position of all thermocouples involved. The accuracy of the positions of the holes depends on the milling machine used to drill them. The mill used to drill the holes in both copper blocks was done by a H.H. Roberts knee and column

mill to an accuracy of 0.25mm. Similar to the position, T is the temperature recorded by the thermocouple and \bar{T} is the average temperature of all thermocouples involved.

The equation for the uncertainty of the temperature gradient is formulated using the standard equation stated in section 3.7 and repeated at the beginning of this appendix.

The values for the uncertainty of the temperature gradient through the hot and cold blocks are 7.4[°C/m] and 7.7[°C/m] respectively.

Surface Temperatures

The temperatures of the hot side and cold side of the TEG are dependent on the temperature gradient. The formula for the extrapolated temperature is:

$$T_{SURF} = \bar{T} - \frac{dT}{dx} \bar{x}$$

The uncertainty equation for the surface temperature a copper block is:

$$u(T_{SURF}) = \sqrt{u(\bar{T})^2 + \left(-u\left(\frac{dT}{dx}\right) \bar{x}\right)^2 + \left(-u(\bar{x}) \frac{dT}{dx}\right)^2}$$
$$u(T_{SURF}) = \sqrt{(0.124)^2 + (7.4 \times 0.0343)^2 + (0.000144 \times 282.95)^2}$$
$$u(T_{SURF}) = 0.2858[^\circ\text{C}]$$

The above value is the uncertainty associated with the extrapolated surface temperature of the hot block. The uncertainty associated with the extrapolated cold surface temperature is 0.2696[°C].

The uncertainty for the average temperature of the TEG can be calculated with these two uncertainties to be 0.206[°C].

Q_{HEATERS}

The heaters only have two variables in their calculations and only two uncertainties.

- Voltage: The Agilent U 1253B Multimeter has two uncertainties depending on the magnitude of the voltage being measured. For voltages over 50V the uncertainty is 0.03% plus five least significant digits. If the voltage is under 50V the uncertainty is 0.025% plus 5 least significant digits.
- Current: The BK 2831D Multimeter has an uncertainty of 1.0% of the reading plus 10 least significant digits.

$$u(Q_{HEATERS}) = \sqrt{\left(u(V) \frac{dQ_{HEATERS}}{dV}\right)^2 + \left(u(I) \frac{dQ_{HEATERS}}{dI}\right)^2}$$

$$u(Q_{HEATERS}) = \sqrt{(0.0753 \times 2.517)^2 + (0.03517 \times 84.38)^2}$$

$$u(Q_{HEATERS}) = 2.9737$$

Q_{HOT} and Q_{COLD}

The equation for the heat flow through the copper blocks is as follows:

$$Q = k_{C110} \times A \times \left(\frac{dT}{dx}\right)$$

The uncertainty of the temperature gradient is known from the above calculations. The uncertainty associated with the area is related the milling machine used to machine the copper blocks. The H.H. Roberts knee and column mill, used to machine the copper, has an associated error of 0.25mm. The conductivity of copper used was evaluated using an equation from the C.R.C. Handbook of materials:

$$k_{C110} = 571.298 - 1.125096 \times T + 02.5411 \times 10^{-3} \times T^2 - 2.528 \times 10^{-6} \times T^3 \\ + 889.684 \times 10^{-12} \times T^4$$

The variable T in the above equation is the average temperature of the three thermocouples temperatures in the block. The uncertainty equation is formulated using the same equation as the other calculated values. The uncertainty of the conductivity of the copper in the hot and cold blocks is 0.004[W/mK] and 0.022[W/mK] respectively.

With the uncertainty of the conductivity of copper known, the calculation of the uncertainty of the heat flux is determined in the standard manner.

$$u(Q) \\ = \sqrt{\left(u(k_{C110}) \times A \times \left(\frac{dT}{dx}\right)\right)^2 + \left(u(A) \times k_{C110} \times \left(\frac{dT}{dx}\right)\right)^2 + \left(u\left(\frac{dT}{dx}\right) \times k_{C110} \times A\right)^2}$$

$$u(Q) = \left(\left((0.004)(0.00168)(281.95)\right)^2 + \left((2.05 \times 10^{-5})(382.56)(281.95)\right)^2\right. \\ \left.+ \left((7.4)(382.95)(0.00168)\right)^2\right)^{-0.5}$$

$$u(Q) = 5.256[W]$$

Using the same equation for uncertainty the uncertainty for the heat flow through the cold block is found to be 5.591[W].

Q_{WATER}

The heat extracted from the system is calculated using the following formula:

$$Q_{WATER} = \dot{m}C_P(\bar{T}_{W,I} - \bar{T}_{W,O})$$

The specific heat capacity of water is calculated from an equation found in the C.R.C. Handbook of Materials. It depends only on the temperature of the water. The specific heat

capacity used in the system is the heat capacity of water at the average temperature of all six thermocouples. The uncertainty associated with this value due to the uncertainty of the thermocouples used is 0.0072[J/kg·K].

There were two mass flow meters used in the experiments for this thesis. The first was an Exact Flow Dual Rotameter with an uncertainty of 0.114%. The second was a Proline Promass 80E Coriolis mass flow meter with an uncertainty of 0.046% of the reading.

$$u(Q_{WATER}) = \left(\left(u(\dot{m})C_P(\bar{T}_{W,I} - \bar{T}_{W,O}) \right)^2 + \left(u(C_P)\dot{m}(\bar{T}_{W,I} - \bar{T}_{W,O}) \right)^2 + \left(u(\bar{T}_{W,I})\dot{m}C_P \right)^2 + \left(u(\bar{T}_{W,O})\dot{m}C_P \right)^2 \right)^{-0.5}$$

The uncertainty of the heat extracted with the chiller is calculated to be 2.14[W].

Thermal Conductivity

The thermal conductivity of a TEG from the measurements of the TEMTester is a relatively simple calculation:

$$K_{TEG} = (Q_{HOT} + Q_{COLD})/[2 \times (T_{HOT} - T_{COLD})]$$

Given that the uncertainties to all the above parameters are known, the uncertainty of the thermal conductivity of the TEG can be calculated easily.

$$u(K_{TEG}) = \left(\left(\frac{u(Q_{HOT})(Q_{COLD})}{2 \times (T_{HOT} - T_{COLD})} \right)^2 + \left(\frac{u(Q_{COLD})(Q_{HOT})}{2 \times (T_{HOT} - T_{COLD})} \right)^2 + \left(\frac{-u(T_{HOT})(Q_{HOT} + Q_{COLD})}{2 \times (T_{COLD} - T_{HOT})} \right)^2 + \left(\frac{u(T_{COLD})(Q_{HOT} + Q_{COLD})}{2 \times (T_{COLD} - T_{HOT})} \right)^2 \right)^{-0.5}$$

The uncertainty of the thermal conductivity of a TEG is 0.0241[W/K]. The effect of the contact resistance is factored into the thermal conductivity of the TEG. The uncertainty of the contact resistance increases the uncertainty of the TEG thermal conductivity to

0.0697[W/K]. Tables of the uncertainties for the experiments conducted can be found in section 3.7.

References:

[B01] Drnovsek, J., Pusnik, I., Bojkovski, J., (1998), “Reduction of uncertainties in temperature calibrations by comparison”, *Measurement Science and Technology*, Vol. 9 (11), pp. 1907-1911.

APPENDIX C

The material used in the commercial thermoelectric generators is doped bismuth telluride. According to testing performed for the P.O.W.E.R. project, the bismuth telluride is doped with selenium and antimony to create the n-type and p-type materials respectively. There are a lot of other materials that are used as semiconductors in thermoelectric generators. In his paper Snyder [C01] presented figure C01 which is a graph of the different figure of merits, ZT, for materials used in thermoelectric generation. In this graph it's quite apparent that the figure of merit is very dependent on temperature. The figure shows that the figure of merit can vary from 0.2 to 0.8 over the temperature differences tested in the experiments for this thesis.

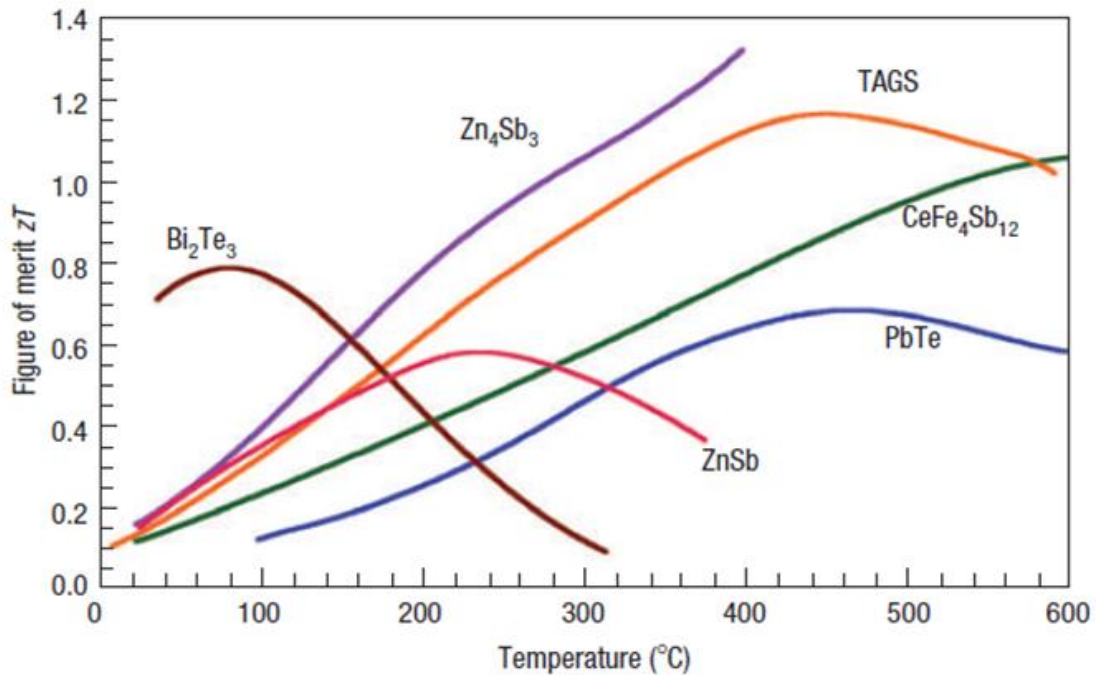


Figure C0.1 Figure of merit of various thermoelectric materials over different ranges of temperatures.

The materials used for thermoelectronics are not only dependent on temperature. They are also highly variable depending on the manufacturing process used to create the material. According to the industry sponsors of the P.O.W.E.R. project the material for the

commercial TEGs tested in this thesis are extruded or grown in ingot form. The material properties can vary within these ingots from the center to the end. In his paper Kanatzidis [C02] graphed the figure of merit for p-type and n-type bismuth telluride as a function of temperature. The materials are shown to be dependent on the different manufacturing processes used.

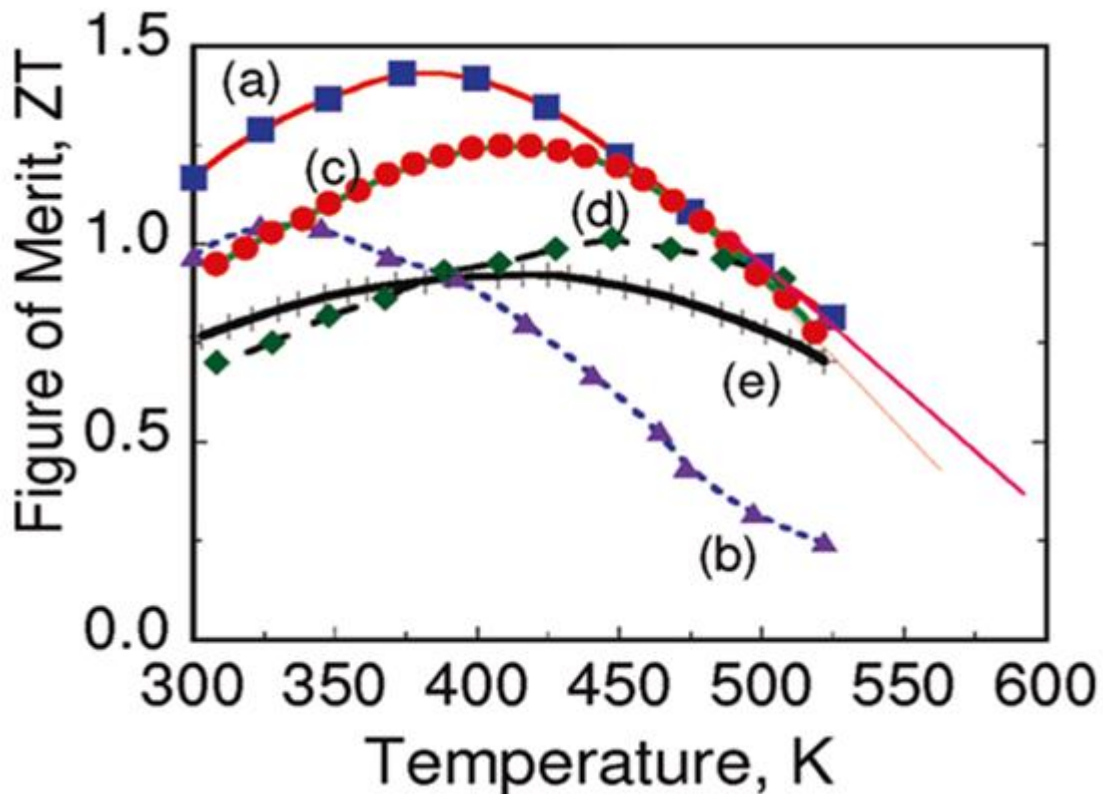


Figure C0.2 Figure of merit, ZT , as a function of temperature for bulk $\text{Bi}_{2-x}\text{Sb}_x\text{Te}_3$ and $\text{Bi}_2\text{Te}_{3-x}\text{Se}_x$ materials prepared by (a) ball milling and hot pressing (p-type), (b) zonemelting (p-type), (c) melt spinning and SPS (p-type), and (d) hydrothermal synthesis (n-type) and (e) conventional $\text{Bi}_{2-x}\text{Sb}_x\text{Te}_3$.

The different manufacturing methods investigated by Kanatzidis involve reducing grain size in the thermoelectric material. This smaller grain size results in more grain boundaries which cause a smaller thermal conductivity due to phonon scattering. The graph in figure C0.2 shows methods used by other researchers which yielded very different results from the conventional and from Kanatzidis's material.

Another factor that determines the figure of merit for a material is the dopants that are used and in what quantities they are used. Figure C0.3 is a very simple example of that fact. The figure is from the paper by Andre et al. [C03]. In this paper they are testing materials manufactured with different dopant levels of selenium and antimony. Figure C0.3 shows the figure of merit of two materials that differ by 2% of antimony. This small change in the material results in a different magnitude of the figure of merit at a different temperature.

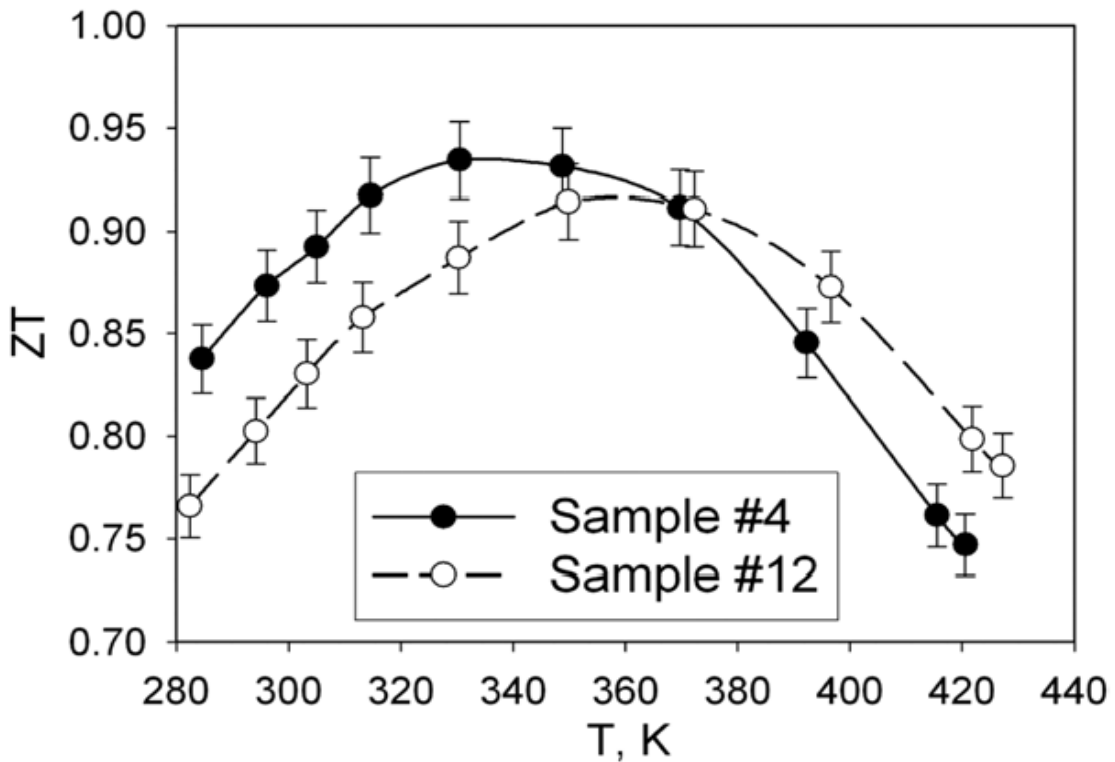


Figure C0.3 Figure of merit, ZT , of two different samples of quaternary alloys (sample 4: 7% Sb, 5% Se, sample 12: 7% Sb, 7% Se), as a function of absolute temperature.

This appendix is written only to give the reader an insight as to the variability of the materials used in thermoelectric generation. There are hundreds of other papers that can be drawn upon as a resource for the material properties of bismuth telluride and other thermoelectric materials.

[C01] Snyder, G. J., (2004), “Disordered zinc in Zn_4Sb_3 with phonon-glass and electron-crystal thermoelectric properties”, *Nature*, Vol. 3, pp.458-463

[C02] Kanatzidis, M. G., (2009), “Nanostructured Thermoelectrics: The New Paradigm?”, *Chemistry of Materials*, Vol. 22 (3), pp. 648-659

[C03] Andre, C., et al., (2011), “Increase in the density of states in n-type extruded $(Bi_{(1-x)}Sb_x)_2(Te_{(1-y)}Se_y)_3$ thermoelectric alloys”, *J. Phys. D: Appl. Phys.*, Vol. 44